TECHNICAL MEMORANDUM

LONGITUDINAL AERODYNAMIC CHARACTERISTICS AT TRANSONIC SPEEDS OF TWO V/STOL AIRPLANE CONFIGURATIONS WITH SKEWED AND VARIABLE-SWEEP WINGS

By Arvo A. Luoma

Langley Research Center
Langley Field, Va.

NATIONAL AERONAUTICS AND SPACE ADMINISTRATION
WASHINGTON
April 1961

[redacted]

NATIONAL AERONAUTICS AND SPACE ADMINISTRATION

TECHNICAL MEMORANDUM X-527

LONGITUDINAL AERODYNAMIC CHARACTERISTICS AT TRANSONIC SPEEDS OF TWO V/STOL AIRPLANE CONFIGURATIONS WITH SKEWED AND VARIABLE-SWEEP WINGS*

By Arvo A. Luoma

SUMMARY

An investigation of the longitudinal aerodynamic characteristics of two versions of a V/STOL airplane design was made in the Langley 8-foot transonic pressure tunnel at Mach numbers from 0.60 to 1.20. A skewed wing and a variable-sweep wing were tested on the models. Wing skew angles of 0°, 30°, 60°, and 90° and wing outboard panels swept 25°, 75°, and 108° with respect to the leading edge were investigated. The tests were made at angles of attack from about -2° to 11°.

Increasing the skew angle to high values produced a positive trim change. A larger horizontal tail substantially reduced nonlinearities evident in the variation of pitching moment with lift for the configuration with the highly skewed wings. The effect of wing sweep and Mach number on the longitudinal aerodynamic characteristics are generally the same as that reported for other V/STOL configurations employing a similar variable-sweep wing.

INTRODUCTION

Recent extensive studies made by the National Aeronautics and Space Administration of airplane configurations employing variable-sweep wings with the pivot point located outboard have indicated that configurations of this type appear to be a satisfactory means of realizing efficient subsonic and supersonic flight characteristics in one airplane (refs. 1 to 6). Further studies have been made at low subsonic speeds, at transonic speeds, and at a Mach number of 1.97 of an advanced version of this wing design on a body more representative of those used on current fighter

*Title, Unclassified.

aircraft (refs. 7 to 9); and, for comparison, of a more conventional variable-sweep wing having the pivot point located within the fuselage (refs. 7 and 9).

A further mission requirement recently studied is that of supersonic flight at low levels over a rather long range. Because of the high drag and gust accelerations associated with the high dynamic pressures at low levels, it appeared desirable to increase the wing sweep until a large portion of the wing was confined either on top of or within the body. References 10 to 13 present the results obtained at transonic and supersonic speeds on configurations having variable-sweep wings which were swept so that a large portion of the wing was on top of the body. Reference 8 includes information at transonic speeds on a configuration which had the wings swept so that a large portion of the wing was within the body.

In order to provide airplanes with V/STOL capability, which enables them to operate from locations with limited ground facilities or from devastated areas, variable-sweep configurations have been designed around a proposed vectored lift-thrust engine. This engine has jet-exit nozzles which rotate through an angle of approximately 120°, from straight back for forward flight to about 30° ahead of the vertical for low-speed operation. The results of studies of such V/STOL variable-wing-sweep airplane configurations are presented in references 14 to 16.

The present paper provides information on the longitudinal aerodynamic characteristics of two further designs of V/STOL airplane configurations based on the proposed vectored lift-thrust engine. Both designs included a scoop-type air inlet on the body. The main differences between the two designs were in the details of the ducting and in the size of the horizontal tails. Two wings were tested on each design: a skewed wing at skew angles of 0°, 30°, 60°, and 90° on one of the designs and 0° and 90° on the other design; and a variable-sweep wing (outboard pivot design) at sweep angles of 25°, 75°, and 108° on both of the designs. The tests were made in the Langley 8-foot transonic pressure tunnel at Mach numbers from 0.60 to 1.20 for an angle-of-attack range from approximately -2° to 11°. The longitudinal and lateral aerodynamic characteristics of one of the two designs of V/STOL airplane configurations were investigated in the Langley 4- by 4-foot supersonic pressure tunnel at a Mach number of 2.20, and the results are presented in reference 17.

SYMBOLS

The longitudinal aerodynamic force and moment data are referred to the wind axes. The yawing-moment, rolling-moment, and lateral-force

data obtained for the skewed-wing configurations are referred to the body axes. The origin of the wind and body axes was the moment reference point shown in figures 1 to 4. This location was 19.69 inches from the body nose and 0.70 inch above the model reference line. All the aerodynamic data presented herein for the configurations with the variable-sweep wing were based on the planform dimensions of the 75° swept wing; all the aerodynamic data presented herein for the configurations with the skewed wing were based on the planform dimensions of the 0° skewed wing. The symbols used are defined as follows:

A aspect ratio of wing, b^2/S

$A_{e,1}$ total area of forward exit of duct

$A_{e,2}$ total area of rearward exit of duct

$A_{e,3}$ area of bypass exit of duct

A_p total projected area of duct inlet on plane perpendicular to reference line of model

b span of wing

C_D external-drag coefficient, $\frac{\text{External drag}}{q_\infty S}$

$C_{D,i}$ internal-drag coefficient,

$$\left\{\frac{w_1}{q_\infty S}\left[V_\infty - V_{e,1}\cos\alpha\cos\theta_1(1 - \tan\alpha\tan\theta_1\sin\theta_2)\right]\right.$$

$$\left. - C_{p,e,1}\frac{A_{e,1}}{S}\cos\alpha\cos\theta_1(1 - \tan\alpha\tan\theta_1\sin\theta_2)\right\}$$

$$+\left\{\frac{w_2}{q_\infty S}\left[V_\infty - V_{e,2}\cos\alpha\cos\theta_1(1 - \tan\alpha\tan\theta_1\sin\theta_2)\right]\right.$$

$$\left. - C_{p,e,2}\frac{A_{e,2}}{S}\cos\alpha\cos\theta_1(1 - \tan\alpha\tan\theta_1\sin\theta_2)\right\}$$

$C_{D,min}$ minimum value of external-drag coefficient

C_L lift coefficient, $\frac{\text{Lift}}{q_\infty S}$

C_l rolling-moment coefficient, $\frac{\text{Rolling moment}}{q_\infty Sb}$

C_m pitching-moment coefficient, $\frac{\text{Pitching moment}}{q_\infty S\bar{c}}$

C_n yawing-moment coefficient, $\frac{\text{Yawing moment}}{q_\infty Sb}$

$C_{p,e,1}$ pressure coefficient of flow in duct at forward exit, $\frac{p_{e,1} - p_\infty}{q_\infty}$

$C_{p,e,2}$ pressure coefficient of flow in duct at rearward exit, $\frac{p_{e,2} - p_\infty}{q_\infty}$

C_Y lateral-force coefficient, $\frac{\text{Lateral force}}{q_\infty S}$

$\bar{c}$ mean aerodynamic chord of wing

L/D lift-drag ratio, C_L/C_D

$(L/D)_{max}$ maximum value of lift-drag ratio

M Mach number of undisturbed stream

$p_{e,1}$ static pressure of flow in duct at forward exit

$p_{e,2}$ static pressure of flow in duct at rearward exit

$p_{t,\infty}$ total pressure of undisturbed stream

p_∞ static pressure of undisturbed stream

q_∞ dynamic pressure of undisturbed stream, $\frac{1}{2}\rho_\infty V_\infty^2$

R Reynolds number, based on $\bar{c}$

S area of wing

$V_{e,1}$ velocity of flow in duct at forward exit

$V_{e,2}$ velocity of flow in duct at rearward exit

V_∞ velocity of undisturbed stream

w total mass flow into inlet of duct, $w_1 + w_2 + w_3$

w_1 mass flow in duct at forward exit

w_2 mass flow in duct at rearward exit

w_3 mass flow in duct at bypass exit

w/w_∞ mass-flow ratio based on projected area of inlet, $\frac{w}{\rho_\infty V_\infty A_p}$

α angle of attack of model, based on reference line of model

δ_h horizontal-tail deflection, determined by angle between exposed root chord and XY-plane of body axes; positive direction when trailing edge is down

ζ skew angle of wing, based on angle of 50-percent-chord line (see fig. 1)

θ_1 angle between duct-exit axis and model reference line (see fig. 2)

θ_2 angle between plane defined by duct-exit axis and model reference line and lateral plane (see fig. 2)

Λ sweep angle of wing, based on sweep of leading edge of outer panel

ρ_∞ mass density of undisturbed stream

$C_{L_\alpha} = \frac{dC_L}{d\alpha}$ per deg

$C_{m_{C_L}} = \frac{dC_m}{dC_L}$

$C_{m_{\delta_h}} = \frac{dC_m}{d\delta_h}$ per deg

Components of model:

B	body (including canopy and air inlet and exits)
H	horizontal tail
V	vertical tail
W	wing

APPARATUS

Tunnel

The investigation was made in the Langley 8-foot transonic pressure tunnel. The test section of this tunnel is square in cross section. The upper and lower walls of the test section are slotted to permit continuous testing through the transonic speed range. The total pressure of the tunnel air can be varied from a minimum value of about 0.25 atmosphere at all test Mach numbers to a maximum value of about 2.0 atmospheres at Mach numbers of 0.4 and less and about 1.5 atmospheres at transonic Mach numbers. The tunnel air is dried sufficiently to avoid condensation effects.

Model

In the present investigation two V/STOL airplane configurations designed around a proposed vectored lift-thrust engine were tested, and they are identified herein as models IV-A and IV-B. Tests on other V/STOL configurations designed for this same engine and designated as models I, II, and III are presented in references 14 to 16. Models IV-A and IV-B represented a four-point vectored-thrust V/STOL arrangement with a large, single, scoop-type air inlet located beneath the body nose. Two wings were tested on each model: a skewed wing and a variable-sweep wing with an outboard pivot. Drawings of model IV-A with the skewed wing are presented in figure 1, and with the variable-sweep wing in figure 2. Drawings of model IV-B with the same skewed and variable-sweep wings are shown in figures 3 and 4, respectively. Photographs of model IV-B with the skewed and variable-sweep wings are shown as figures 5 and 6, respectively. Some of the geometric characteristics of the models are presented in table I. The main differences between models IV-A and IV-B were in the details of the ducting and in the size of the horizontal tails.

Each model had four duct exits with two located on each side of the body. The axis of the duct exits of model IV-A was deflected 30° away from the model reference line (fig. 2). The axis of the duct exits of model IV-B was parallel to the model reference line. A bypass exit located just aft of the inlet was incorporated on model IV-B to increase the mass flow into the inlet (figs. 3, 4, and 6(e)).

The airfoil section (streamwise) of the 0° skewed wing was 3 percent thick with a flat lower surface and a circular-arc upper surface. The pivot point of the skewed wing was at the 50-percent point of the root chord of the $\zeta = 0°$ position. The airfoil section (streamwise) of the outboard panel of the 25° swept wing was 6 percent thick with a flat lower surface and an upper surface which conformed to the upper-surface ordinates of the NACA 65A012 airfoil section. The leading edge was rounded. The pivot point about which the outboard panel was swept was located laterally at 48.2 percent of the semispan of the 75° swept wing. The inboard (fixed) panel of the variable-sweep wing had a leading-edge sweep of 60°. Both the skewed and the variable-sweep wings had 0° dihedral and incidence.

The same vertical tail was used on both models IV-A and IV-B. The leading-edge sweep of the horizontal tail was 60° on model IV-A and 54° on model IV-B. The span and area of the horizontal tail of model IV-B were 33 percent and 29 percent larger, respectively, than those of model IV-A. The horizontal and vertical tails were constructed of 1/8-inch flat steel plate with rounded leading edges and beveled trailing edges.

The longitudinal distribution of cross-sectional area of model IV-A is shown in figure 7. In order to account for internal flow, the cross-sectional area has been reduced to correspond to a mass-flow ratio w/w_∞ of 0.82, with 43 percent of the mass flow being exited at the forward exit and 57 percent at the rearward exit. Model IV-A with the skewed wing had a small amount of area added to the sides and top of the body forward of the wing to improve the area distribution in this region. This area addition was left on for model IV-B with both the skewed and variable-sweep wings. The longitudinal distribution of cross-sectional area of model IV-B is shown in figure 8. In order to account for internal flow, the cross-sectional area has been reduced to correspond to a mass-flow ratio w/w_∞ of 1.00, with 32 percent of the mass flow being exited at the bypass exit, 25 percent at the forward exit, and 43 percent at the rearward exit.

Instrumentation

A six-component strain-gage balance, which was housed in the body, was used for determining the overall forces and moments on the model.

A strain-gage attitude transmitter was used for getting the no-load angle of attack of the model. Because the attitude transmitter was housed in the extension of the model sting, a correction to the reading of the attitude transmitter was necessary to obtain the model angle of attack because of the flexibility under aerodynamic load of the balance, model sting, and sting extension.

A static orifice located within the chamber surrounding the strain-gage balance was connected to a pressure transducer. Rakes were used at all duct exits when mass-flow and internal-drag measurements were made.

The overall forces and moments on the model, the angle of attack, and the static pressure in the chamber surrounding the strain-gage balance were recorded electronically on punch cards for all configurations. During the mass-flow runs the total and static pressures at the duct exits were measured by use of a multiple-tube manometer containing tetrabromoethane. All manometer tubes were photographed simultaneously.

TESTS, CORRECTIONS, AND ACCURACY

Tests

All the tests were made with transition fixed on the model. Narrow strips of No. 80 carborundum grains were shellacked to the wings and tail surfaces at 10 percent chord, to the inlet lip, and to the body at 10 percent body length.

The effect of wing skew angle, wing sweep, horizontal-tail deflection, and model components on the longitudinal aerodynamic characteristics was determined. All of the tests were made at an angle of sideslip of 0°.

Model IV-A with the skewed wing was investigated at wing skew angles of 0°, 30°, 60°, and 90° at a horizontal-tail deflection of 0°. Model IV-A with the variable-sweep wing was investigated for outboard wing panels swept back 25°, 75°, and 108° with respect to the leading edge. Model IV-A with the 75° swept wing was tested at horizontal-tail deflections of 0° and -4.15°, and also with the horizontal tail off. The horizontal-tail deflection was -4.15° on model IV-A with the 25° swept wing and 0° on model IV-A with the 108° swept wing.

Model IV-B with the skewed wing was tested at wing skew angles of 0° and 90° at a horizontal-tail deflection of -4.15°. Model IV-B with the 90° skewed wing was also tested at a horizontal-tail deflection

of 0° and with the horizontal tail off. Model IV-B with the variable-sweep wing was tested at sweep angles of 25°, 75°, and 108° at a horizontal-tail deflection of -4.15°.

All the configurations except the configurations with the 25° swept wing were investigated at five Mach numbers from 0.60 to 1.20 and through an angle-of-attack range from approximately -2° to 11°. The configurations with the 25° swept wing were tested at Mach numbers from 0.60 to 0.95 through the same angle-of-attack range. Minimum-drag data were also obtained at a few intermediate Mach numbers. The configurations generally were tested at total pressures of 1,060 pounds per square foot (1/2 atmosphere) or 530 pounds per square foot (1/4 atmosphere), depending on wing or balance load limits. The Reynolds number corresponding to these total pressures is shown in figure 9.

L 1 4 8 7

All the configurations were investigated with internal flow in the model. The mass flow and internal drag of model IV-A with the 108° swept wing (configuration BWVH; $\delta_h = 0°$) and model IV-B with the 90° skewed wing (configuration BWV) were measured. Internal-flow data were obtained at Mach numbers from 0.60 to 1.20 and at angles of attack from 0° to about 10°.

Corrections

The external-drag coefficient C_D was corrected by adjusting the static pressure in the balance chamber and at the body base to the free-stream value. The external-drag coefficient also includes the correction for the internal-drag coefficient $C_{D,i}$. The internal-drag coefficient measured for model IV-A with the 108° swept wing and shown in figure 10 was used in correcting all the configurations of model IV-A. The internal-drag coefficient measured for model IV-B with the 90° skewed wing and shown in figure 11 was used in correcting all the configurations of model IV-B. Mass-flow results are also presented in figures 10 and 11.

Data presented herein at supersonic Mach numbers consist of minimum-drag results at a Mach number of 1.03 and of force and moment results for the angle-of-attack range at a Mach number of 1.20. At a Mach number of 1.03 the flow over the model was subject to influence by wall-reflected disturbances. The effect on drag was probably small. The configurations were clear of wall-reflected disturbances at a Mach number of 1.2. No corrections have been made to the data for wall-reflected disturbances except to the extent of the partial correction for wall-reflected disturbances inherent in the base-pressure correction.

No sting-interference corrections have been made to the data except to the extent of the partial correction for sting interference inherent in the base-pressure correction.

Accuracy

The accuracy of the data, based primarily on the static calibrations and the repeatability of the data, is estimated to be as follows:

C_L	±0.01
C_D	±0.0015
C_m	±0.003
C_n	±0.002
C_l	±0.0006
C_Y	±0.01
α, deg	±0.1
M	±0.003

PRESENTATION OF RESULTS

The basic longitudinal aerodynamic characteristics of model IV-A are presented in figures 12 to 15 and those of model IV-B in figures 16 to 18. Figure 12 also presents information on the effect of wing skew angle on the lateral force-and-moment components. The basic data are presented in the following order:

	Figure
Model IV-A:	
Wing skewed 0°, 30°, 60°, and 90°	12
Wing swept 25°	13
Wing swept 75°	14
Wing swept 108°	15
Model IV-B:	
Wing skewed 0°	16
Wing skewed 90°	17
Wing swept 25°, 75°, and 108°	18

Summary data on performance and longitudinal stability and control derivatives are presented in figures 19 to 26 for model IV-A and in figures 27 to 34 for model IV-B. A comparison of the minimum drags of models IV-A and IV-B is given in figure 35. The derivatives C_{L_α} and

$C_{m_{C_L}}$ are for an angle of attack of approximately 0°. The summary plots are presented in the following order:

SUMMARY OF RESULTS

A detailed discussion of the results obtained in the investigation at transonic speeds of two V/STOL airplane configurations with skewed and variable-sweep wings has been omitted in order to expedite publication of the data. A few observations are made, however, in order to point out some of the more important results obtained.

Skewed-Wing Configurations

The longitudinal-stability characteristics of model IV-B (figs. 16(d), 17(d), and 33(a)) were generally more satisfactory than those of model IV-A (figs. 12(c) and 25(a)). The noticeable nonlinearity evident in the pitching-moment curves of model IV-A with the 60° and 90° skewed wings (fig. 12(c)) was not present in the pitching-moment curves of model IV-B with the 90° skewed wing (fig. 17(d)). Skewing the wing from 0° to 90° resulted in a positive trim change for both models (figs. 12(c), 16(d), and 17(d)), in a forward movement of the aerodynamic center for model IV-A (fig. 25(a)), and in a rearward movement of the aerodynamic center for model IV-B (fig. 33(a)). The differences in the longitudinal-stability characteristics of the two models with the highly skewed wings appear to be due mainly to a greater effectiveness of the larger horizontal tail on model IV-B. Presumably, the tips of the small horizontal tail were in the strong downwash flow field just inboard of the wing-tip vortex cores, whereas the tips of the large horizontal tail extended outboard of the wing-tip vortex cores into an upwash flow field.

The maximum lift-drag ratio of model IV-A with the 0° skewed wing was somewhat higher than that for model IV-B with the 0° skewed wing (figs. 24(a) and 32(a), respectively). The minimum-drag coefficients of these two configurations were not greatly different (figs. 19 and 27). The drag due to lift, however, was lower for model IV-A with the 0° skewed wing (figs. 12(b) and 16(b)).

Variable-Sweep-Wing Configurations

The effect of wing sweep and Mach number on the longitudinal aerodynamic characteristics (figs. 20, 29, 23(b), 31(b), 24(b), 32(b), 25(b), and 33(b)) is generally the same as that reported in reference 14 for V/STOL configurations employing a similar variable-sweep wing. The maximum lift-drag ratios of the present tests, especially those of model IV-A, are somewhat higher than those found in the tests of reference 14. The minimum-drag coefficient of the configurations of the present tests (figs. 20 and 29) was somewhat higher than that found in reference 14.

Comparisons of the minimum-drag force (i.e., drag coefficients based on same wing area) of the configurations with the skewed and variable-sweep wing showed that the minimum-drag force of the configurations with the 75° swept wing was lower at all test Mach numbers than that of the configurations with the 0° skewed wing. The minimum-drag force of the configurations with the 0° and 90° skewed wings, however, was generally lower than that of the configurations with the 25° and 108° swept wings, respectively.

The maximum lift-drag ratio of the configurations with the 25° swept wing was higher than that of the configurations with the 0° skewed wing at Mach numbers below approximately 0.85. The maximum lift-drag ratios of the configurations with the 75° swept wing and the 0° skewed wing were about the same at Mach numbers of 1.00 and 1.20. (See figs. 24 and 32.)

Langley Research Center,
National Aeronautics and Space Administration,
Langley Field, Va., February 15, 1961.

REFERENCES

1. Alford, William J., Jr., and Henderson, William P.: An Exploratory Investigation of the Low-Speed Aerodynamic Characteristics of Variable-Wing-Sweep Airplane Configurations. NASA TM X-142, 1959.

2. Alford, William J., Jr., Luoma, Arvo A., and Henderson, William P.: Wind-Tunnel Studies at Subsonic and Transonic Speeds of a Multiple-Mission Variable-Wing-Sweep Airplane Configuration. NASA TM X-206, 1959.

3. Spearman, M. Leroy, and Foster, Gerald V.: Stability and Control Characteristics at a Mach Number of 2.01 of a Variable-Wing-Sweep Configuration With Outboard Wing Panels Swept Back 75°. NASA TM X-32, 1959.

4. Spearman, M. Leroy, and Foster, Gerald V.: Effects of Various Modifications on the Supersonic Stability Characteristics of a Variable-Wing-Sweep Configuration at a Mach Number of 2.01. NASA TM X-260, 1960.

5. Foster, Gerald V.: Stability and Control Characteristics at Mach Numbers of 2.50, 3.00, and 3.71 of a Variable-Wing-Sweep Configuration With Outboard Wing Panels Swept Back 75°. NASA TM X-267, 1960.

6. Foster, Gerald V.: Effects of Spoiler-Slot-Deflector Control on the Aerodynamic Characteristics at a Mach Number of 2.01 of a Variable-Wing-Sweep Configuration With the Outer Wing Panels Swept Back 75°. NASA TM X-273, 1960.

7. Spencer, Bernard, Jr.: Stability and Control Characteristics at Low Subsonic Speeds of an Airplane Configuration Having Two Types of Variable-Sweep Wings. NASA TM X-303, 1960.

8. Luoma, Arvo A.: Stability and Control Characteristics at Transonic Speeds of a Variable-Wing-Sweep Airplane Configuration With Wing Outboard Panels Swept 113.24° and 75°. NASA TM X-342, 1960.

9. Foster, Gerald V., and Morris, Odell A.: Stability and Control Characteristics at a Mach Number of 1.97 of an Airplane Configuration Having Two Types of Variable-Sweep Wings. NASA TM X-323, 1960.

10. Bielat, Ralph P., Robins, A. Warner, and Alford, William J., Jr.: The Transonic Aerodynamic Characteristics of Two Variable-Sweep Airplane Configurations Capable of Low-Level Supersonic Attack. NASA TM X-304, 1960.

11. Spearman, M. Leroy, and Robinson, Ross B.: Stability and Control Characteristics at a Mach Number of 2.01 of a Variable-Sweep Airplane Configuration Capable of Low-Level Supersonic Attack - Outer Wing Swept 75°. NASA TM X-310, 1960.

12. Robinson, Ross B., and Howard, Paul W.: Stability and Control Characteristics at a Mach Number of 1.41 of a Variable-Sweep Airplane Configuration Capable of Low-Level Supersonic Attack - Outer Wing Swept 75° and 108°. NASA TM X-320, 1960.

13. Robinson, Ross B., and Spearman, M. Leroy: Stability and Control Characteristics at a Mach Number of 2.2 of a Variable-Sweep Airplane Configuration Capable of Low-Level Supersonic Attack - Outer Wing Swept 75°. NASA TM X-330, 1960.

14. Luoma, Arvo A., and Alford, William J., Jr.: Performance, Stability, and Control Characteristics at Transonic Speeds of Three V/STOL Airplane Configurations With Wings of Variable Sweep. NASA TM X-321, 1960.

15. Foster, Gerald V., and Morris, Odell A.: Aerodynamic Characteristics in Pitch at a Mach Number of 1.97 of Two Variable-Wing-Sweep V/STOL Configurations With Outboard Wing Panels Swept Back 75°. NASA TM X-322, 1960.

16. Foster, Gerald V., and Morris, Odell A.: Static Longitudinal and Lateral Aerodynamic Characteristics at a Mach Number of 2.20 of a Variable-Wing-Sweep STOL Configuration. NASA TM X-329, 1960.

17. Morris, Odell A., and Foster, Gerald V.: Static Longitudinal and Lateral Aerodynamic Characteristics at a Mach Number of 2.20 of a V/STOL Airplane Configuration With a Variable-Sweep Wing and With a Skewed Wing Design. NASA TM X-521, 1961.

TABLE I.- GEOMETRIC CHARACTERISTICS OF MODELS

Model IV-A:	
With variable-sweep wing; $\Lambda = 75^{\circ}$:	
Area, S, sq ft	0.858
Span, b, ft	1.309
Mean aerodynamic chord, $\bar{c}$, ft	0.740
Aspect ratio, A	1.997
With skewed wing; $\zeta = 0^{\circ}$:	
Area, S, sq ft	0.586
Span, b, ft	1.562
Mean aerodynamic chord, $\bar{c}$, ft	0.431
Aspect ratio, A	4.163
Duct:	
Projected inlet area, A_p, sq ft	0.05210
Exit area:	
Forward, $A_{e,1}$, sq ft	0.01843
Rearward, $A_{e,2}$, sq ft	0.02749
Bypass, $A_{e,3}$, sq ft	0
Total, sq ft	0.04592
Exit angles:	
Forward:	
θ_1, deg	30
θ_2, deg	30
Rearward:	
θ_1, deg	30
θ_2, deg	45
Body base area, sq ft	0.01670
Model IV-B:	
With variable-sweep wing; $\Lambda = 75^{\circ}$:	
Area, S, sq ft	0.858
Span, b, ft	1.309
Mean aerodynamic chord, $\bar{c}$, ft	0.740
Aspect ratio, A	1.997
With skewed wing; $\zeta = 0^{\circ}$:	
Area, S, sq ft	0.586
Span, b, ft	1.562
Mean aerodynamic chord, $\bar{c}$, ft	0.431
Aspect ratio, A	4.163
Duct:	
Projected inlet area, A_p, sq ft	0.05007
Exit area:	
Forward, $A_{e,1}$, sq ft	0.01757
Rearward, $A_{e,2}$, sq ft	0.02576
Bypass, $A_{e,3}$, sq ft	0.01604
Total, sq ft	0.05937
Exit angles:	
Forward:	
θ_1, deg	0
θ_2, deg	30
Rearward:	
θ_1, deg	0
θ_2, deg	45
Body base area, sq ft	0.01670

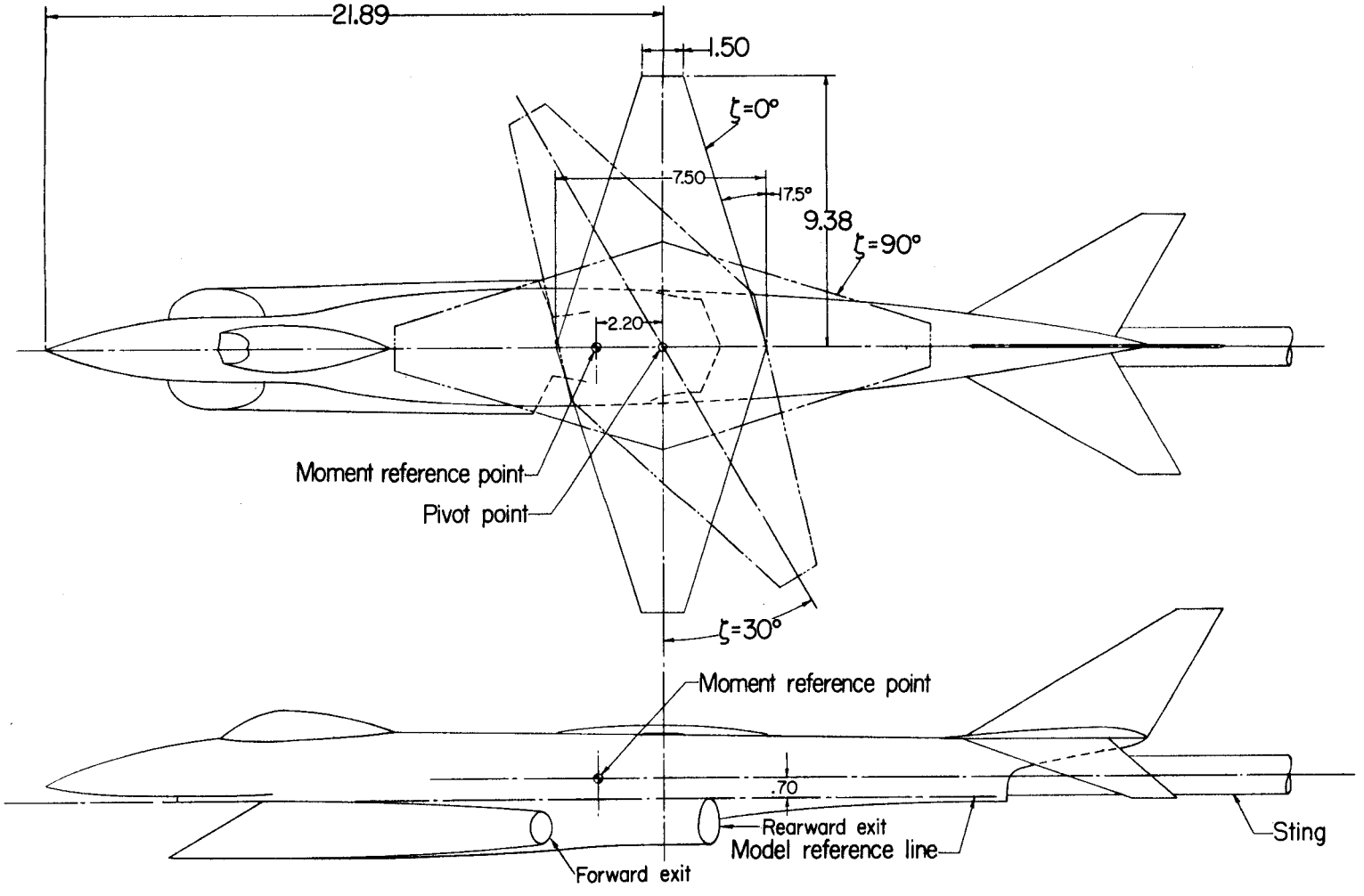

Figure 1.- Drawing of model IV-A with skewed wing. Configuration BWVH. All dimensions are in inches unless otherwise noted.

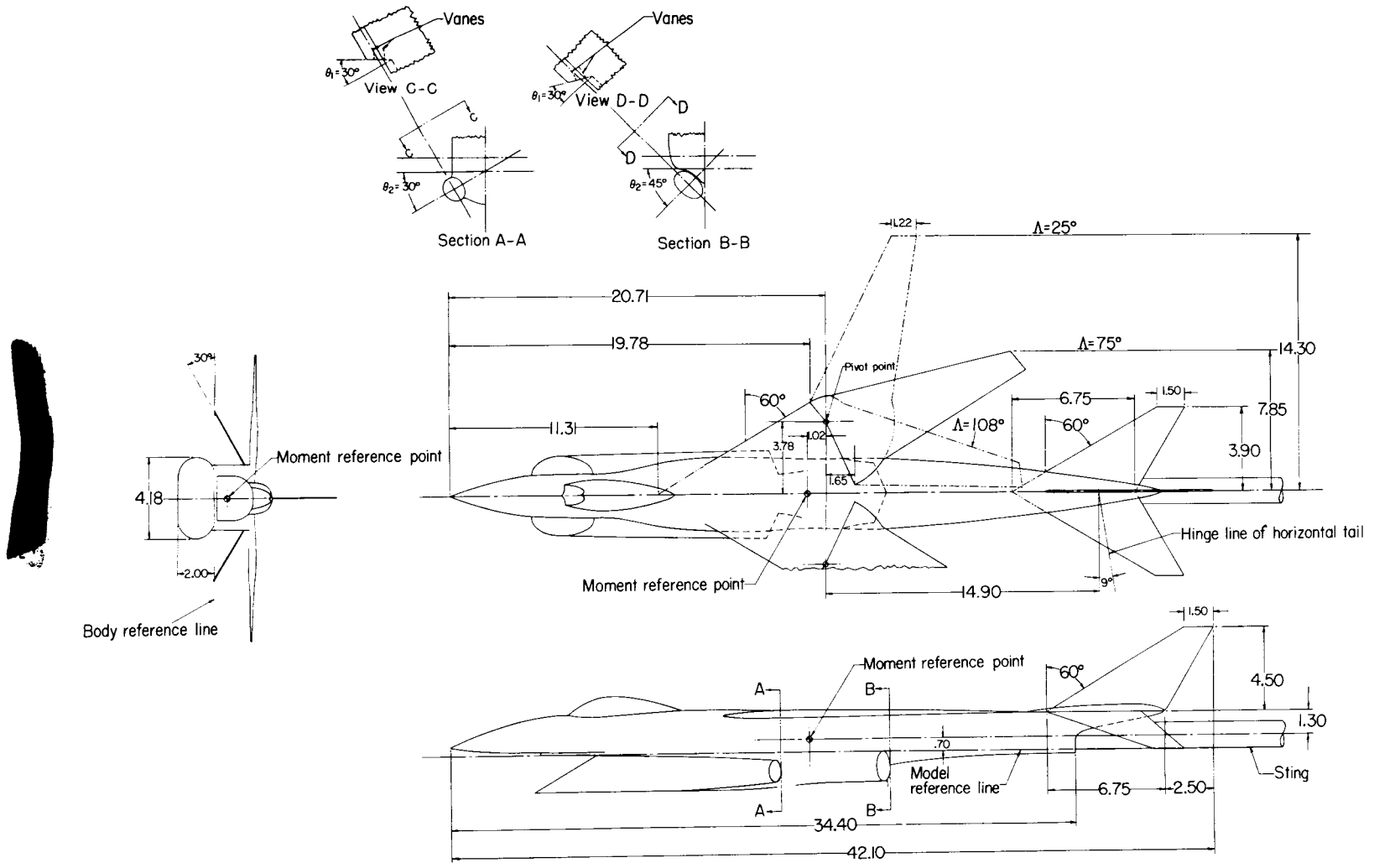

Figure 2.- Drawing of model IV-A with variable-sweep wing. Configuration BWVH. All dimensions are in inches unless otherwise noted.

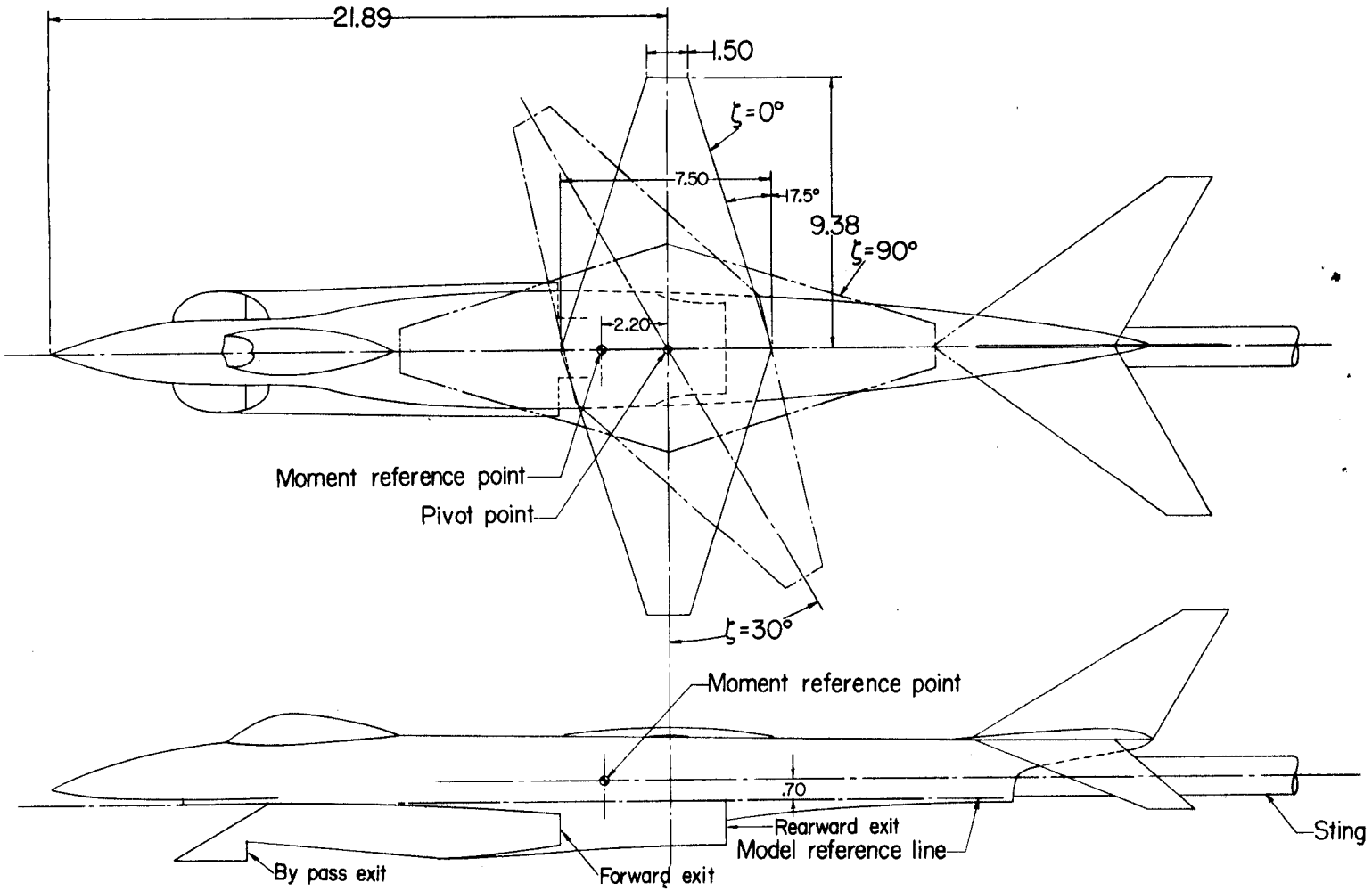

Figure 3.- Drawing of model IV-B with skewed wing. Configuration BWVH. All dimensions are in inches unless otherwise noted.

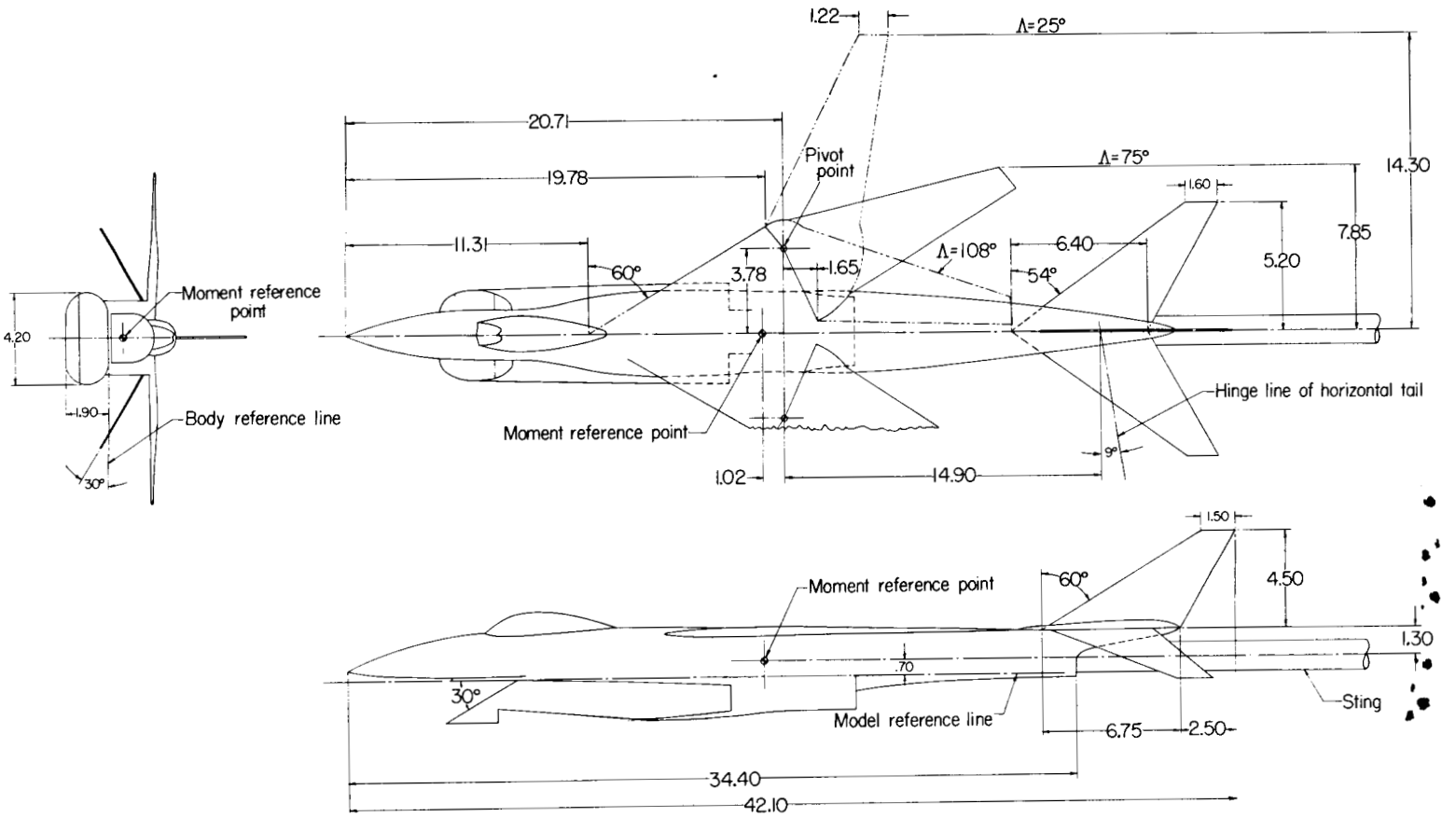

Figure 4.- Drawing of model IV-B with variable-sweep wing. Configuration BWVH. All dimensions are in inches unless otherwise noted.

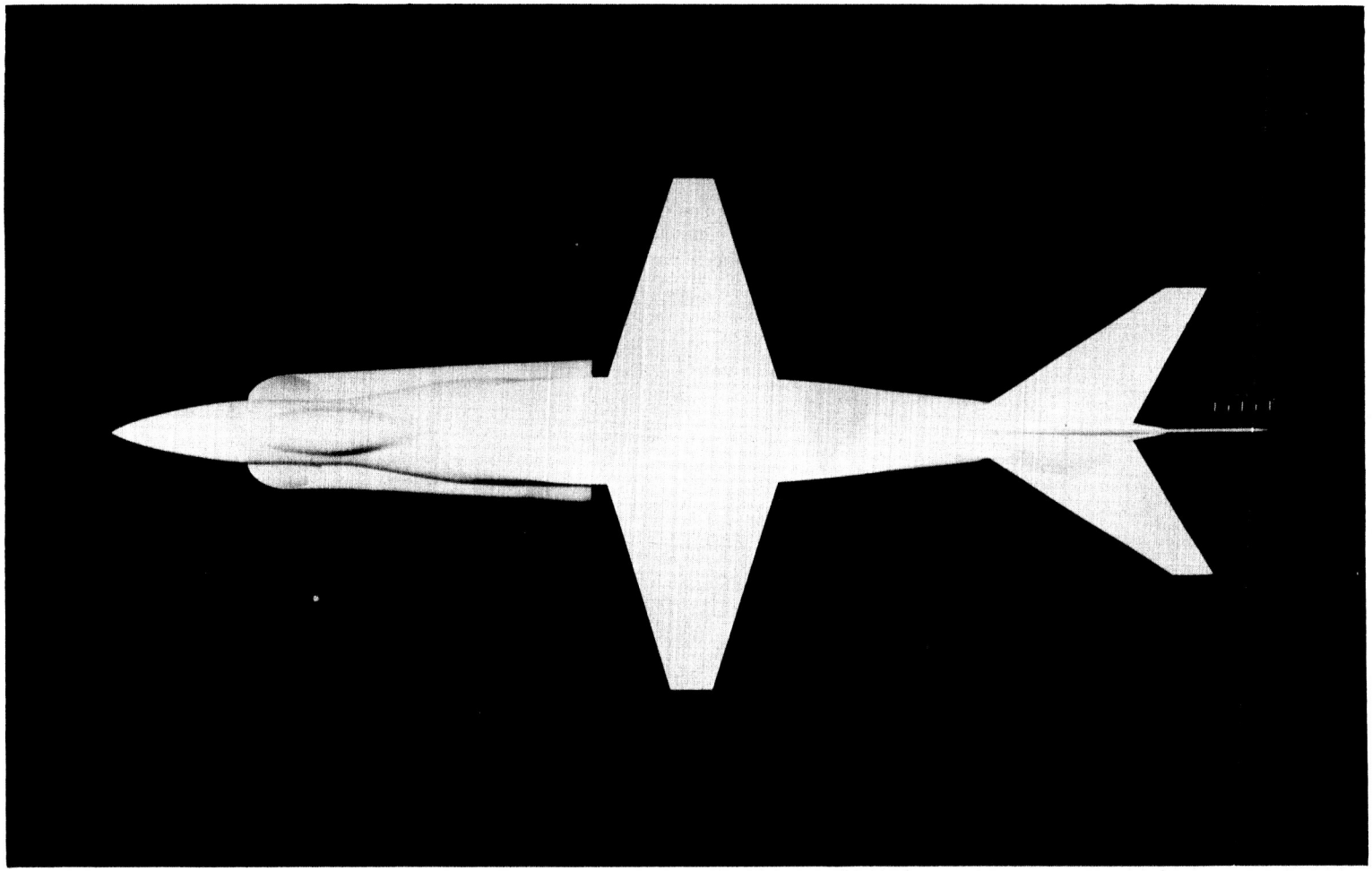

(a) Plan view; $\zeta = 0^{\circ}$. L-60-6217

Figure 5.- Photographs of model IV-B with skewed wing. Configuration BWVH; $\delta_h = -4.15^{\circ}$.

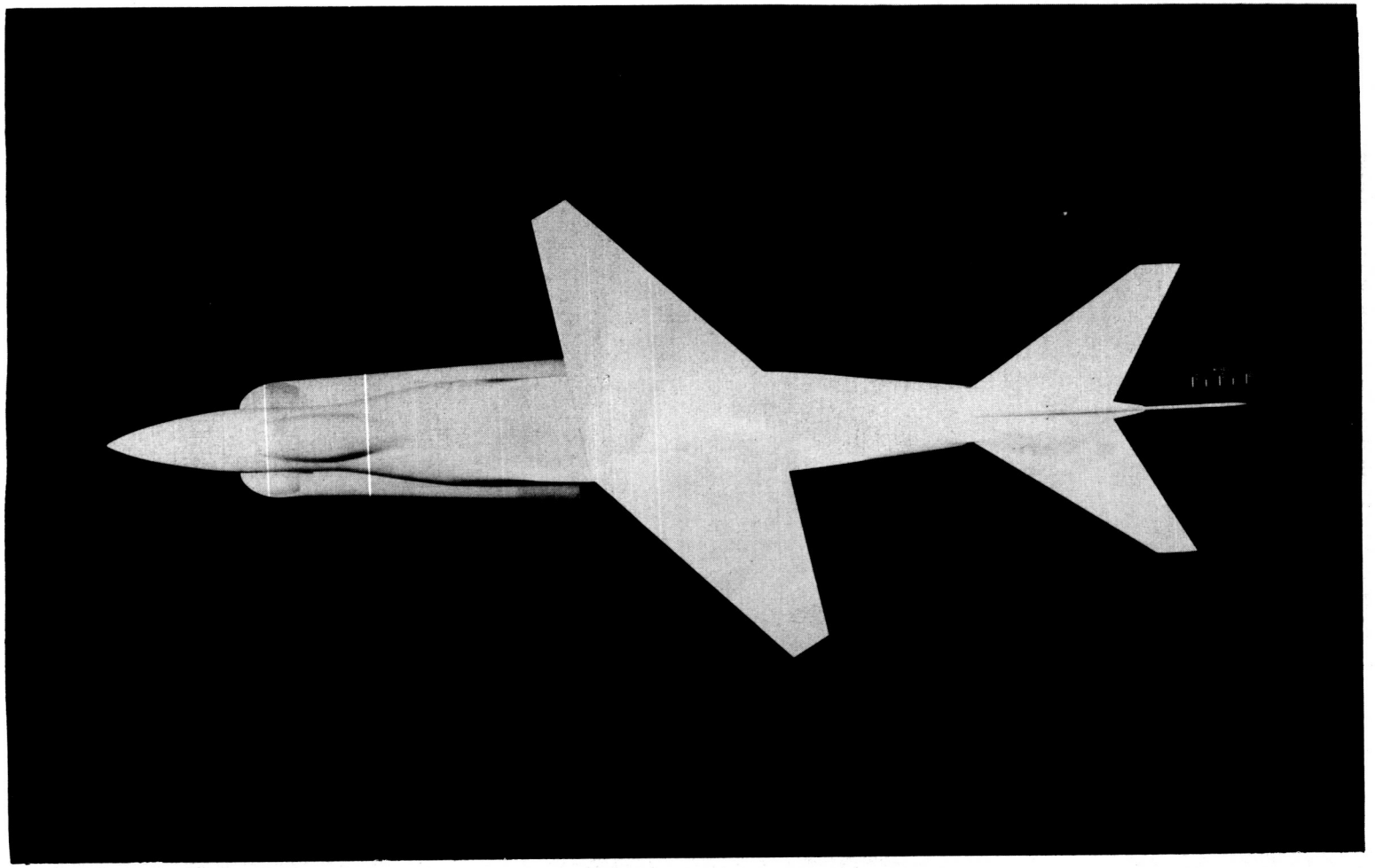

(b) Plan view; $\zeta = 30^{\circ}$. L-60-6218

Figure 5.- Continued.

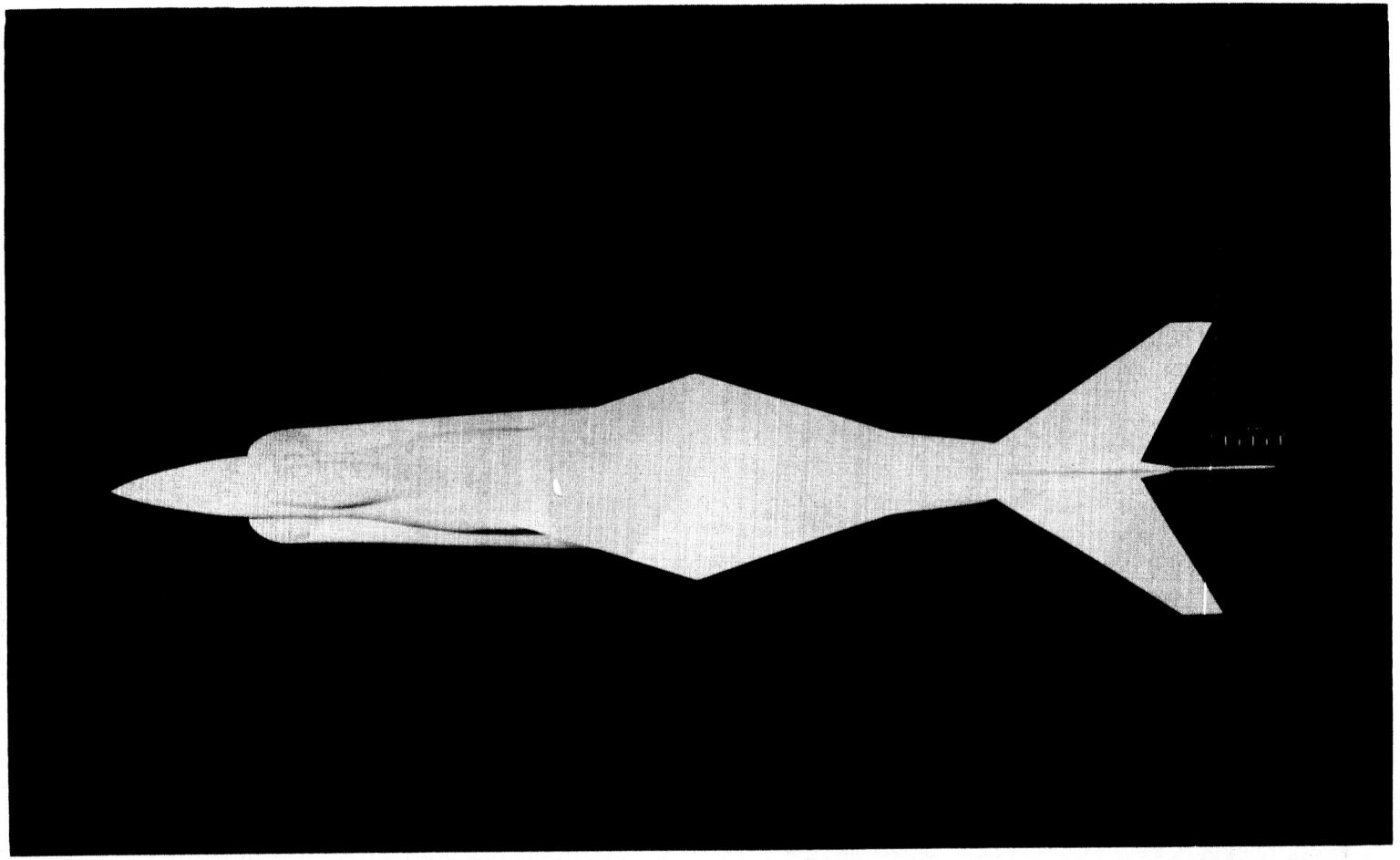

(c) Plan view; $\zeta = 90^{\circ}$. L-60-6219

Figure 5.- Concluded.

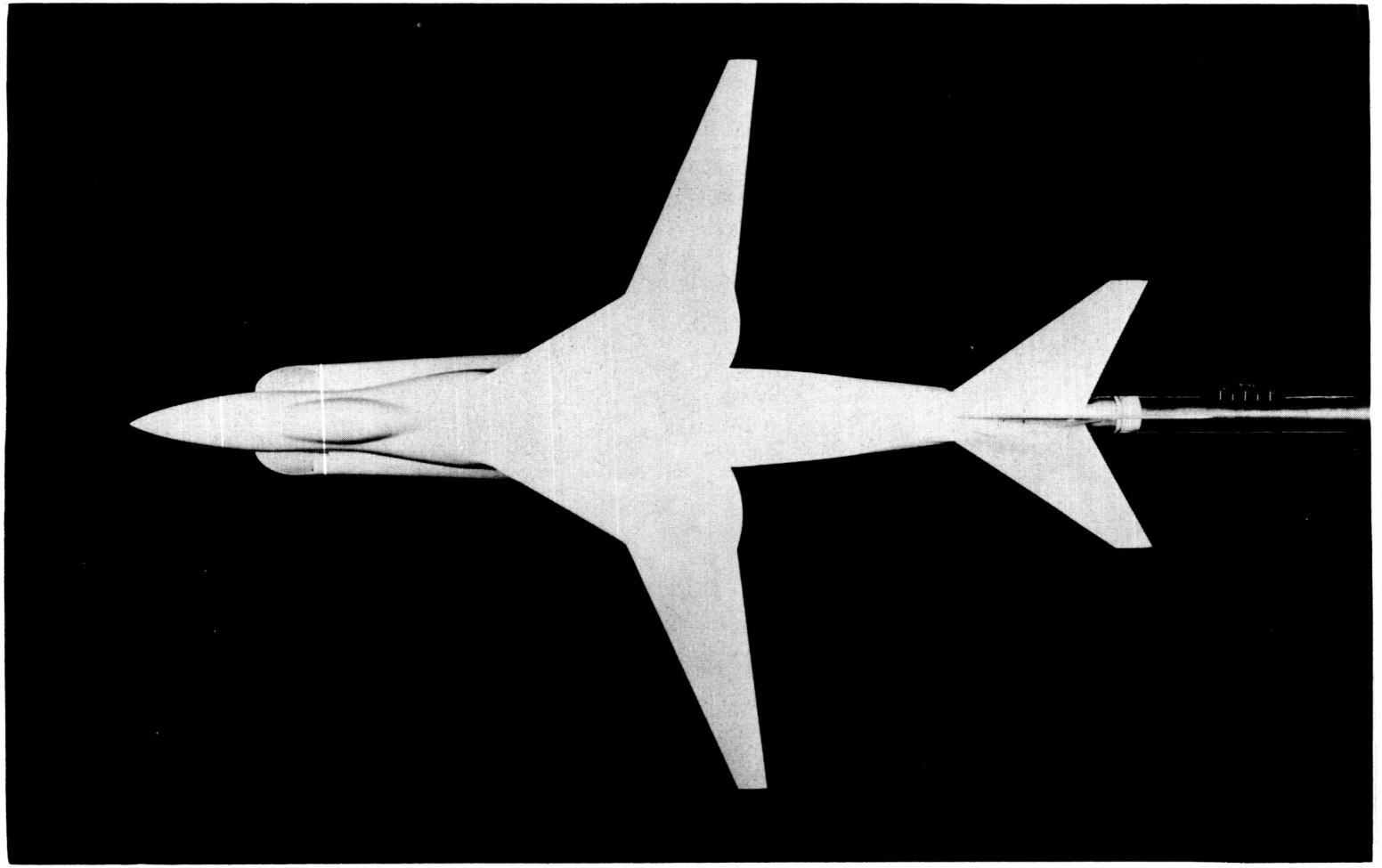

(a) Plan view; $\Lambda = 25^{\circ}$. L-60-6213

Figure 6.- Photographs of model IV-B with variable-sweep wing. Configuration BWVH; $\delta_h = -4.15^{\circ}$.

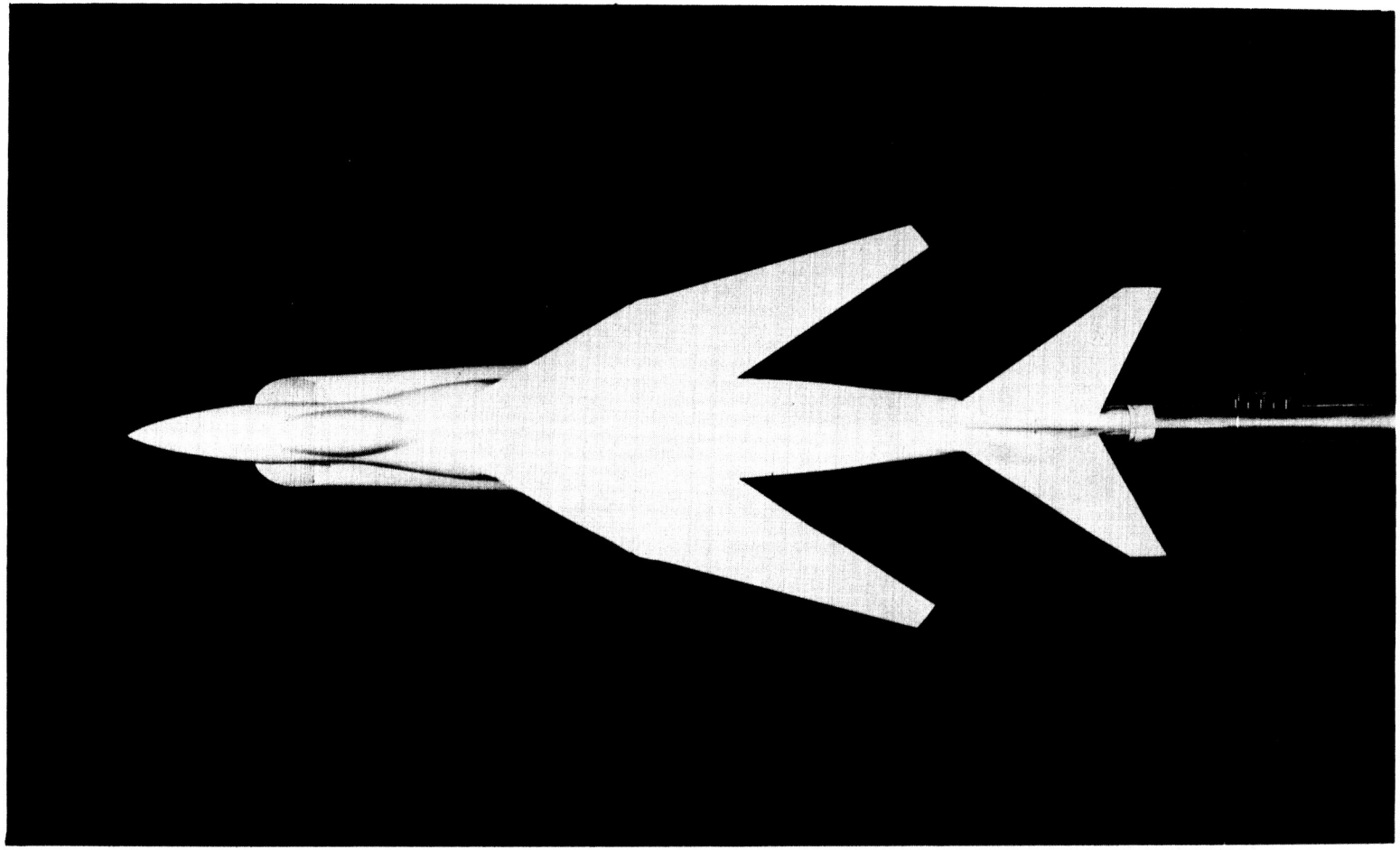

(b) Plan view; $\Lambda = 75^{\circ}$. L-60-6214

Figure 6.- Continued.

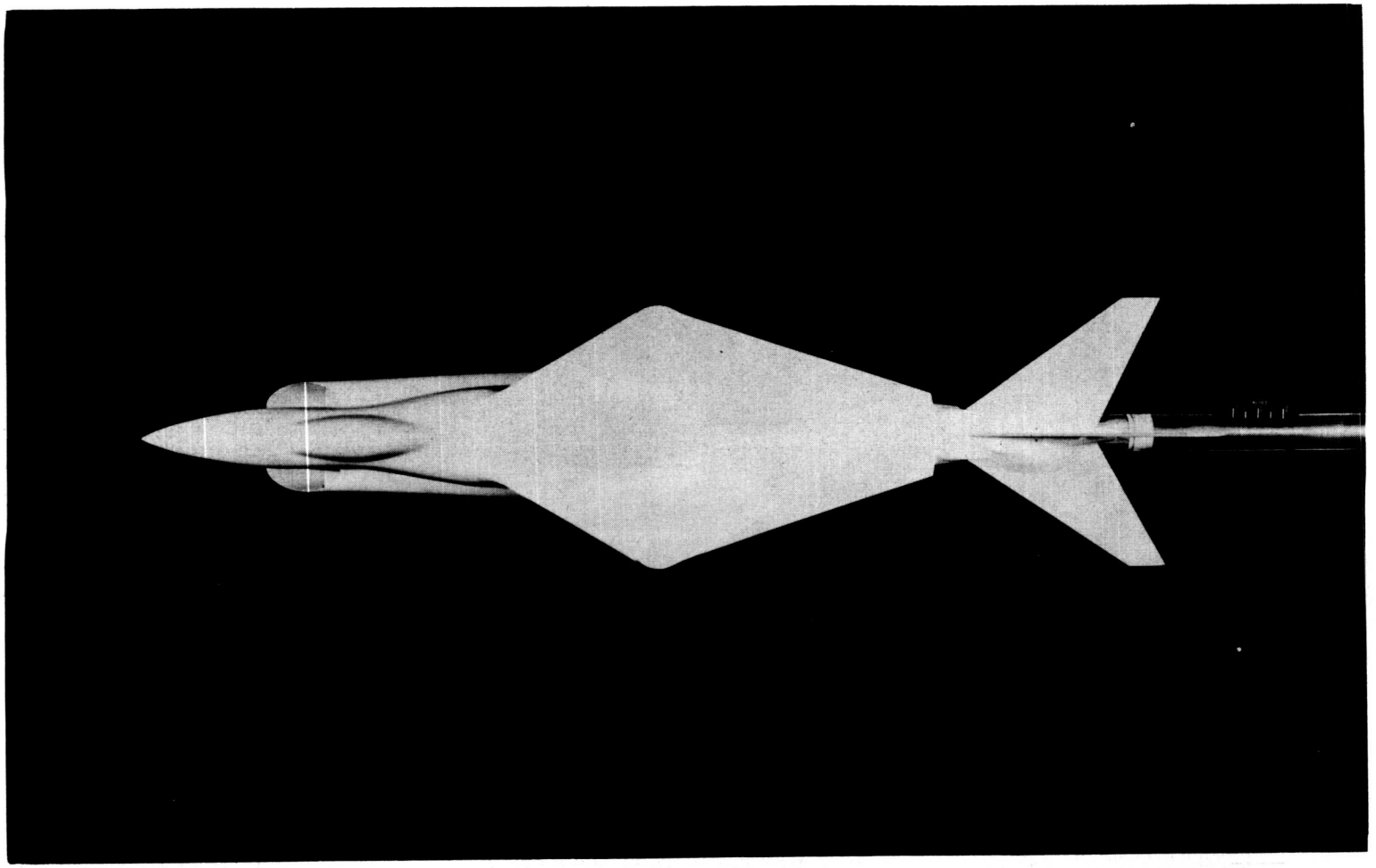

(c) Plan view; $\Lambda = 108^{\circ}$. L-60-6215

Figure 6.- Continued.

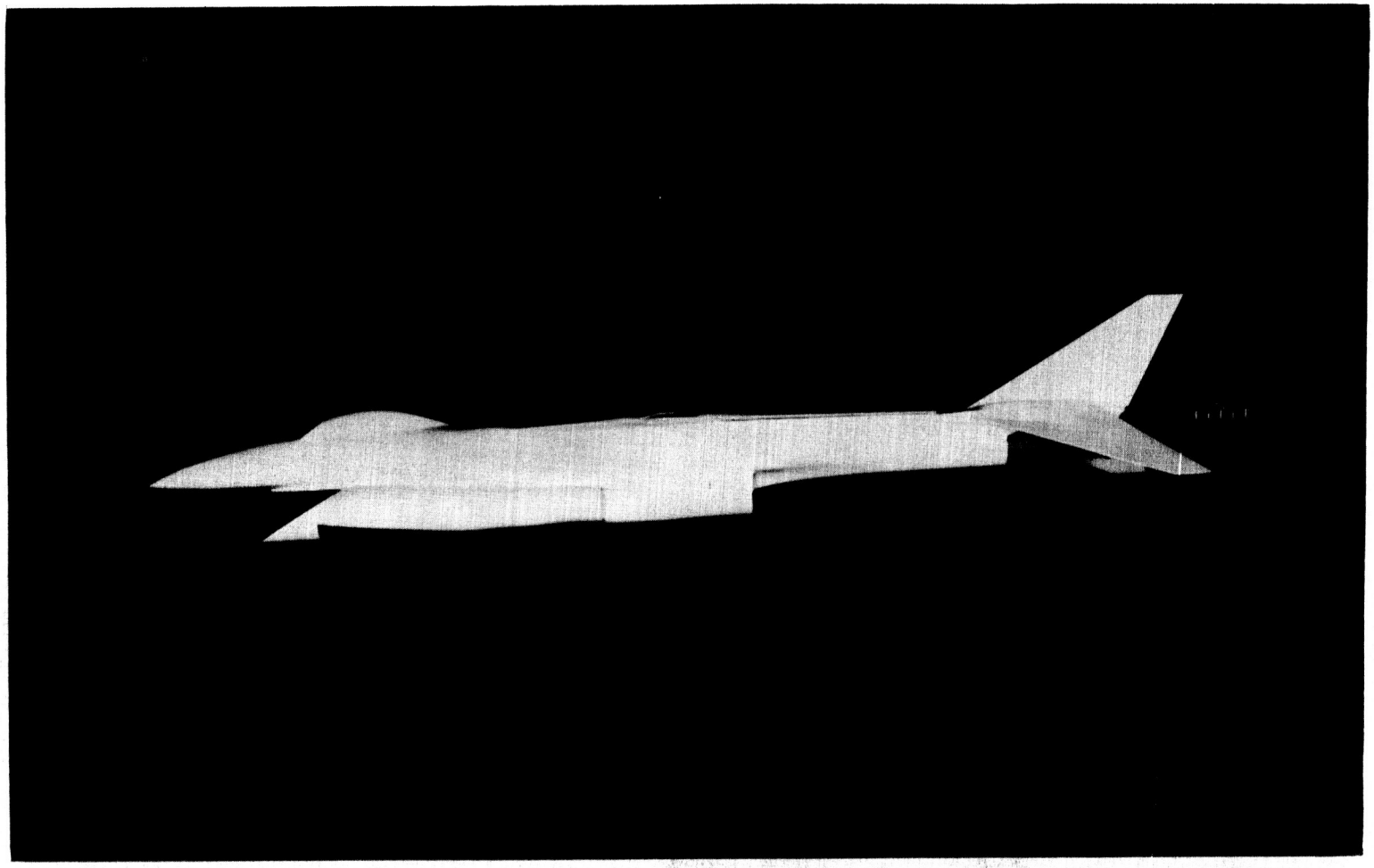

(d) Side view; $\Lambda = 108^{\circ}$. L-60-6212

Figure 6.- Continued.

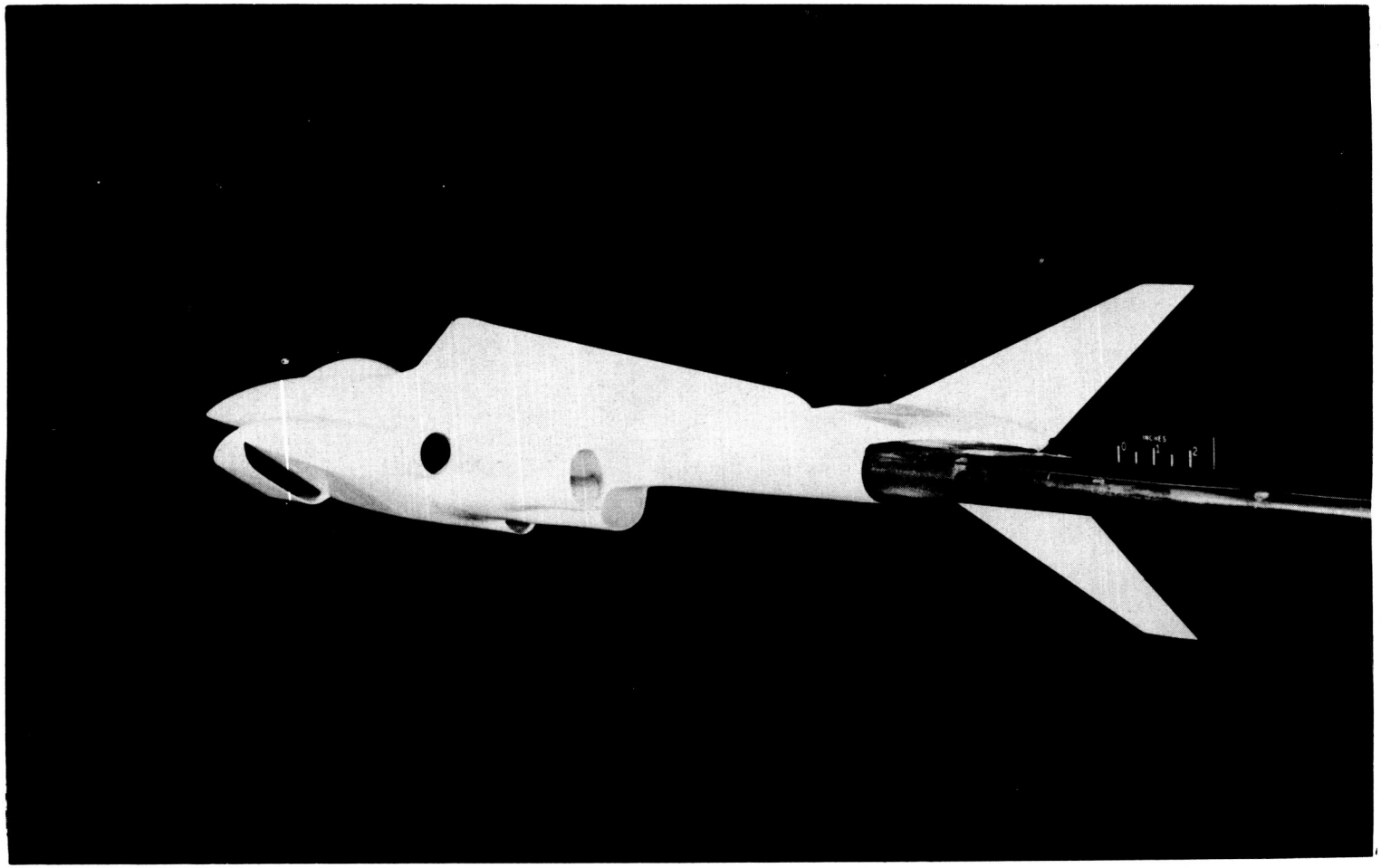

(e) Three-quarter rear view. $\Lambda = 108^{\circ}$. L-60-6216

Figure 6.- Concluded.

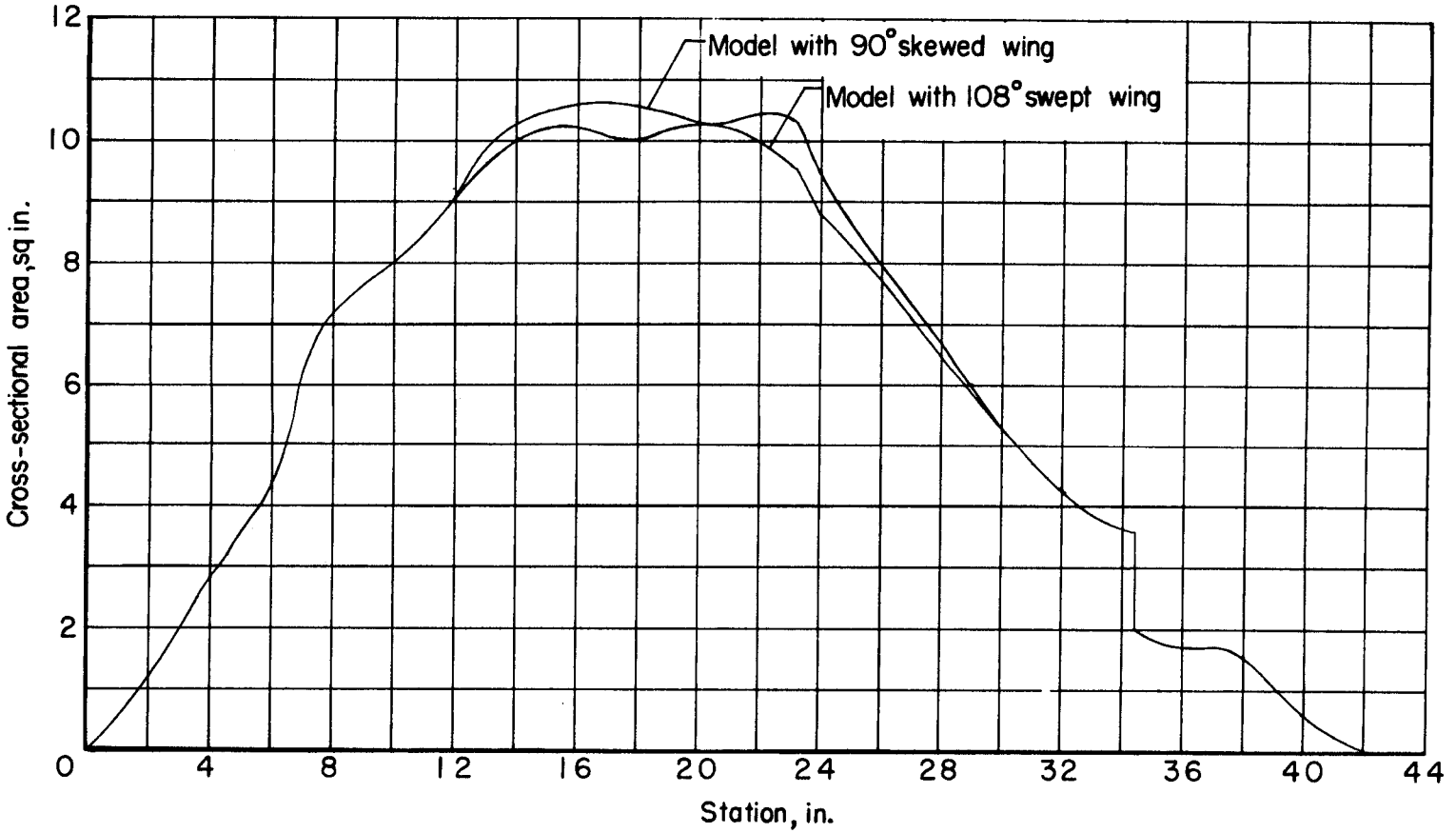

Figure 7.- Longitudinal distribution of normal cross-sectional area of model IV-A with skewed and variable-sweep wings. Configuration BWVH.

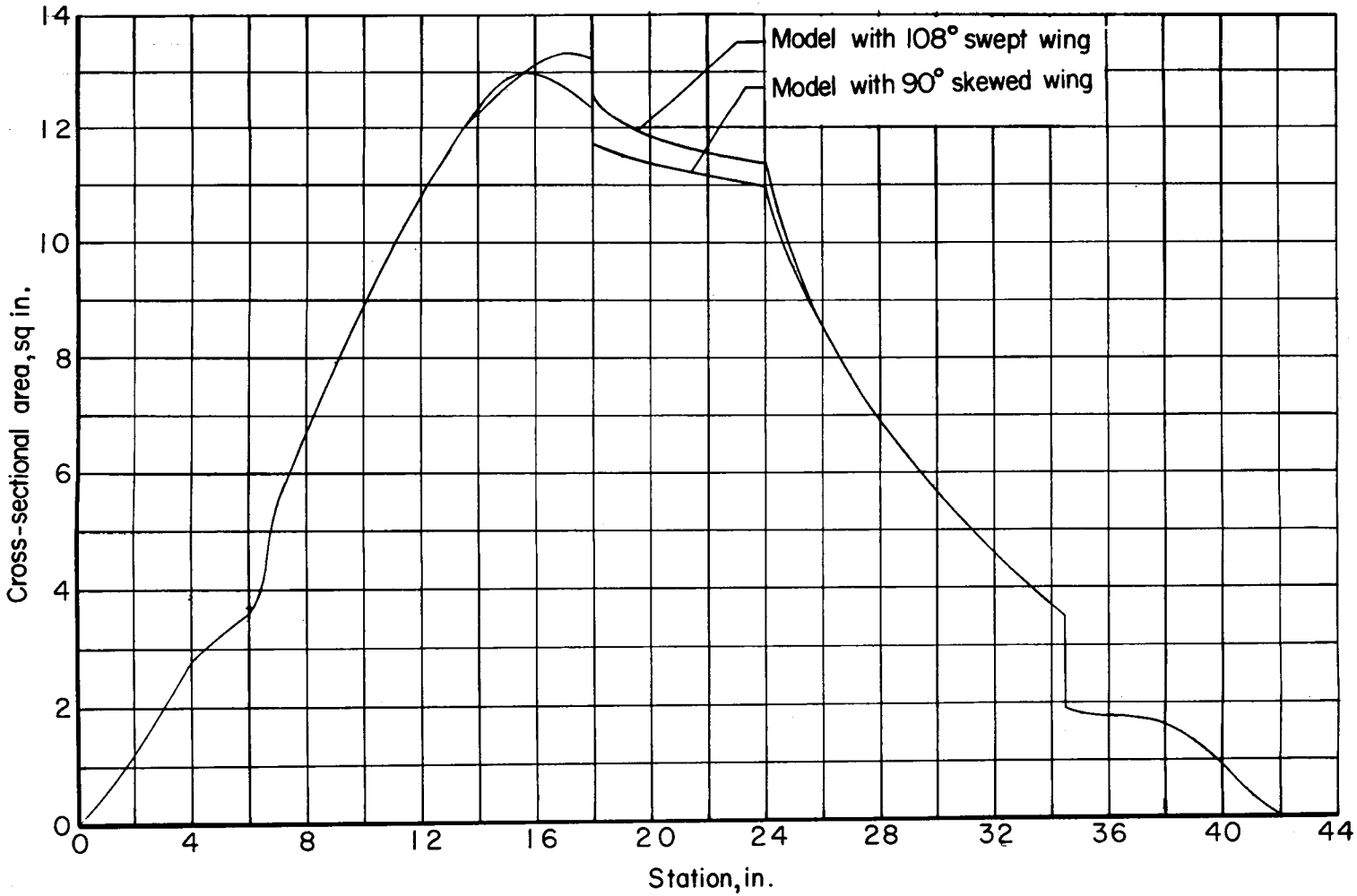

Figure 8.- Longitudinal distribution of normal cross-sectional area of model IV-B with skewed and variable-sweep wings. Configuration BWVH.

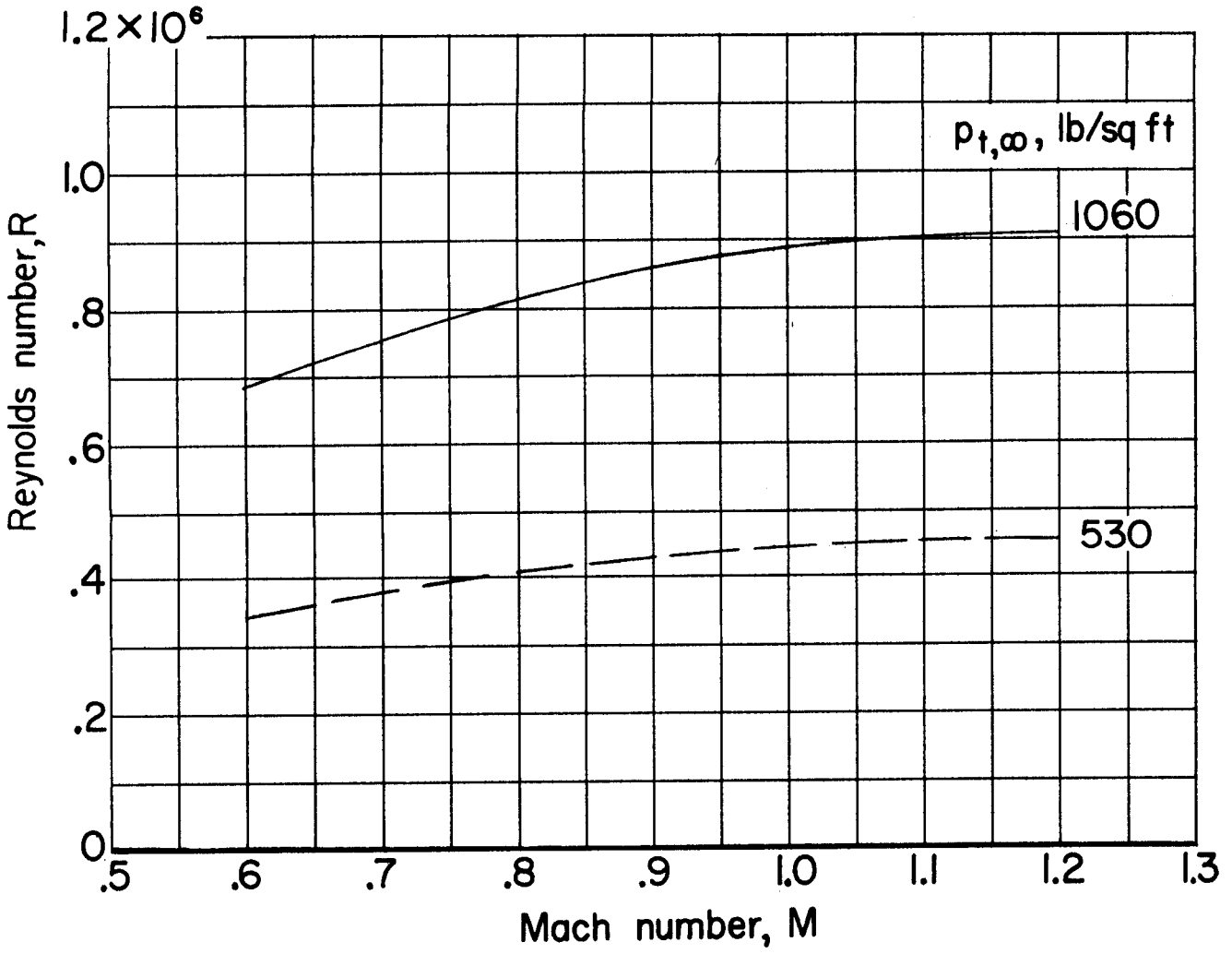

Figure 9.- Variations of Reynolds number (based on mean aerodynamic chord of skewed wing of 0.431 ft) with Mach number.

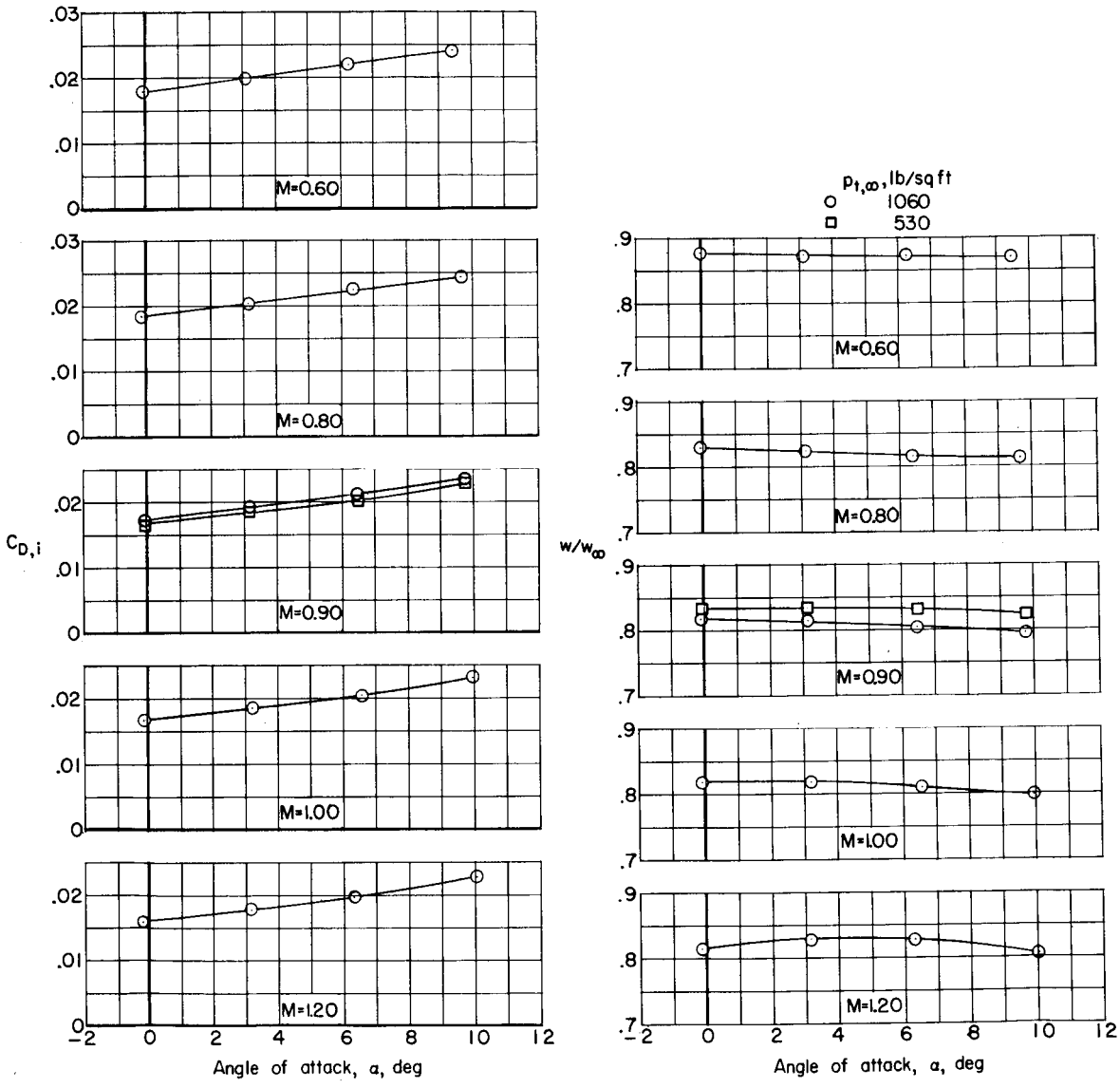

(a) Variation of $C_{D,i}$ and w/w_∞ with α.

Figure 10.- Internal-drag coefficient and mass-flow ratio of model IV-A with 108° swept wing. Configuration BWVH; $\delta_h = 0°$.

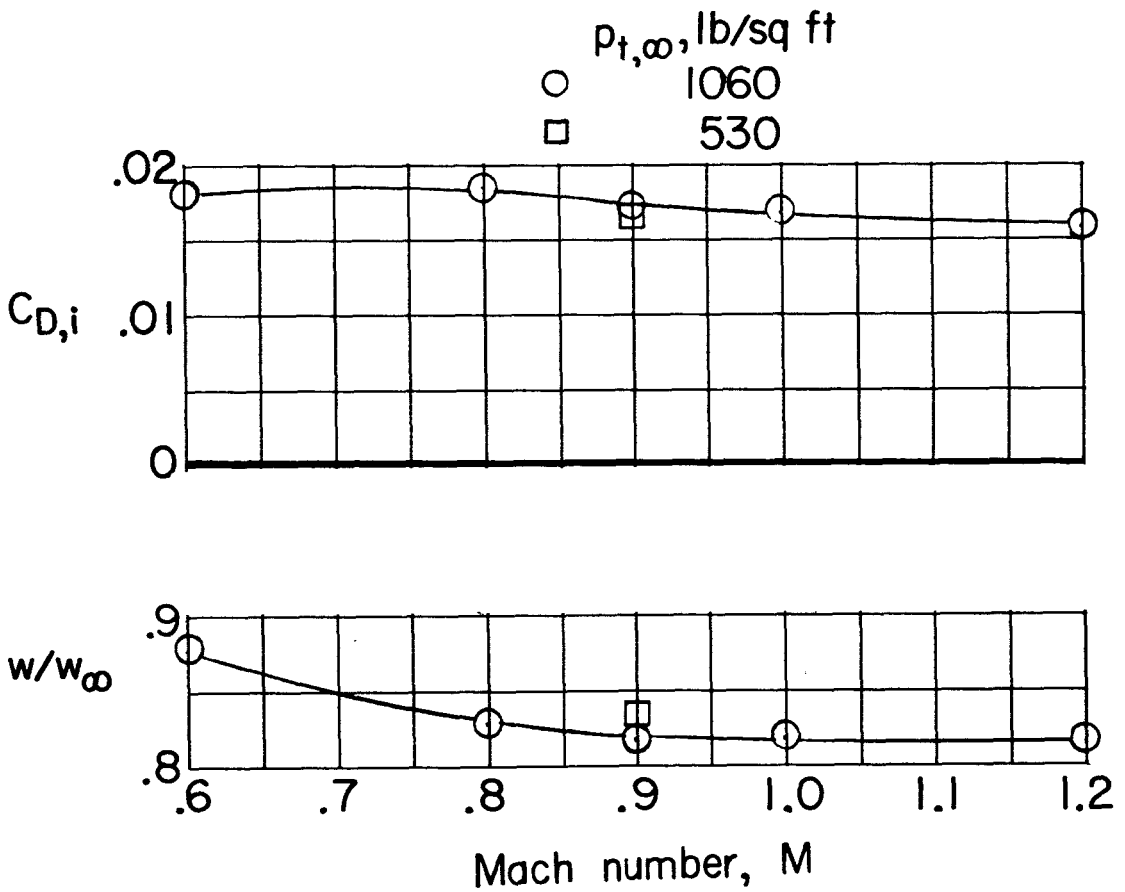

(b) Variation of $C_{D,i}$ and w/w_∞ with M; $\alpha = 0^\circ$.

Figure 10.- Concluded.

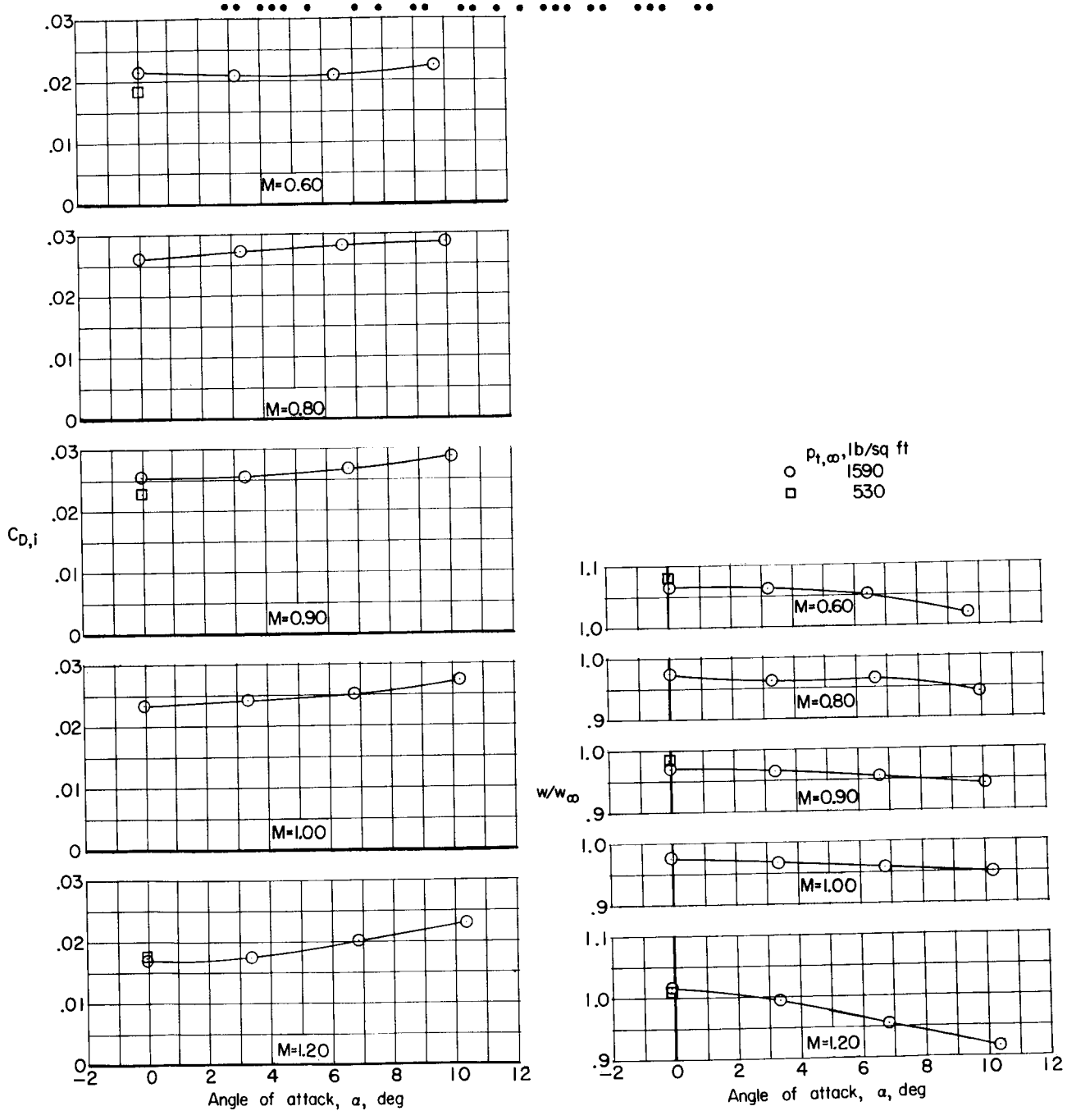

(a) Variation of $C_{D,i}$ and w/w_∞ with α.

Figure 11.- Internal-drag coefficient and mass-flow ratio of model IV-B with 90° skewed wing. Configuration BWV.

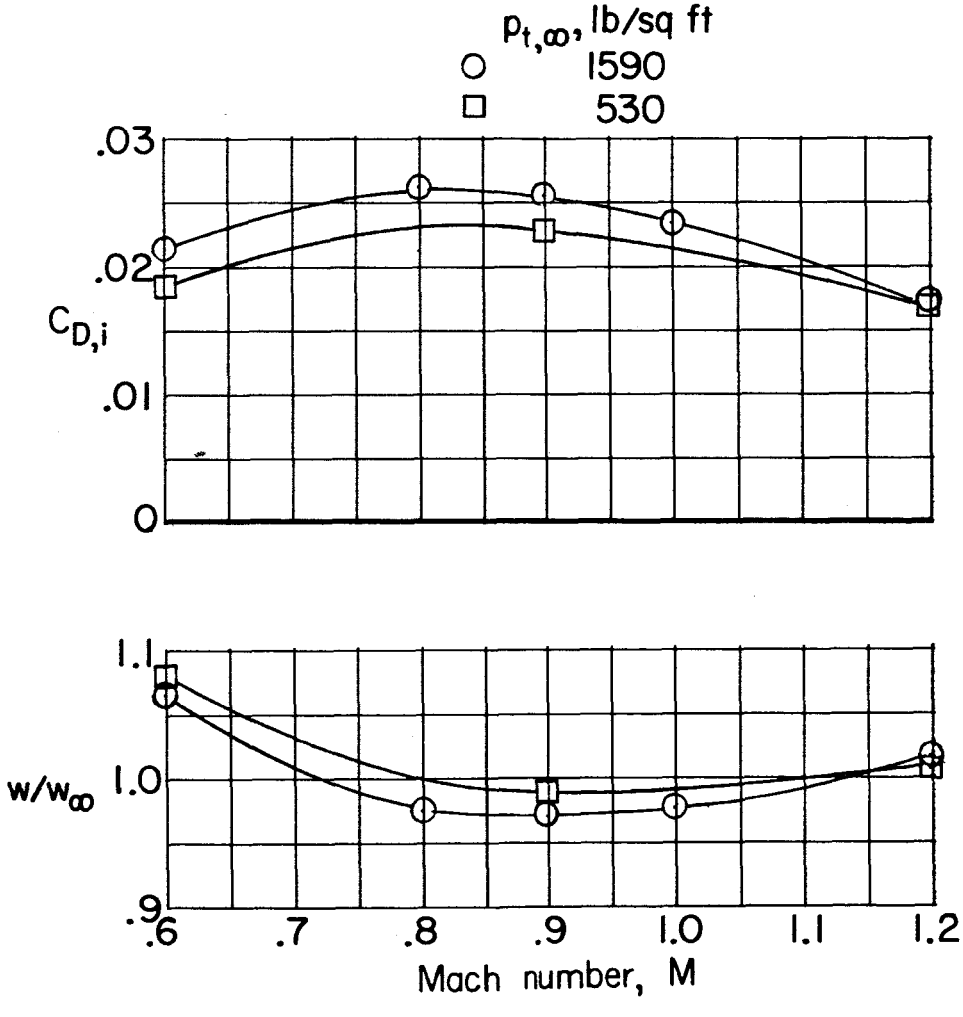

(b) Variation of $C_{D,i}$ and w/w_∞ with M; $\alpha = 0^\circ$.

Figure 11.- Concluded.

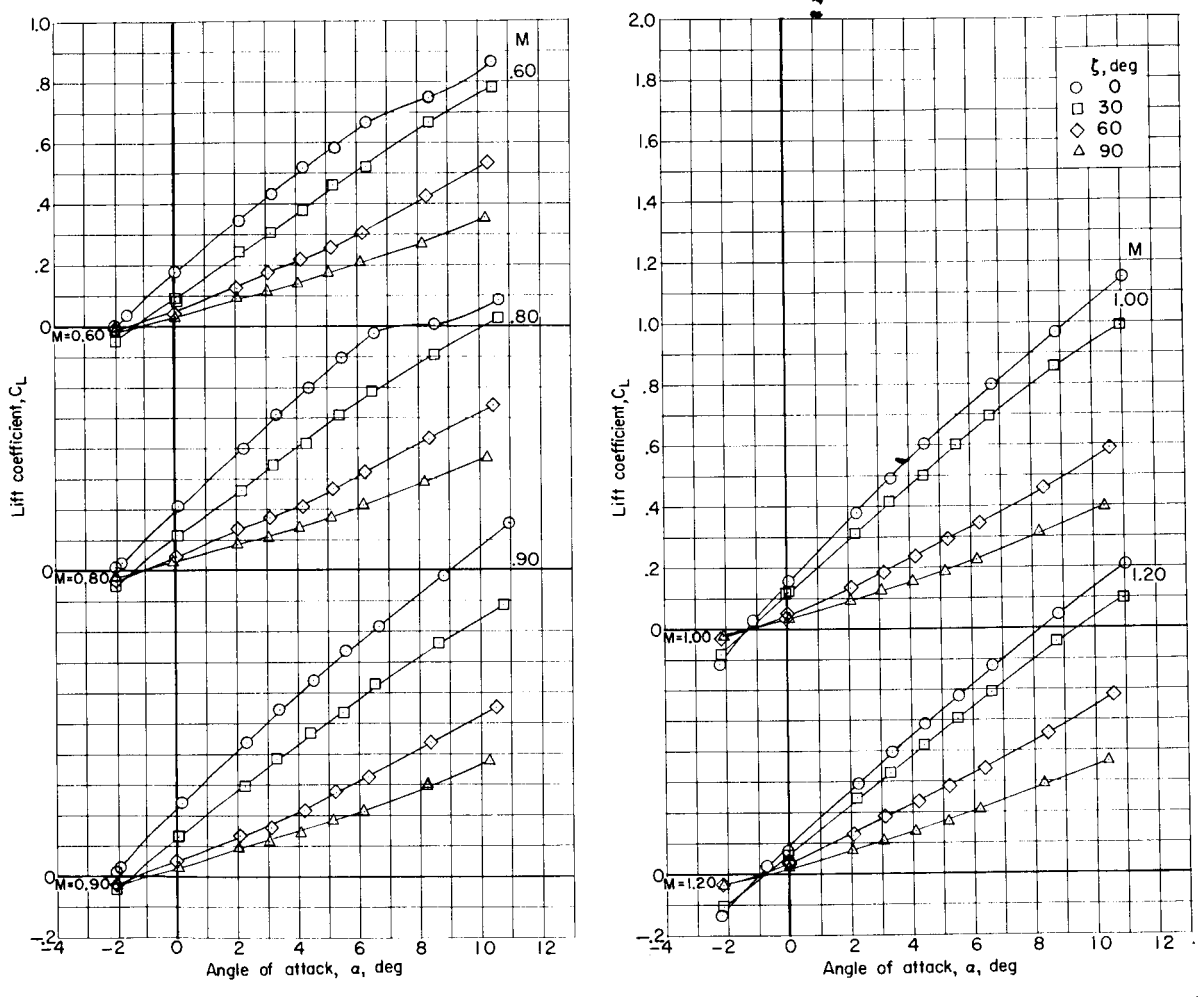

(a) Variation of C_L with α.

Figure 12.- Effect of wing skew angle on longitudinal aerodynamic characteristics of model IV-A. Configuration BWVH; $\delta_h = 0^o$; $p_{t,\infty} = 530$ lb/sq ft.

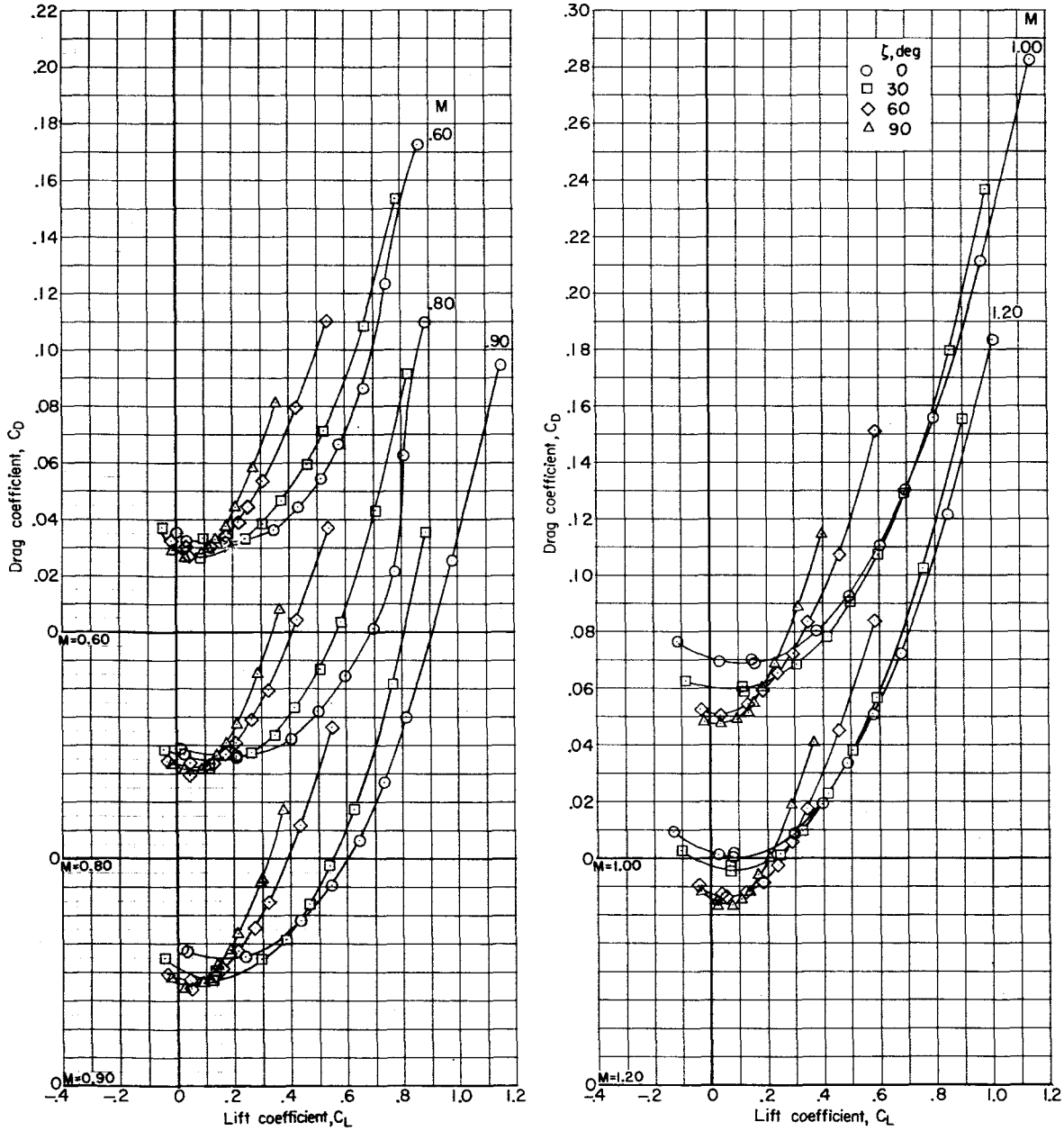

(b) Variation of C_D with C_L.

Figure 12.- Continued.

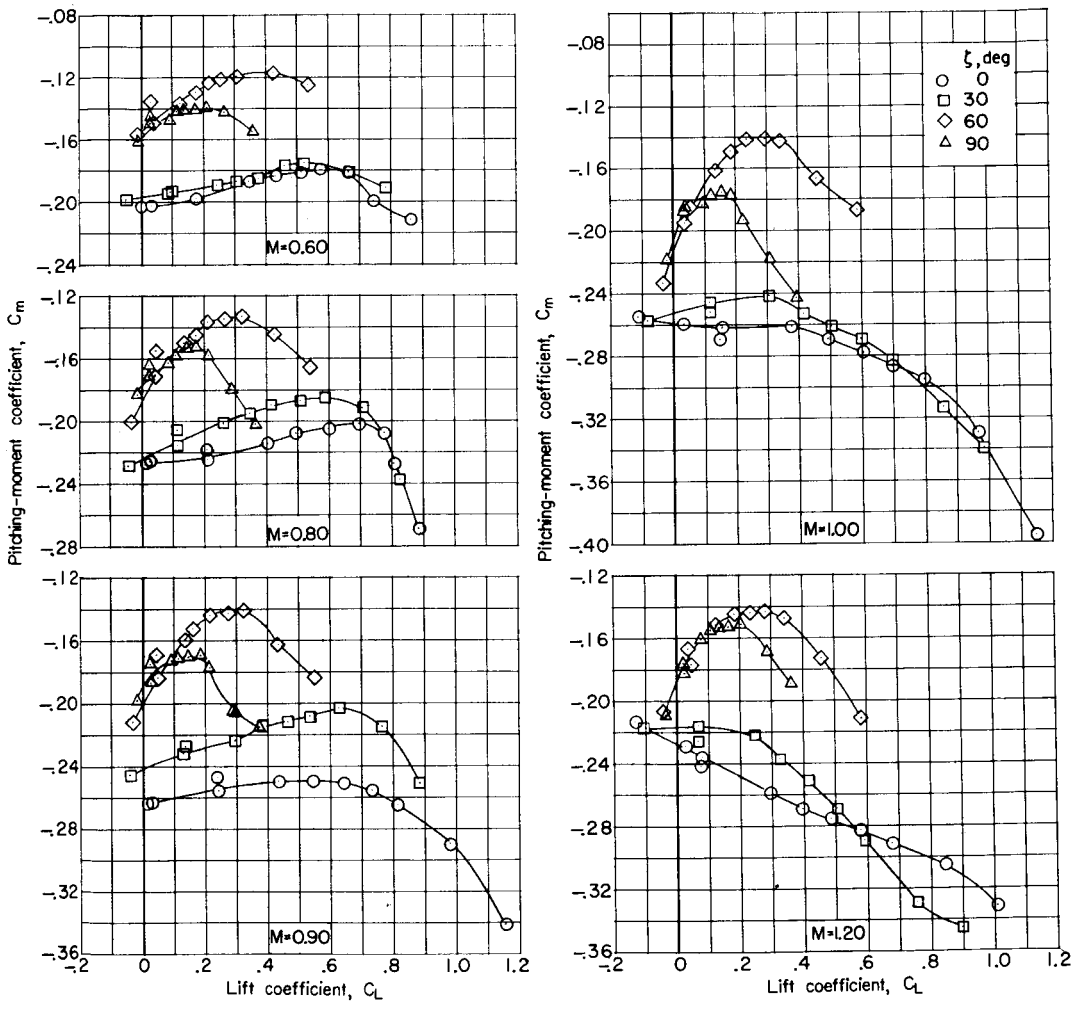

(c) Variation of C_m with C_L.

Figure 12.- Continued.

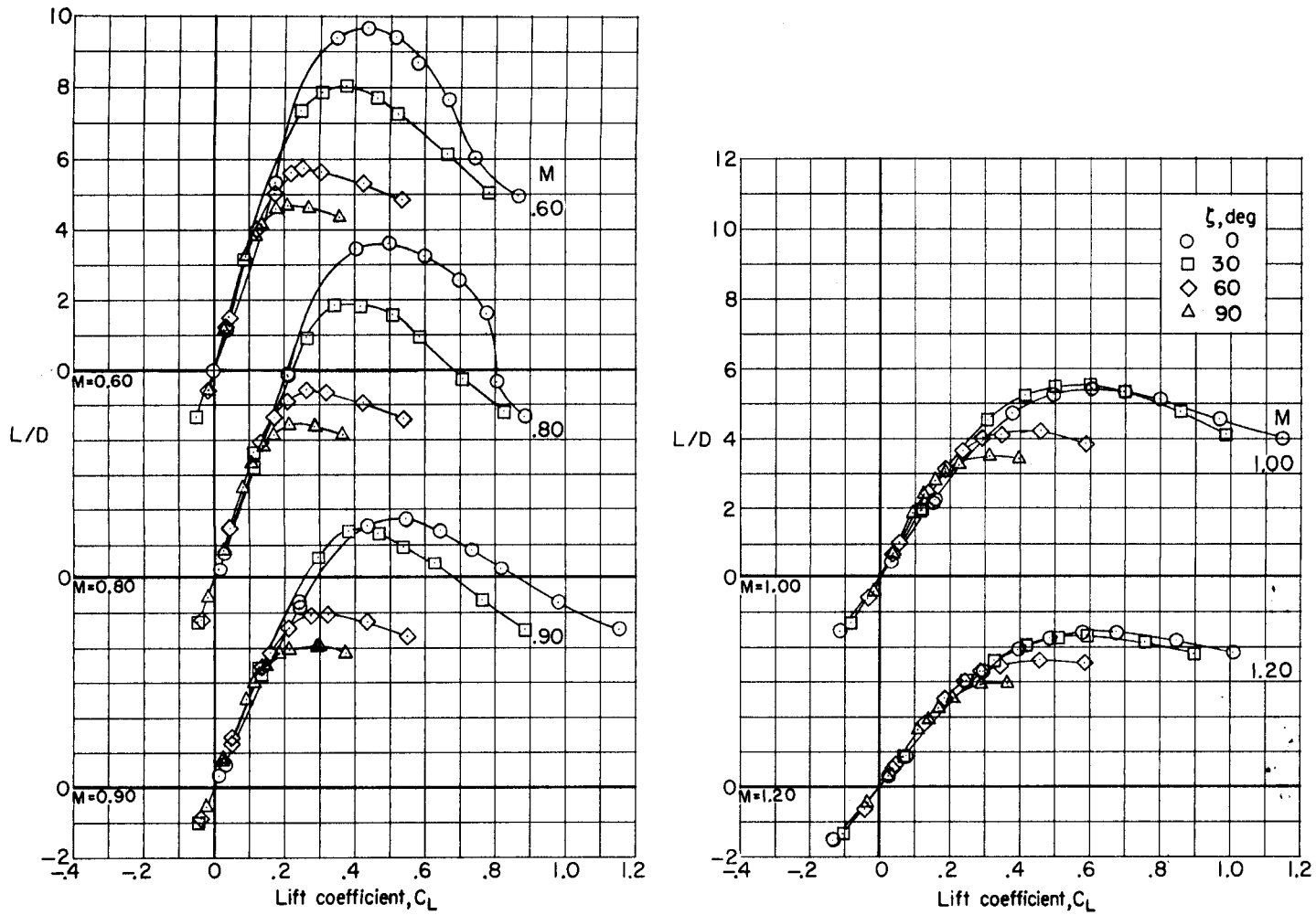

(d) Variation of L/D with C_L.

Figure 12.- Continued.

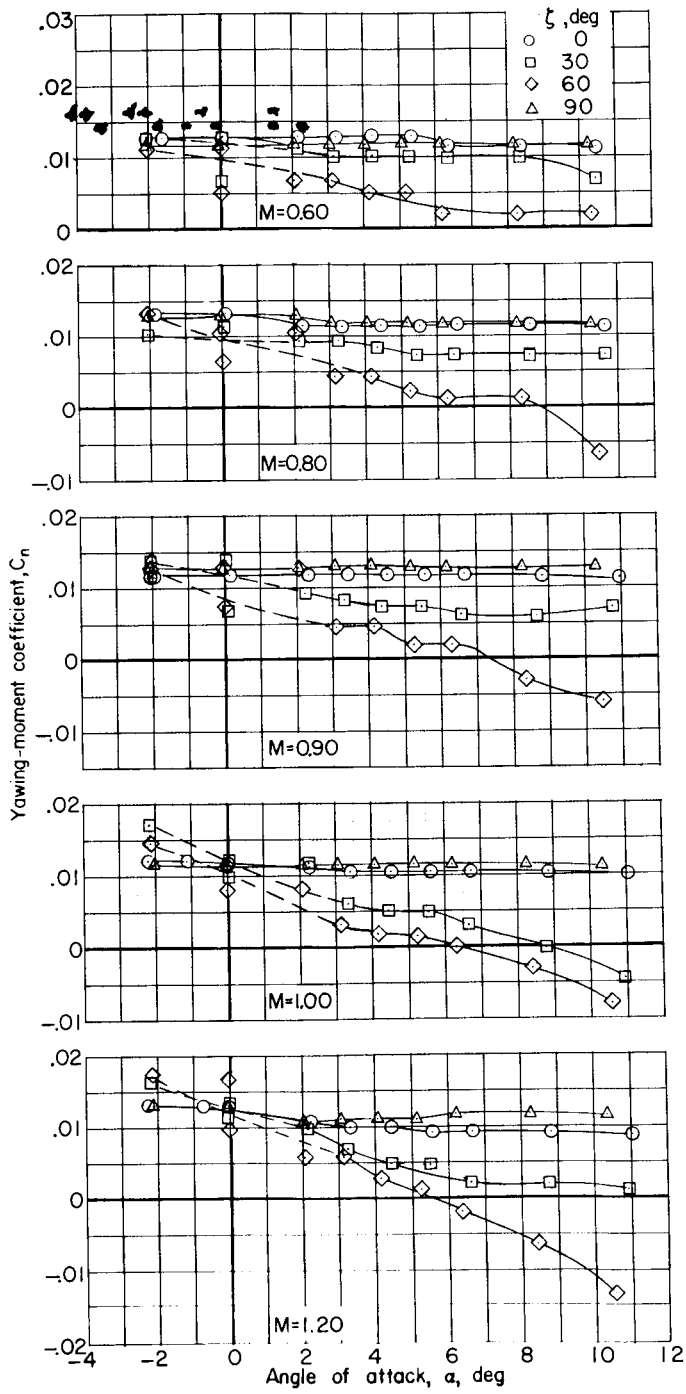

(e) Variation of C_n with α.

Figure 12.- Continued.

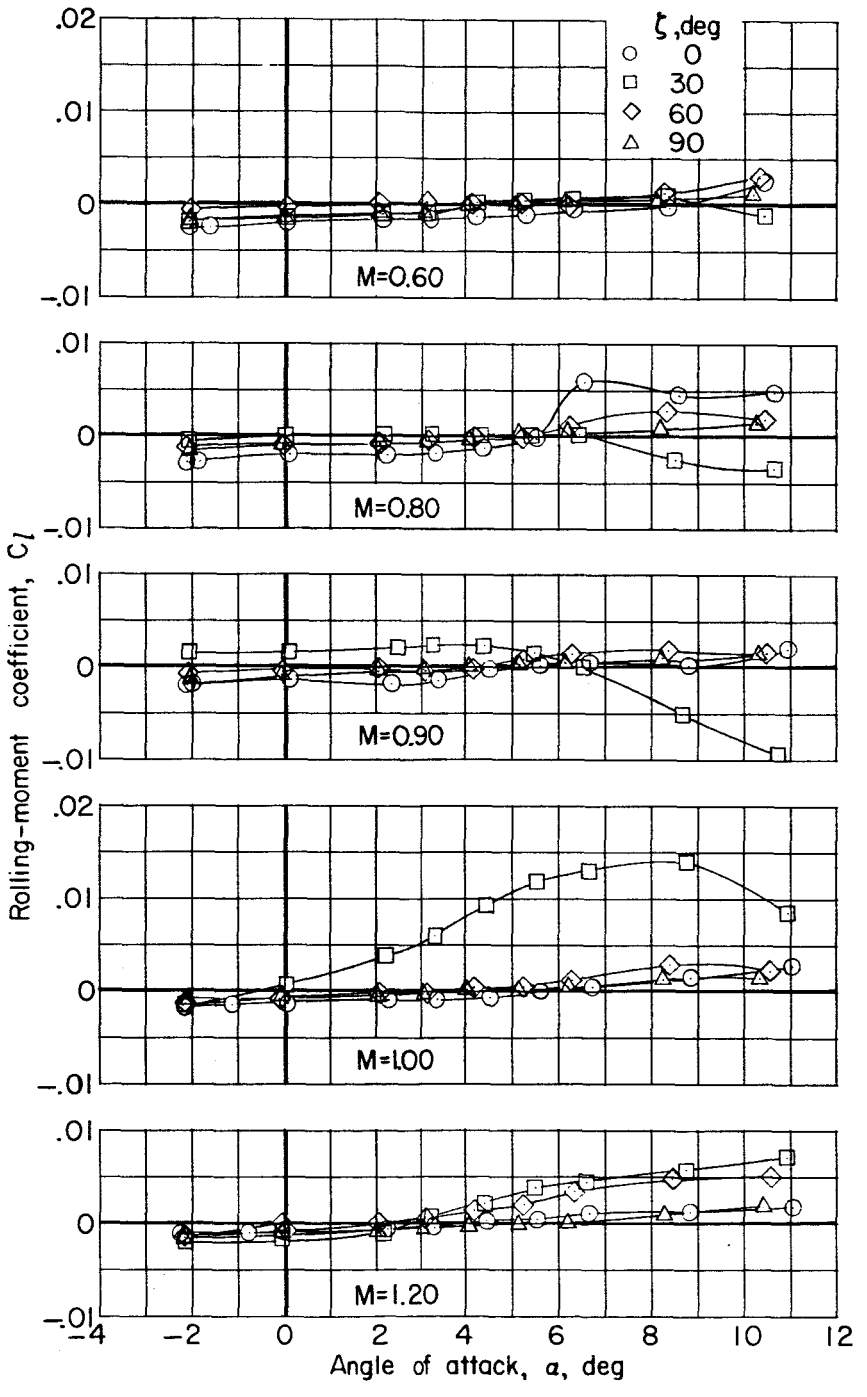

(f) Variation of C_l with α.

Figure 12.- Continued.

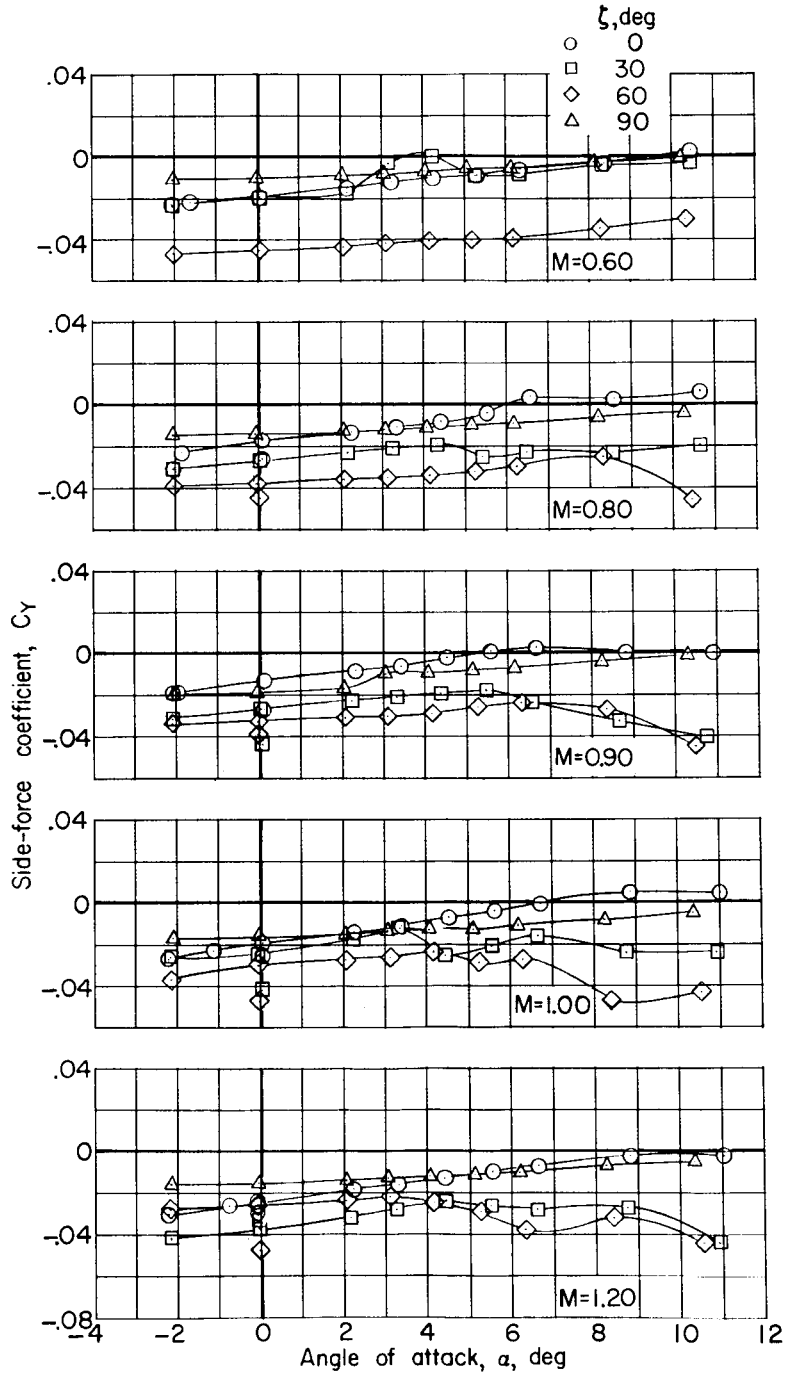

(g) Variation of C_Y with α.

Figure 12.- Concluded.

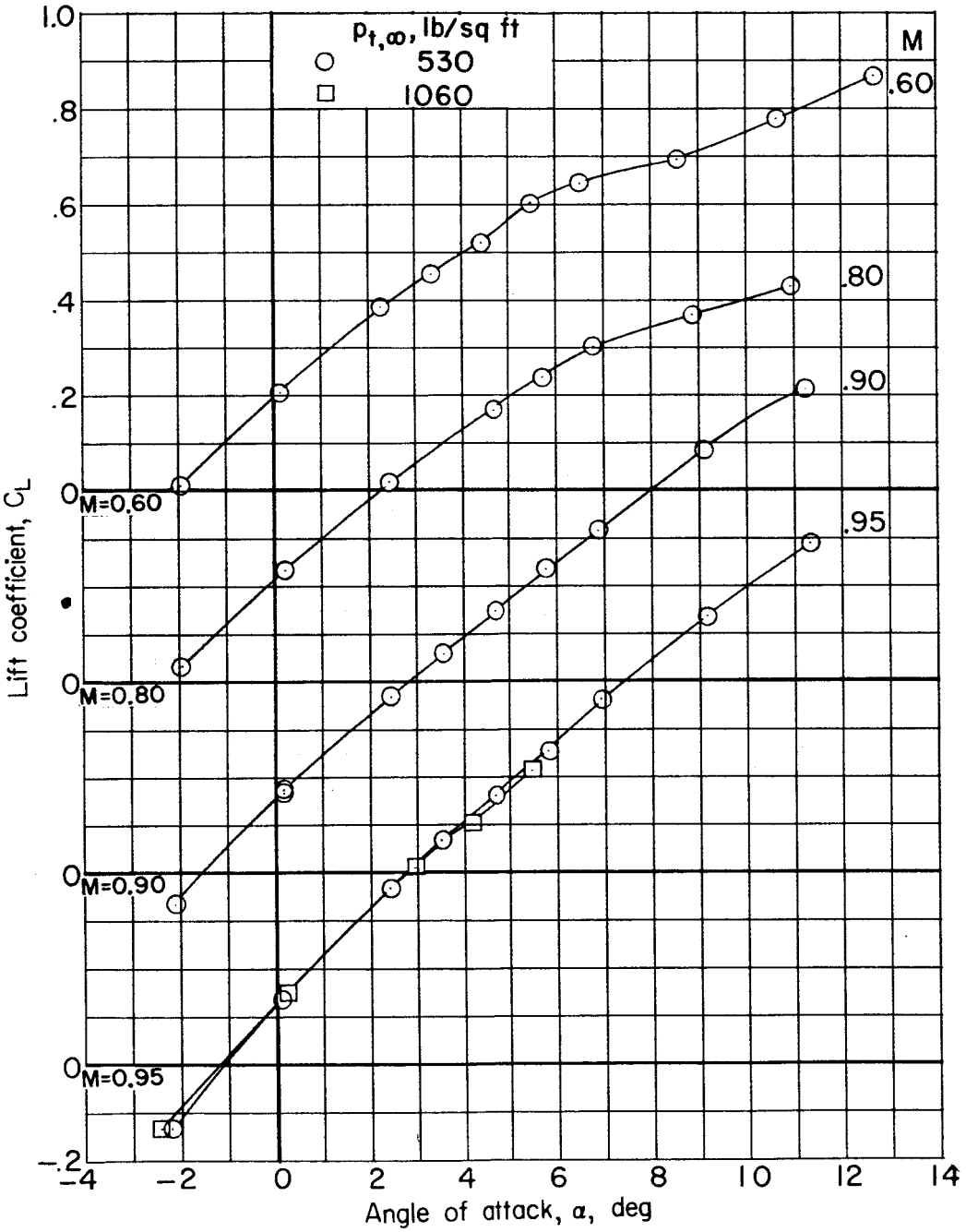

(a) Variation of C_L with α.

Figure 13.- Longitudinal aerodynamic characteristics of model IV-A with 25° swept wing. Configuration BWVH; $\delta_h = -4.15°$.

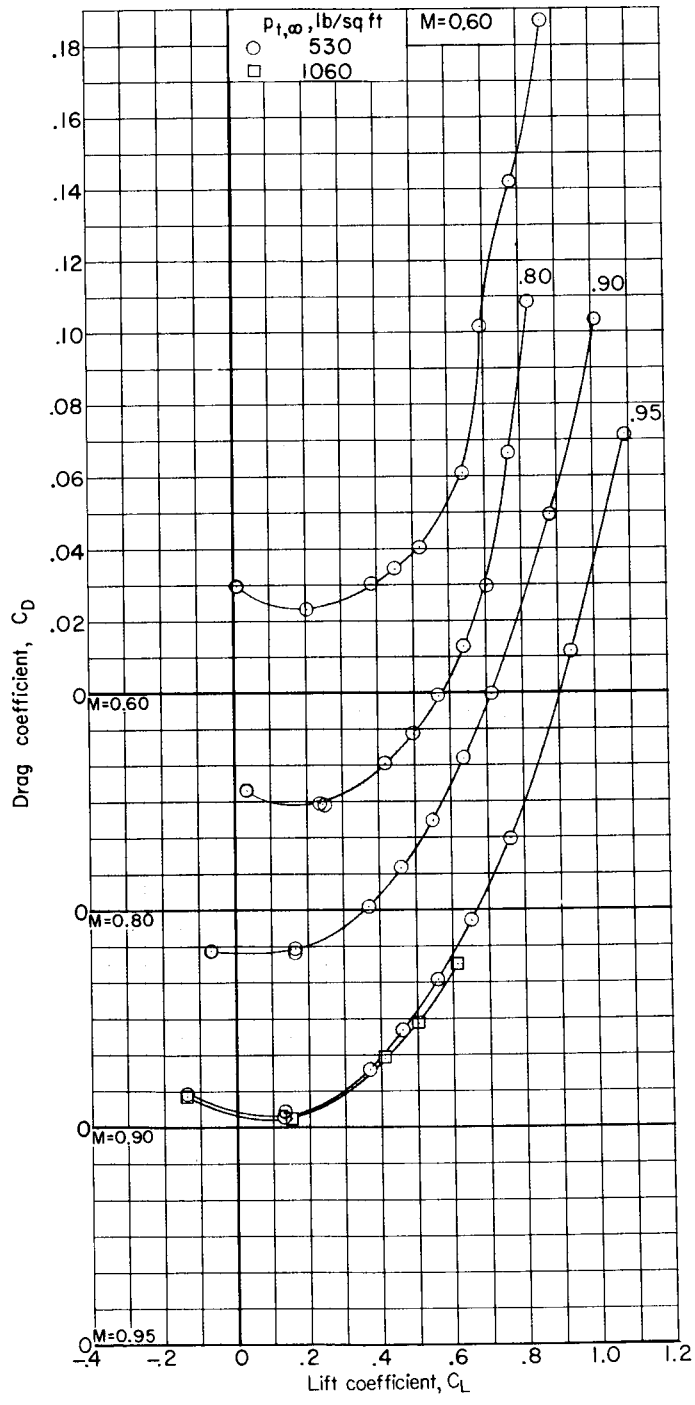

(b) Variation of C_D with C_L.

Figure 13.- Continued.

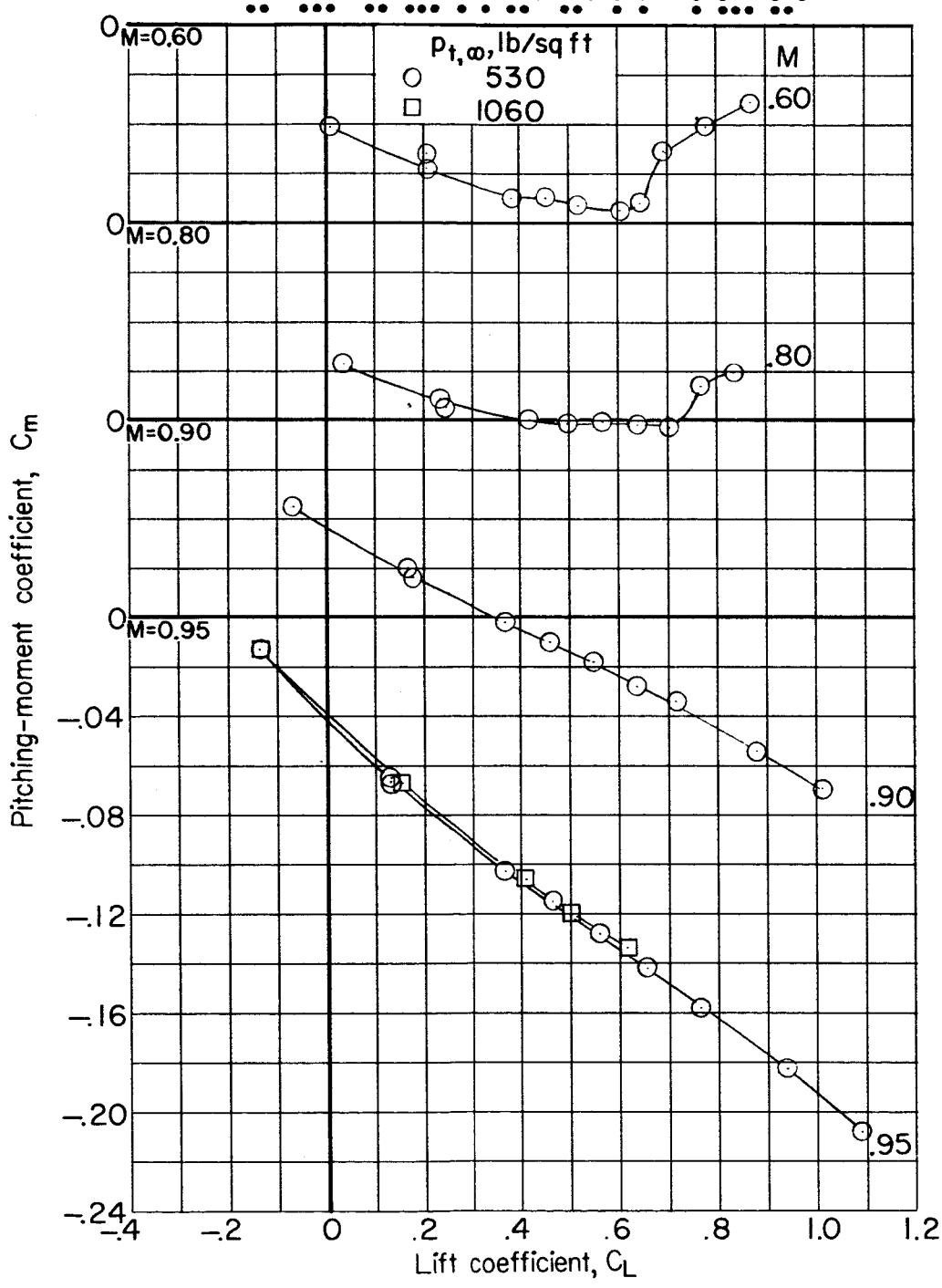

(c) Variation of C_m with C_L.

Figure 13.- Continued.

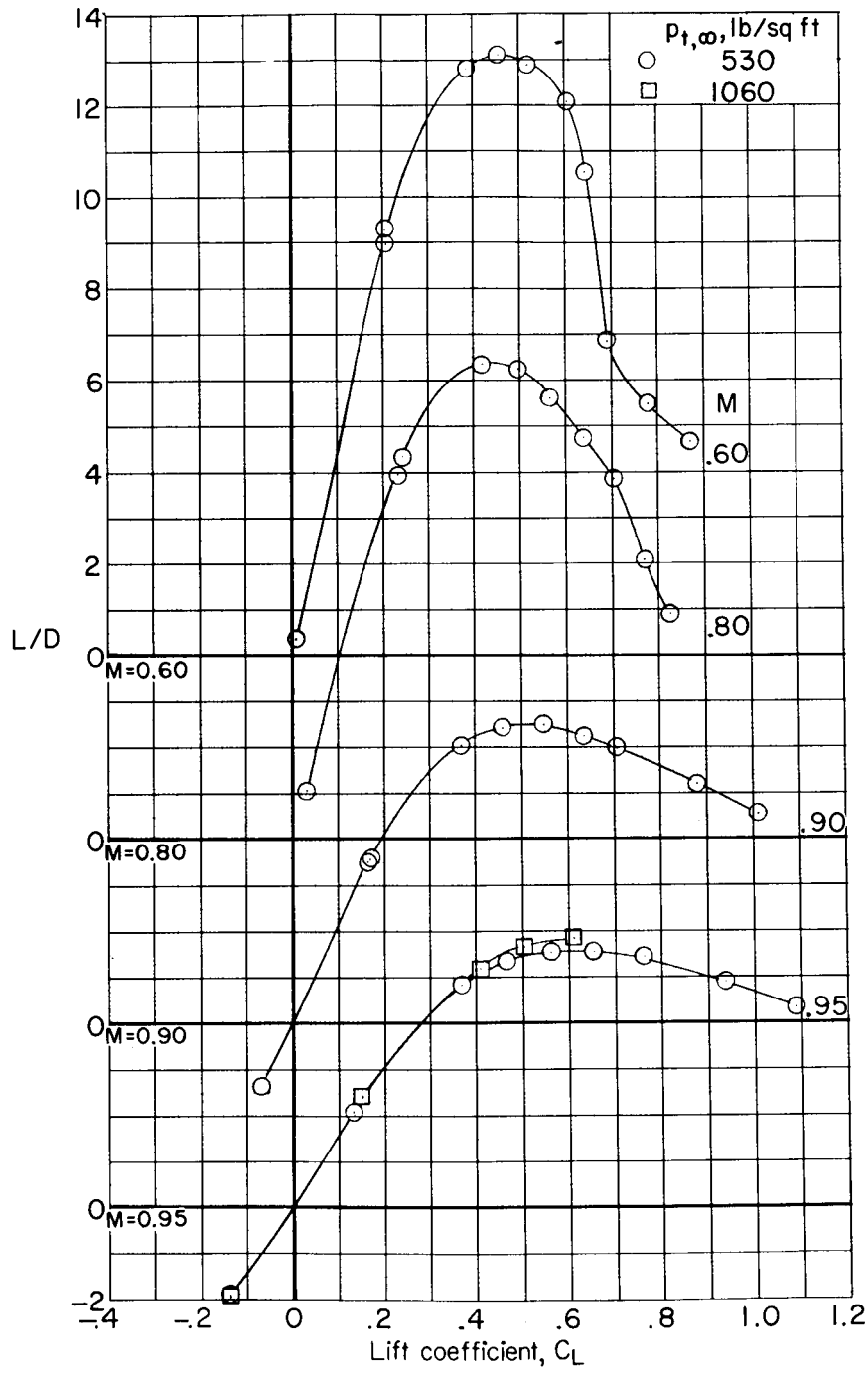

(d) Variation of L/D with C_L.

Figure 13.- Concluded.

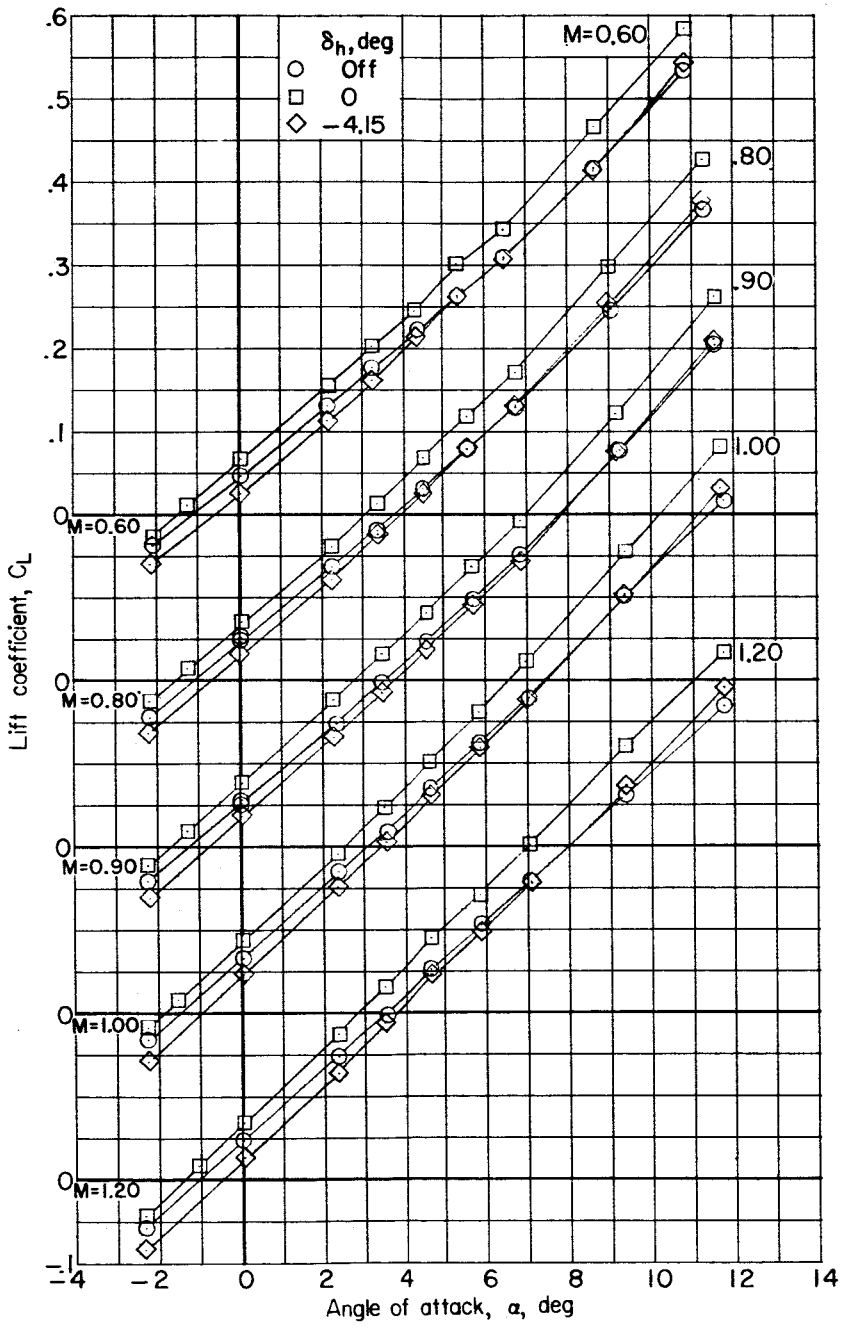

(a) Variation of C_L with α.

Figure 14.- Effect of horizontal-tail deflection on longitudinal aerodynamic characteristics of model IV-A with 75° swept wing. Configuration BWVH; $p_{t,\infty}$ = 1,060 lb/sq ft.

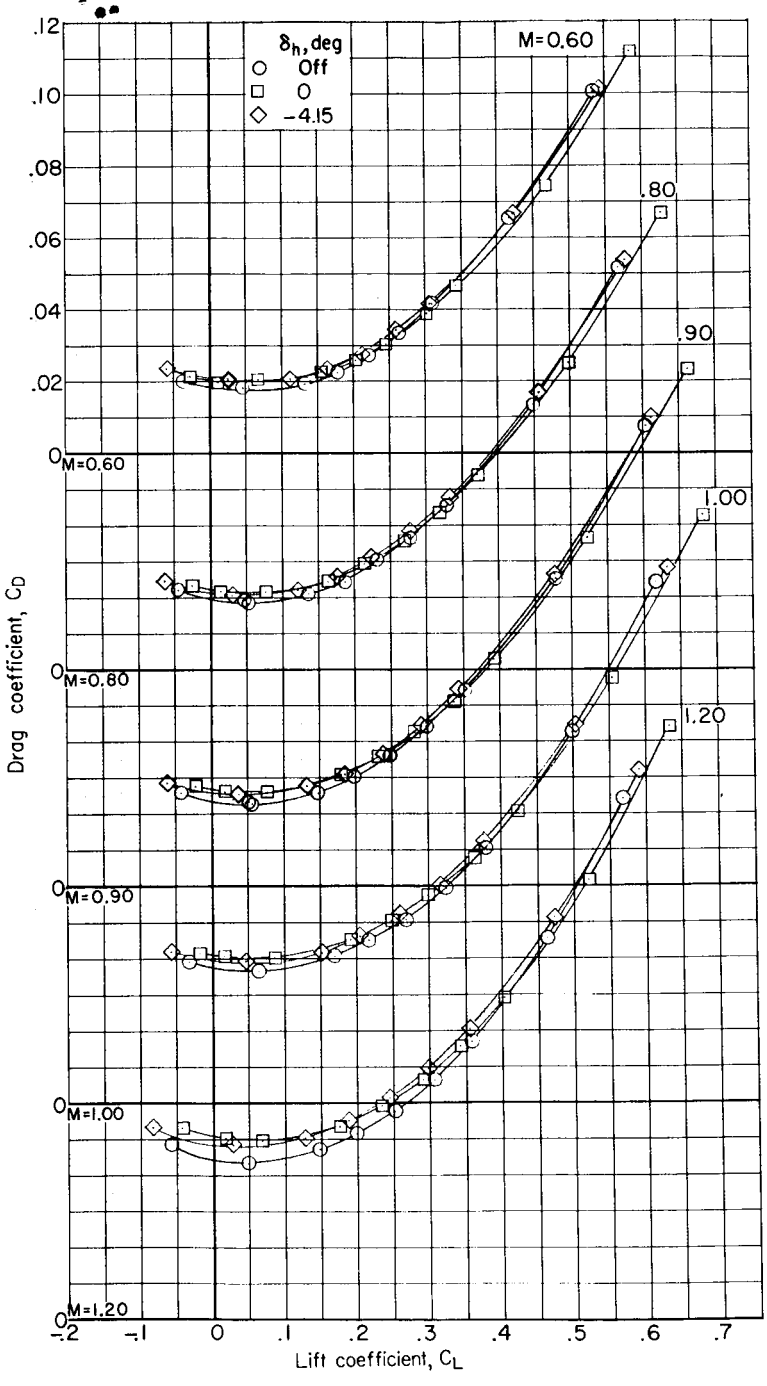

(b) Variation of C_D with C_L.

Figure 14.- Continued.

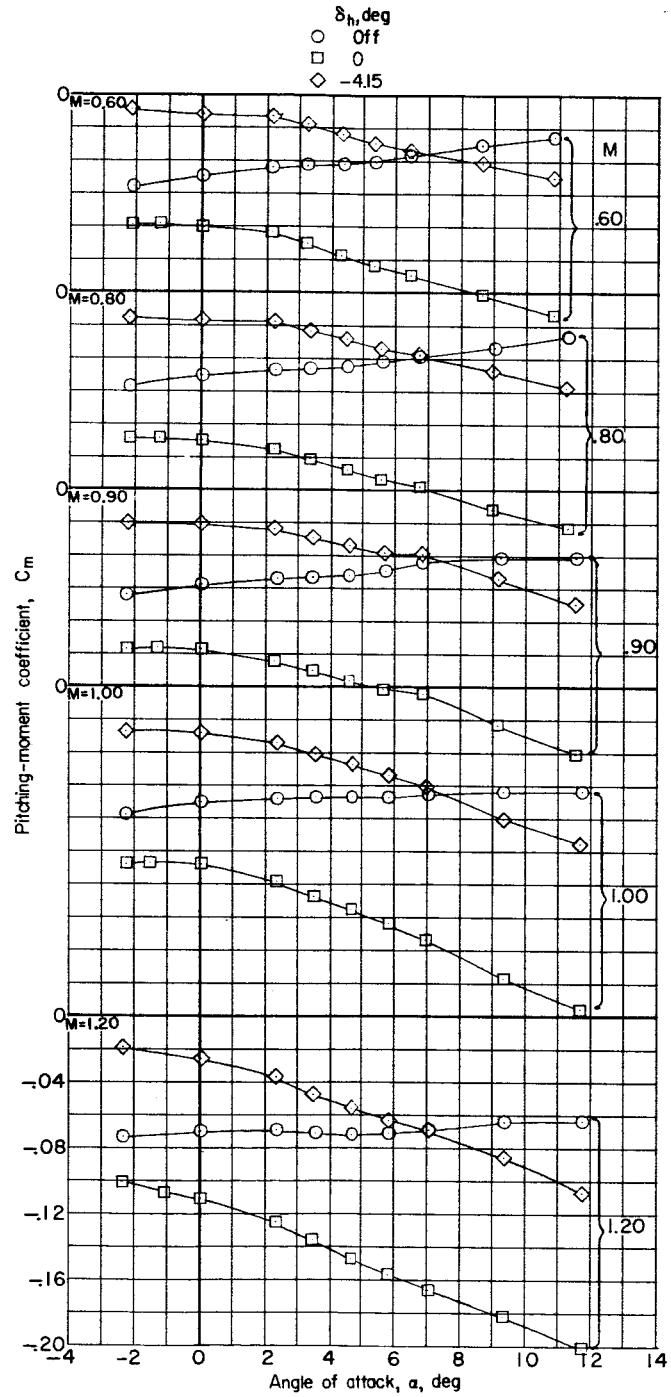

(c) Variation of C_m with α.

Figure 14.- Continued.

[redacted]

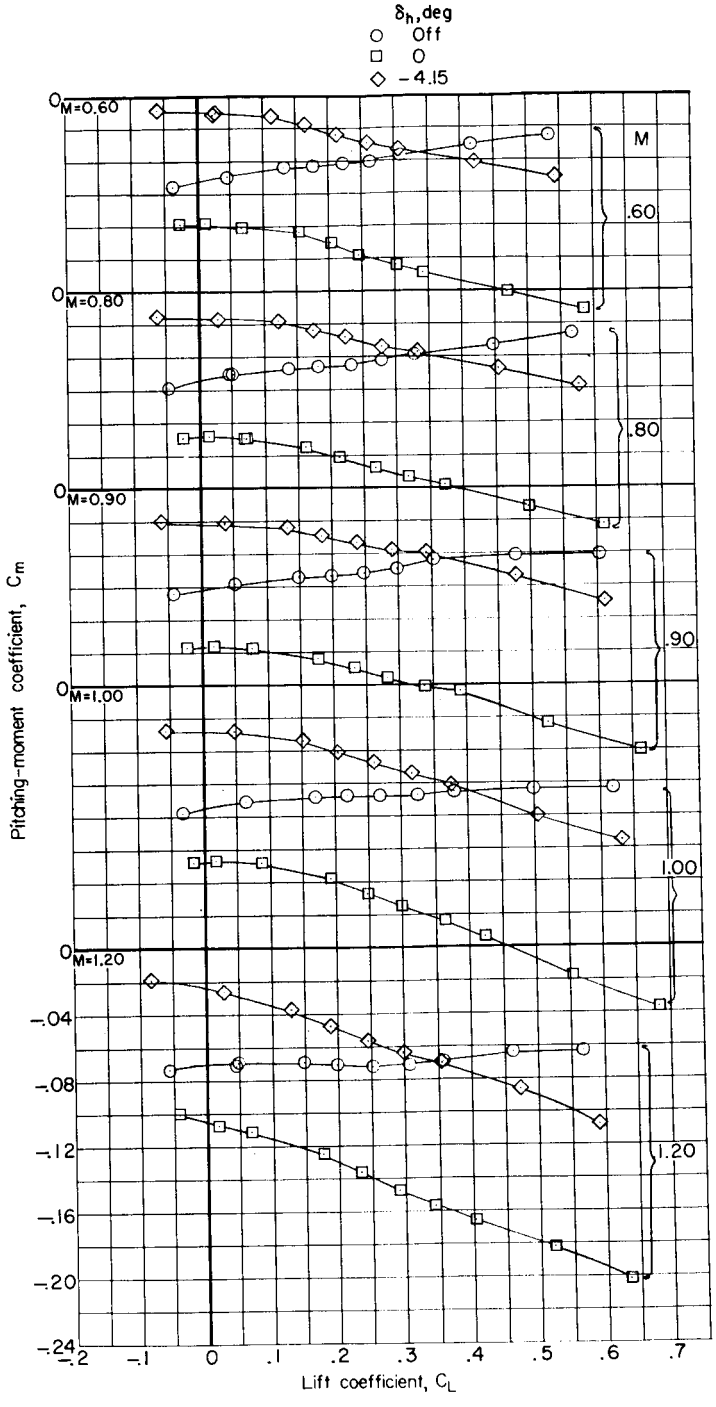

(d) Variation of C_m with C_L.

Figure 14.- Continued.

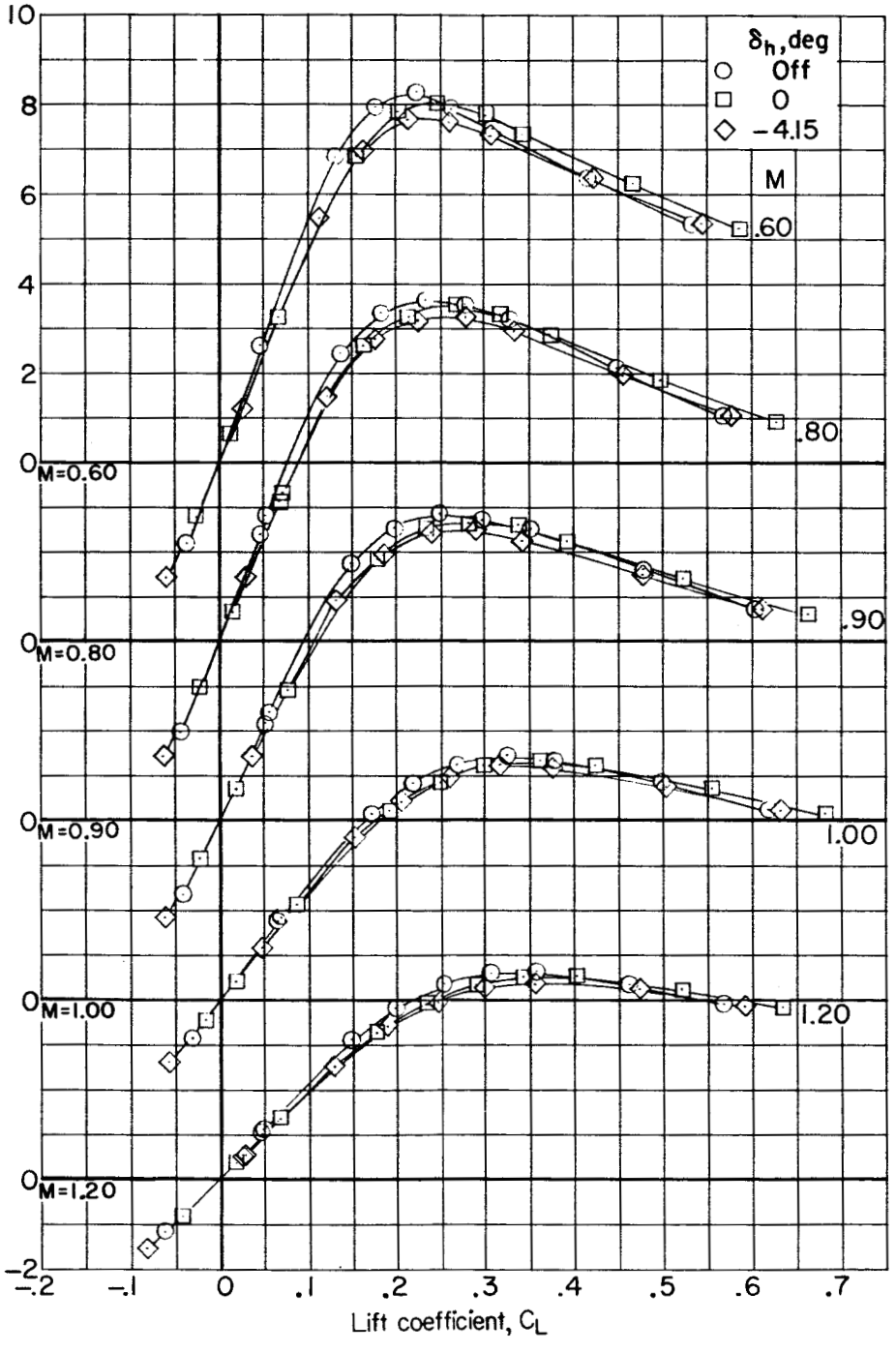

(e) Variation of L/D with C_L.

Figure 14.- Concluded.

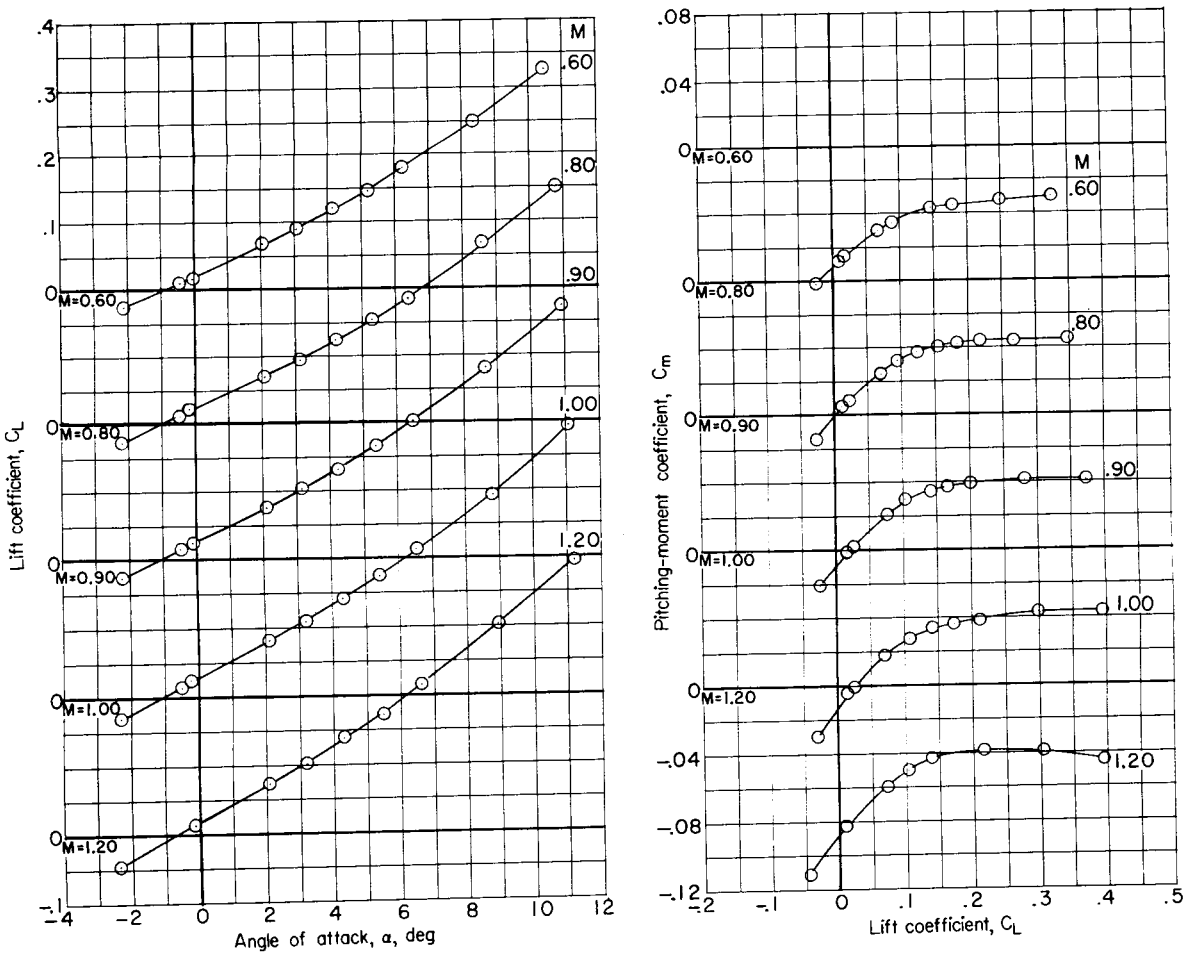

(a) Variation of C_L with α and C_m with C_L.

Figure 15.- Longitudinal aerodynamic characteristics of model IV-A with 108° swept wing. Configuration BWVH; $\delta_h = 0°$; $p_{t,\infty} = 1{,}060$ lb/sq ft.

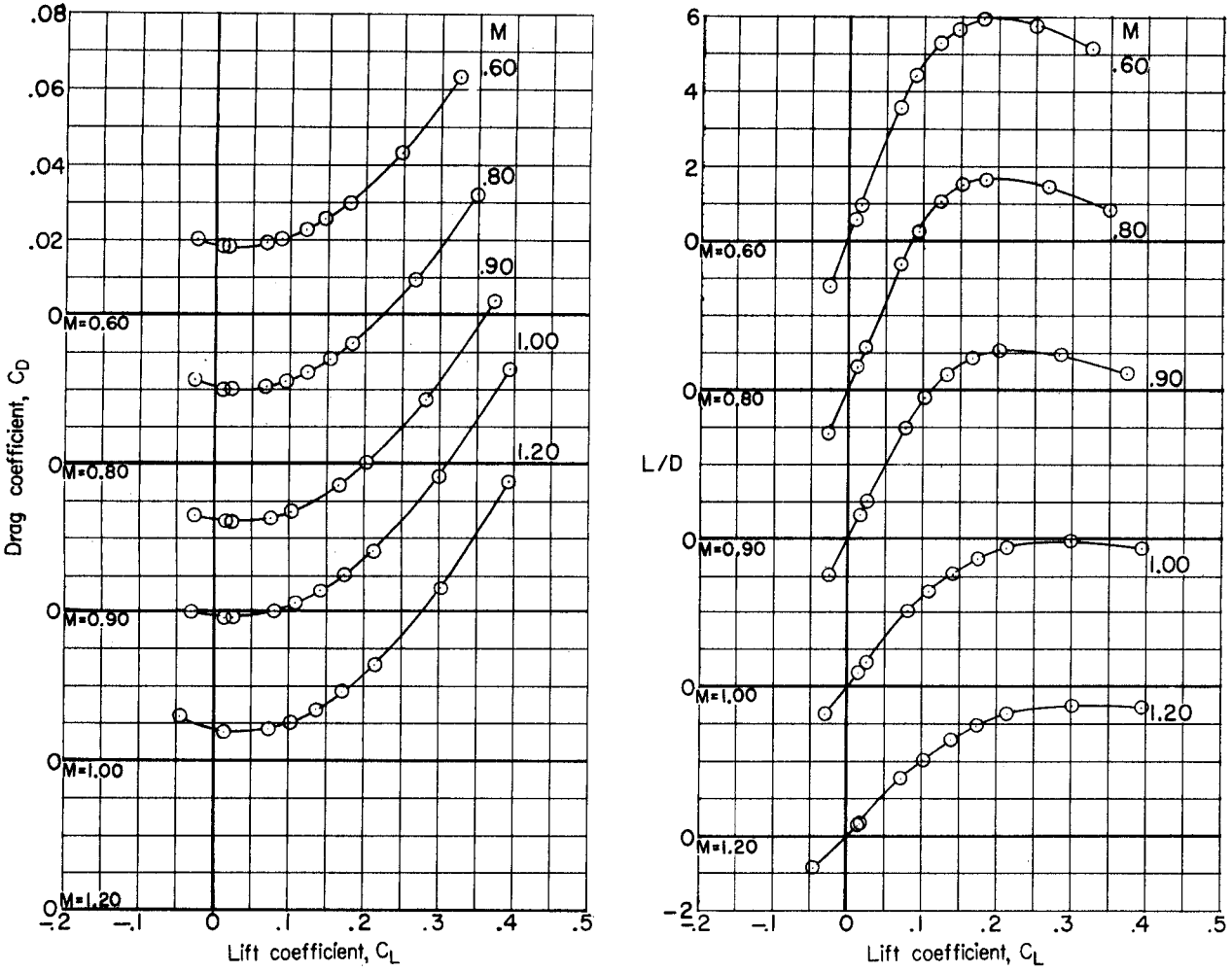

(b) Variation of C_D with C_L and L/D with C_L.

Figure 15.- Concluded.

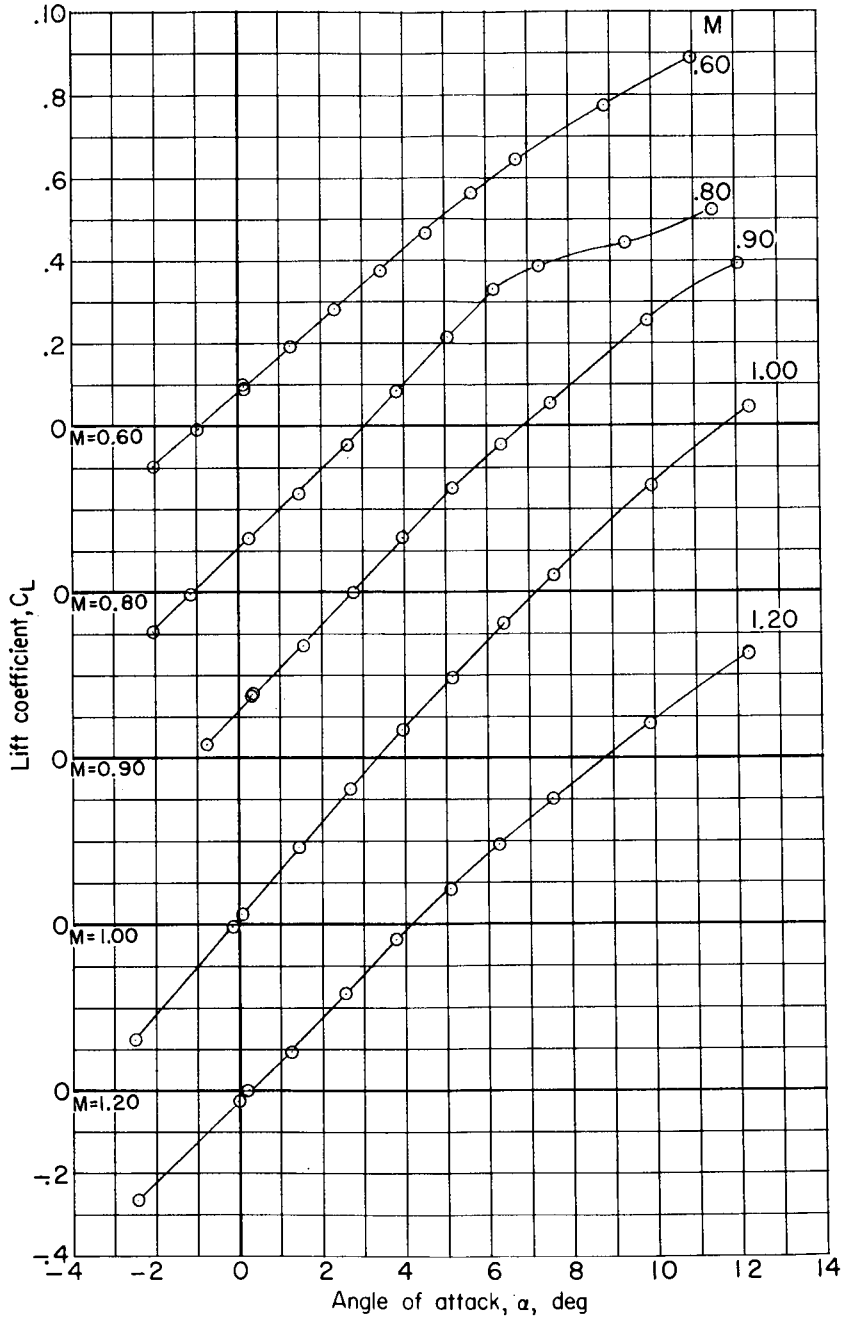

(a) Variation of C_L with α.

Figure 16.- Longitudinal aerodynamic characteristics of model IV-B with 0° skewed wing. Configuration BWVH; $\delta_h = -4.15°$; $p_{t,\infty} = 1{,}060$ lb/sq ft.

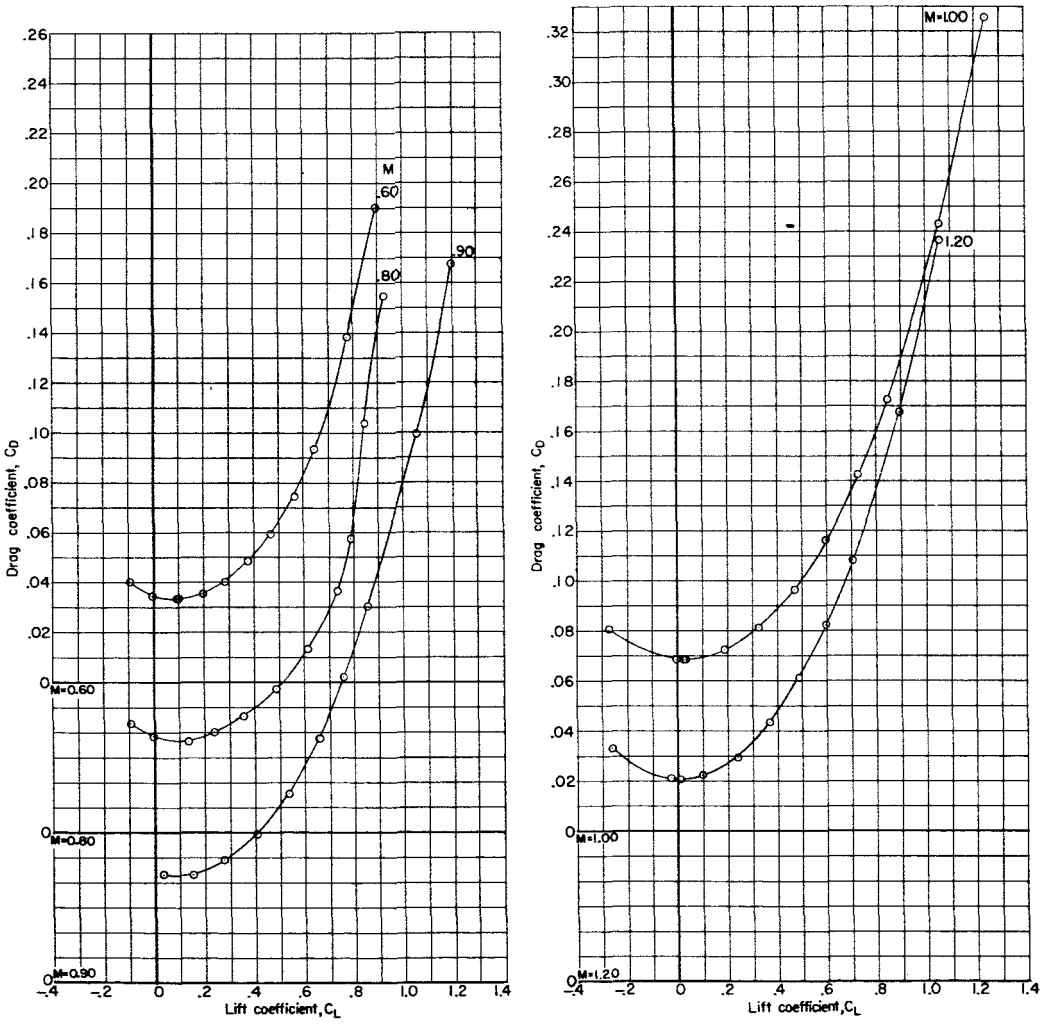

(b) Variation of C_D with C_L.

Figure 16.- Continued.

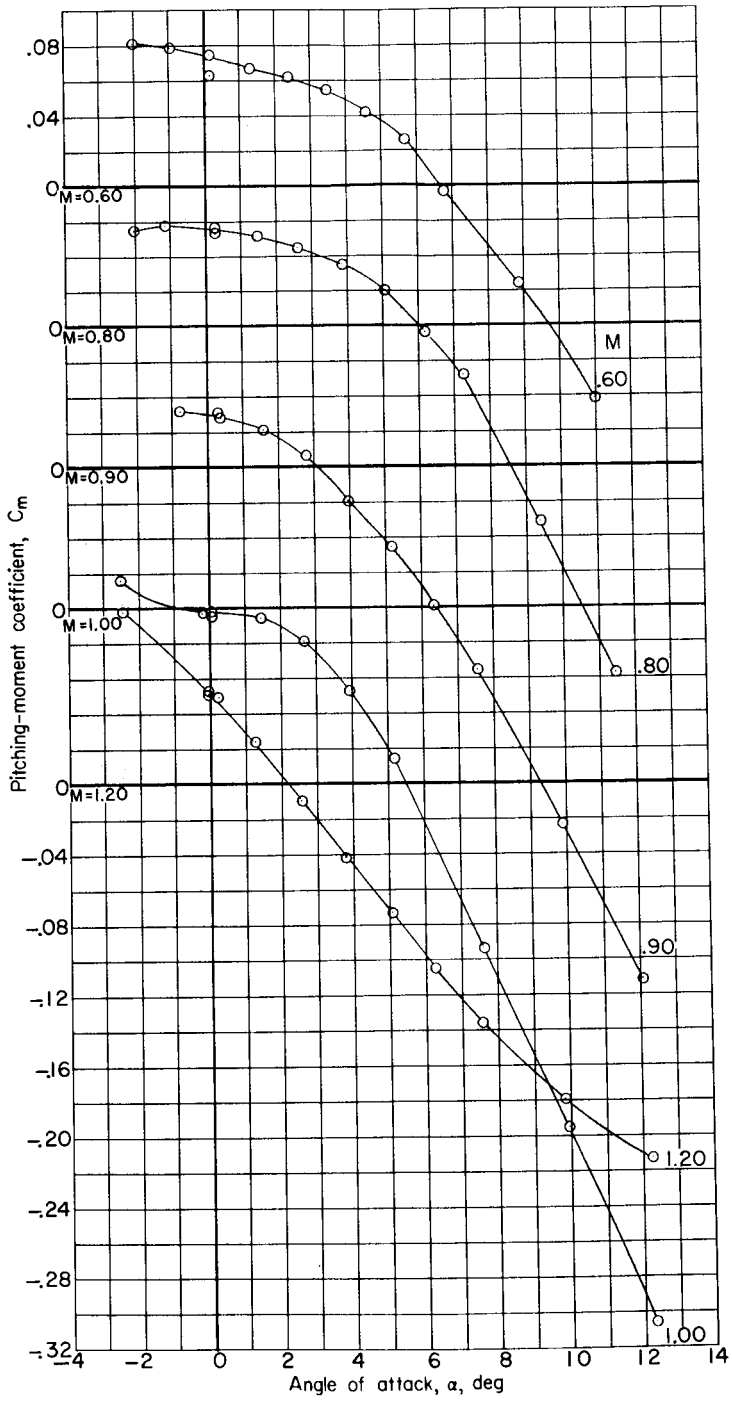

(c) Variation of C_m with α.

Figure 16.- Continued.

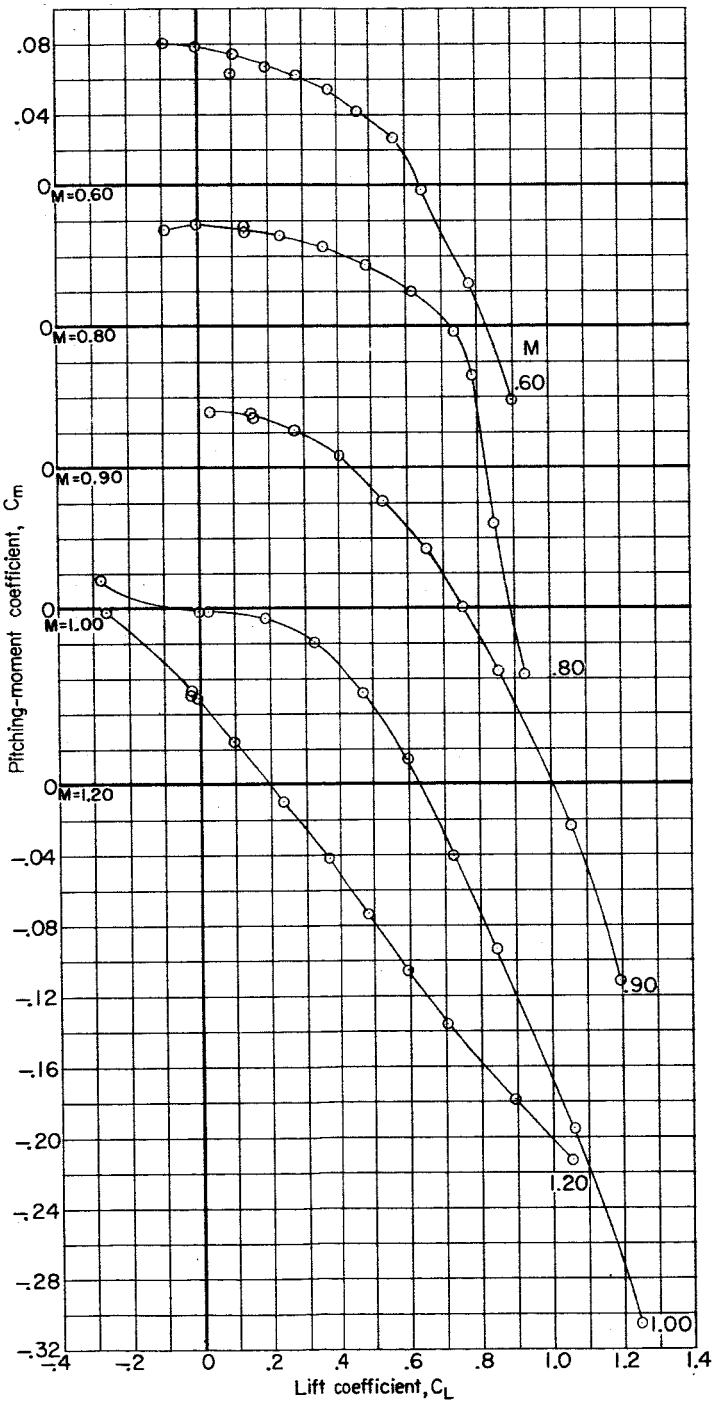

(d) Variation of C_m with C_L.

Figure 16.- Continued.

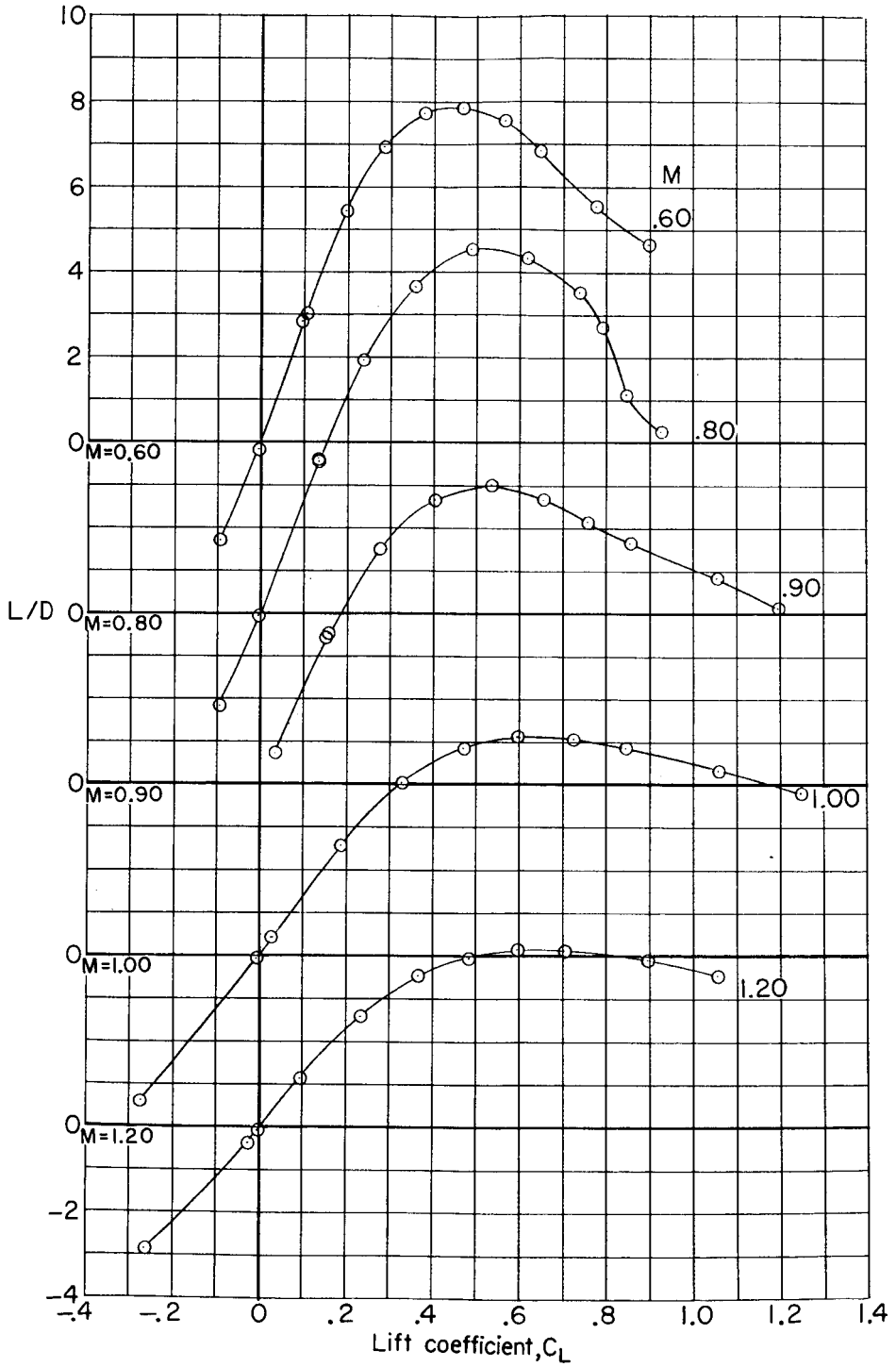

(e) Variation of L/D with C_L.

Figure 16.- Concluded.

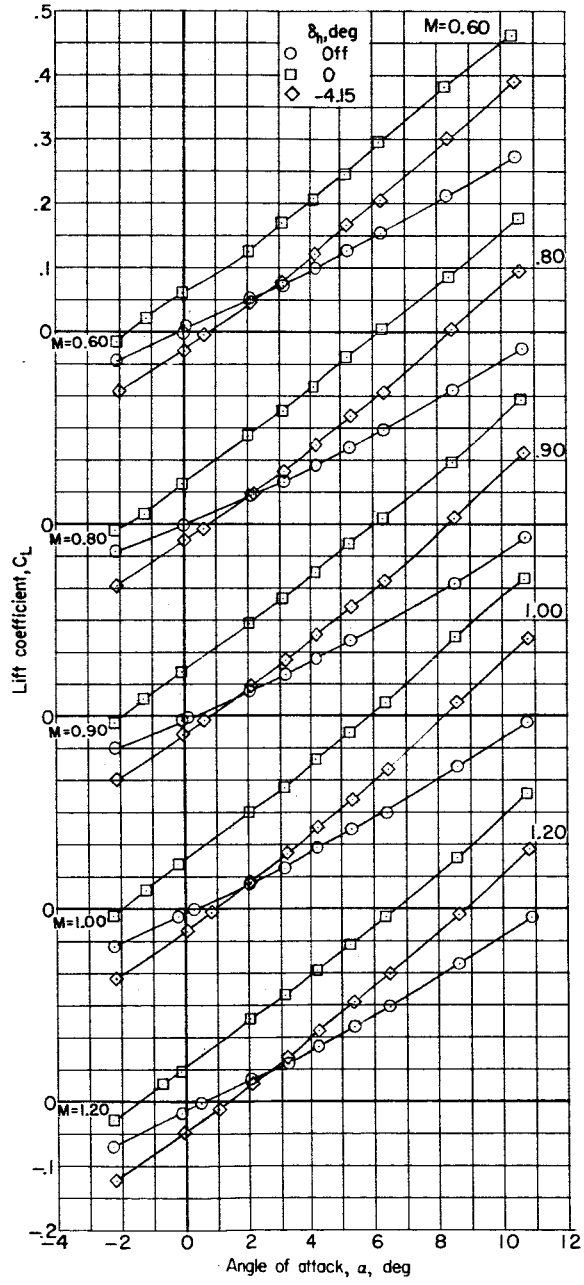

(a) Variation of C_L with α.

Figure 17.- Effect of horizontal-tail deflection on longitudinal aerodynamic characteristics of model IV-B with 90° skewed wing. Configuration BWVH; $p_{t,\infty}$ = 1,060 lb/sq ft.

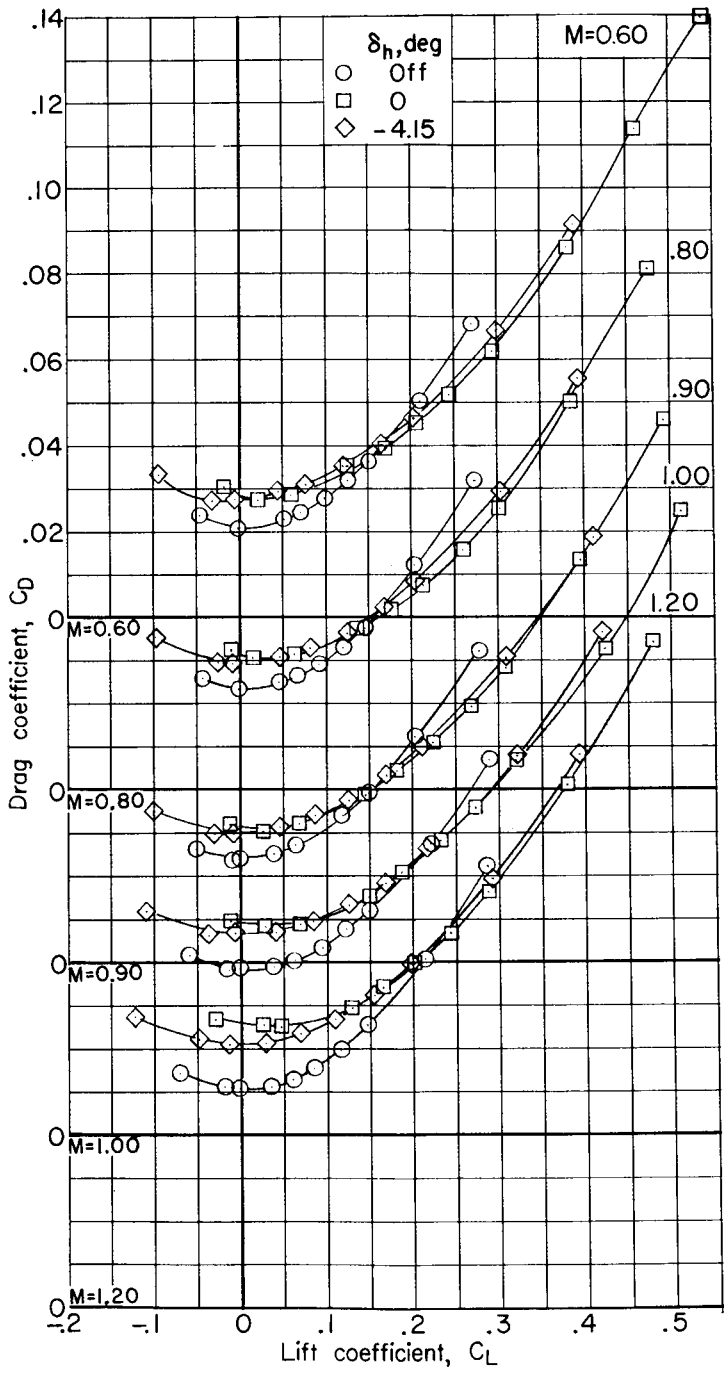

(b) Variation of C_D with C_L.

Figure 17.- Continued.

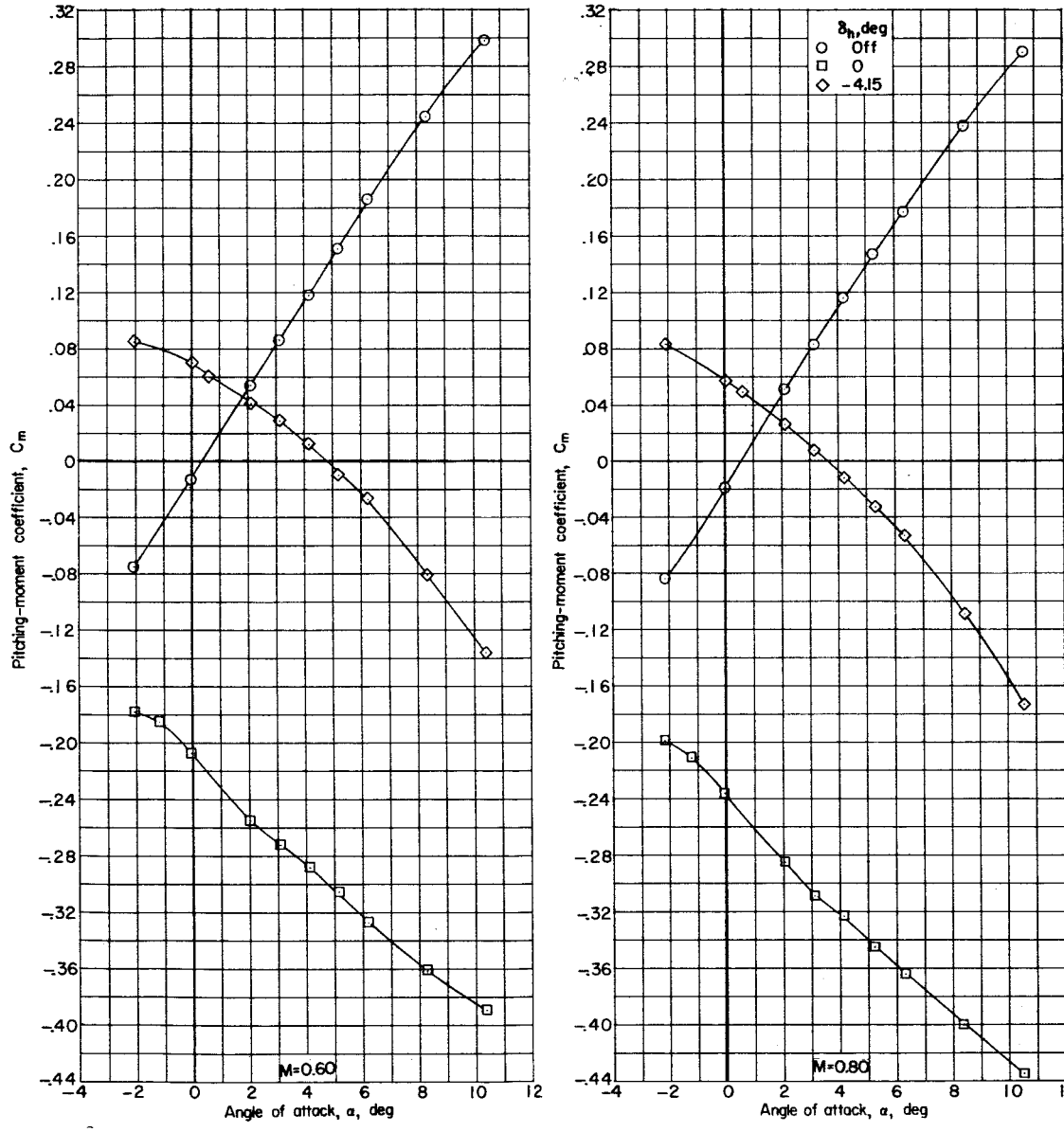

(c) Variation of C_m with α.

Figure 17.- Continued.

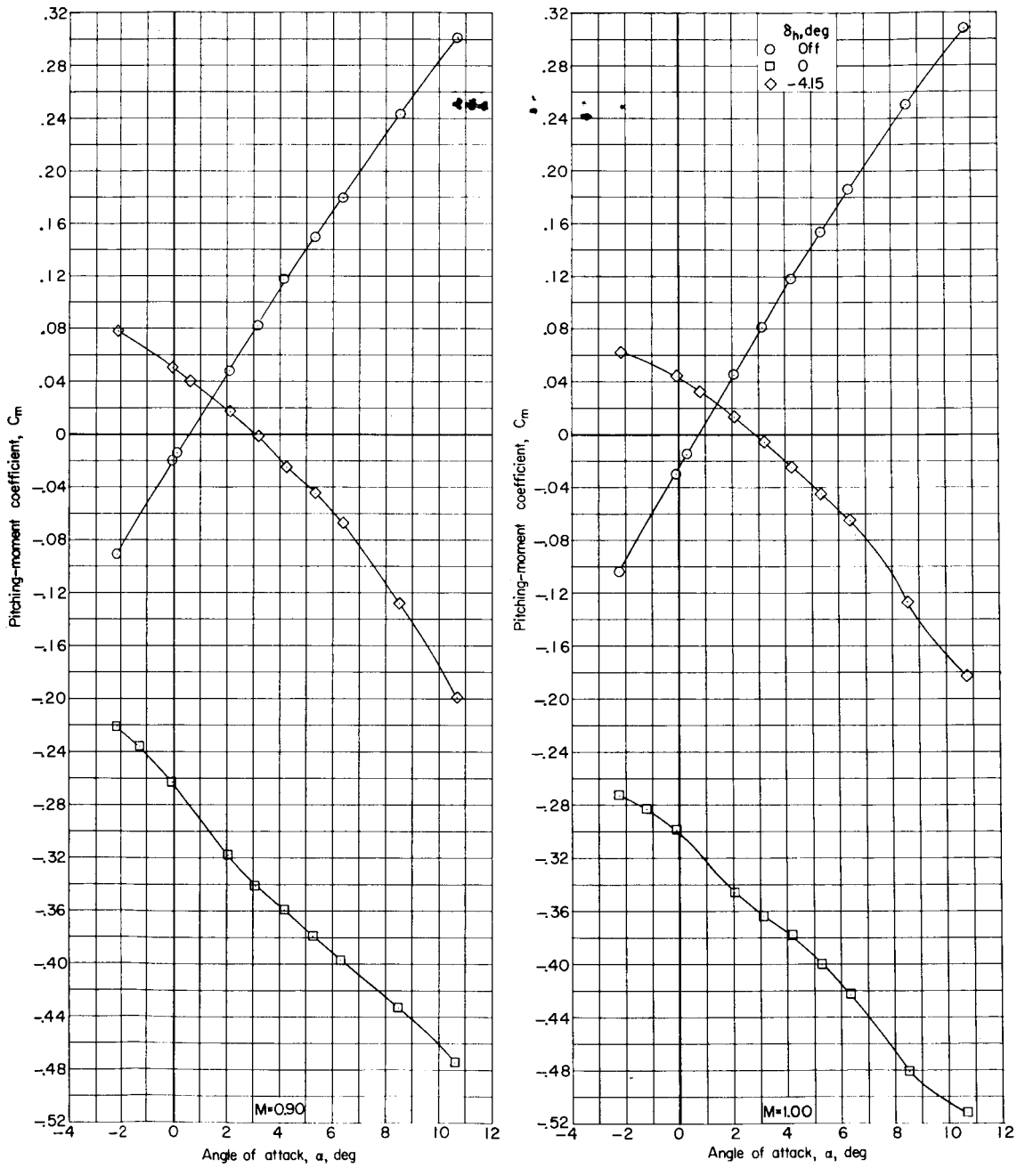

(c) Continued.

Figure 17.- Continued.

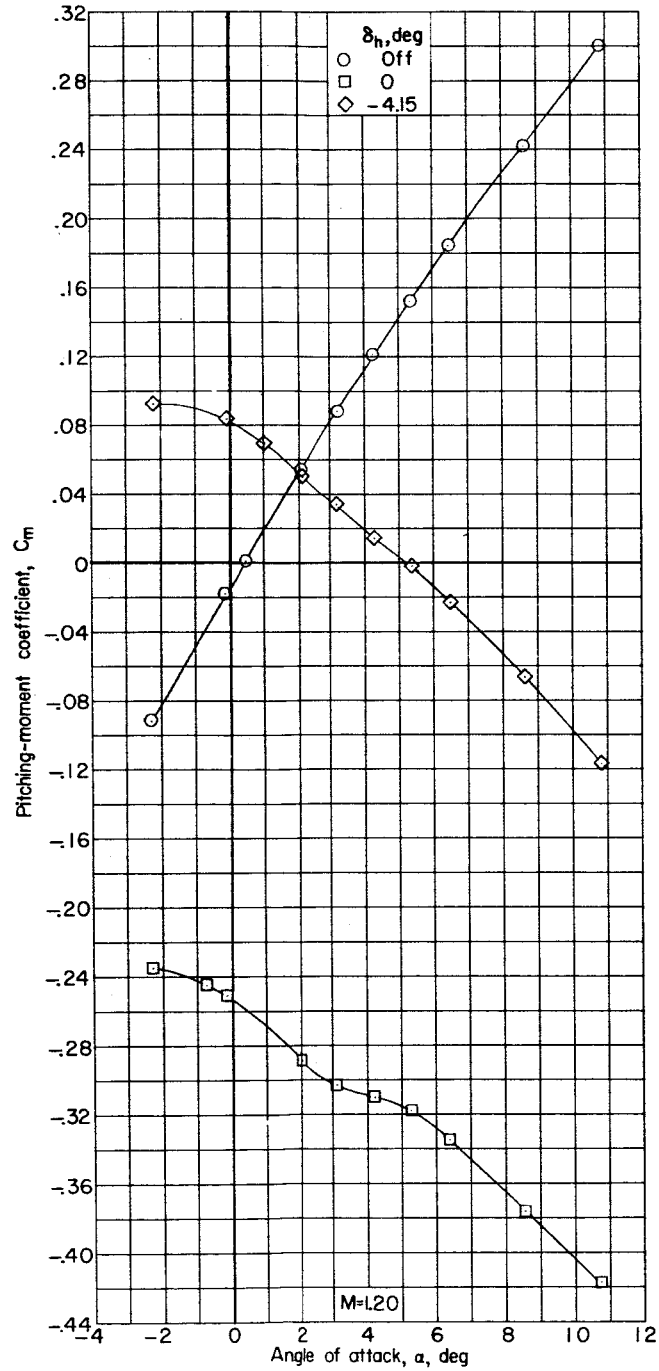

(c) Concluded.

Figure 17.- Continued.

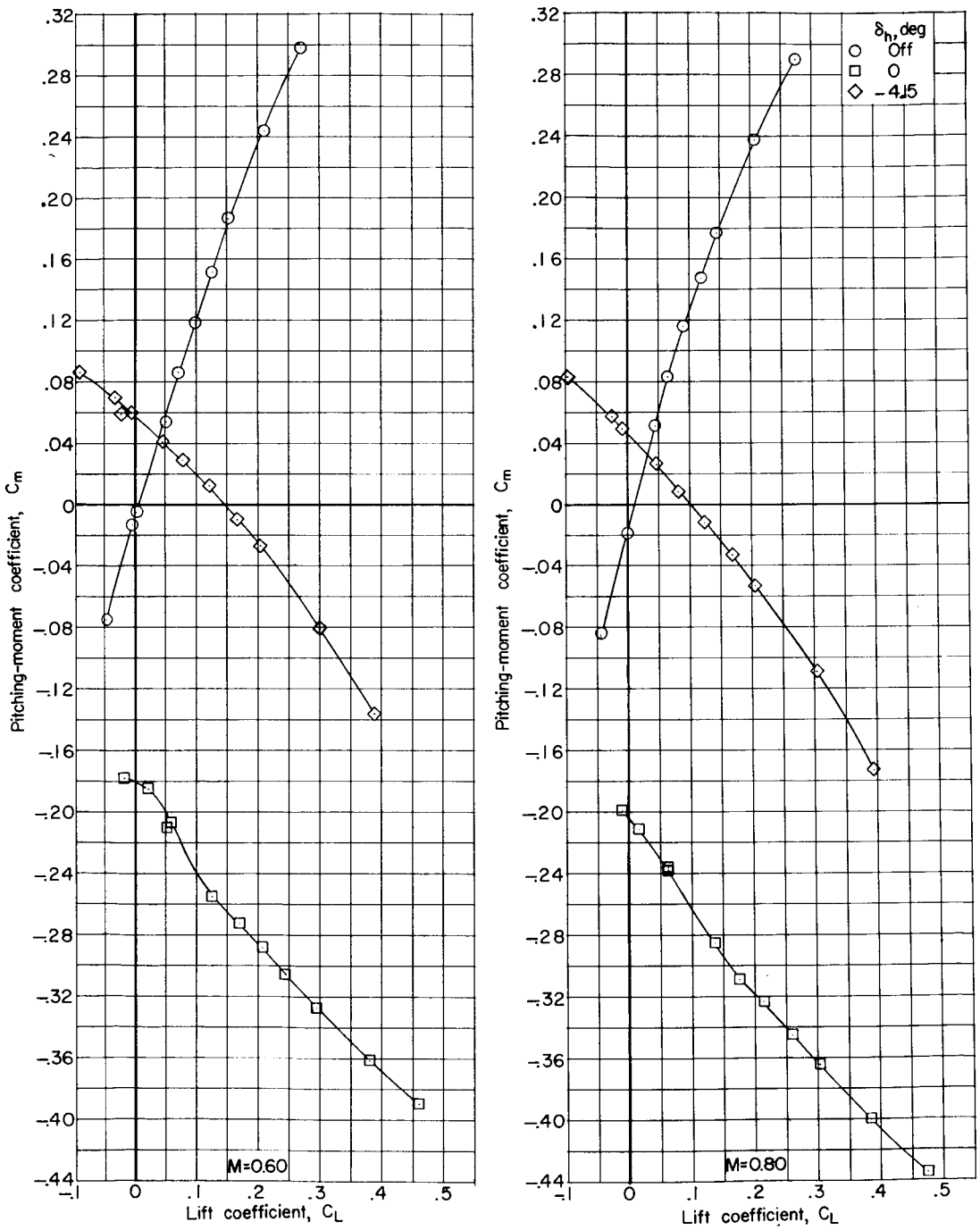

(d) Variation of C_m with C_L.

Figure 17.- Continued.

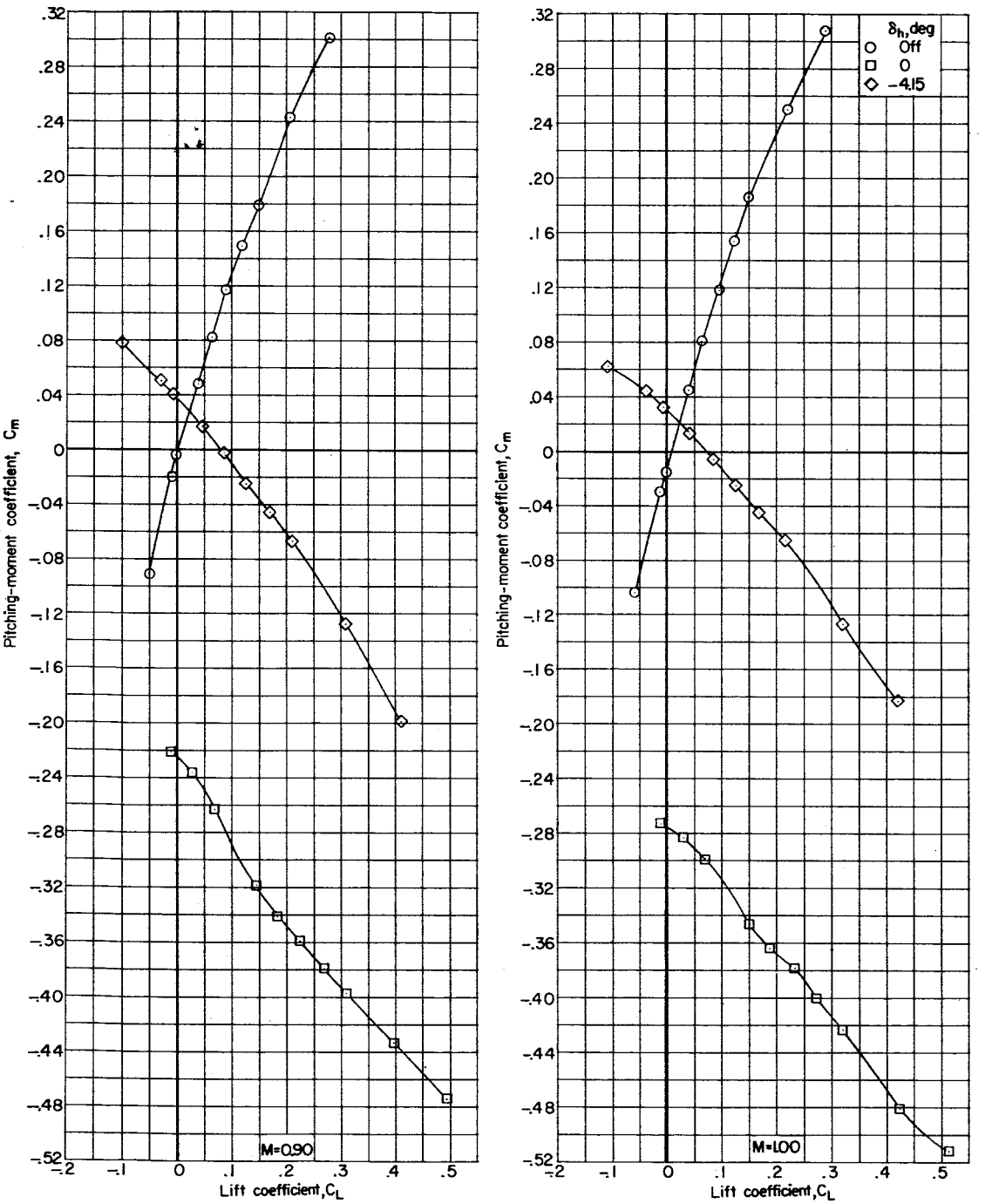

(d) Continued.

Figure 17.- Continued.

[redacted]

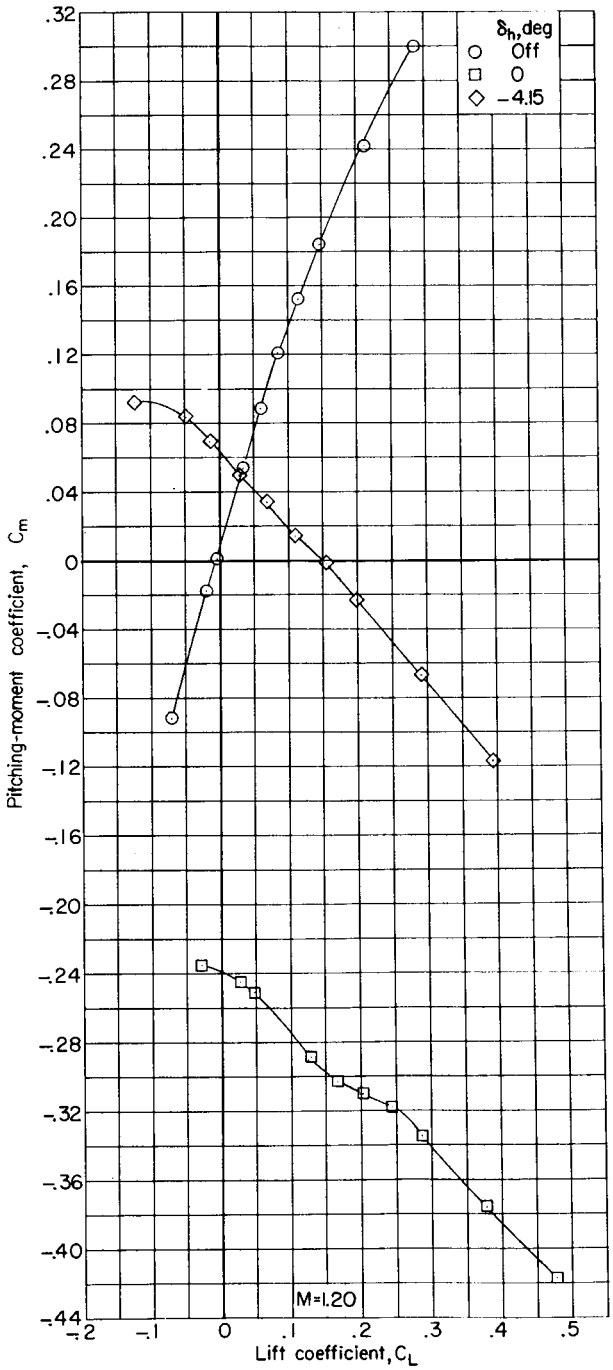

(d) Concluded.

Figure 17.- Continued.

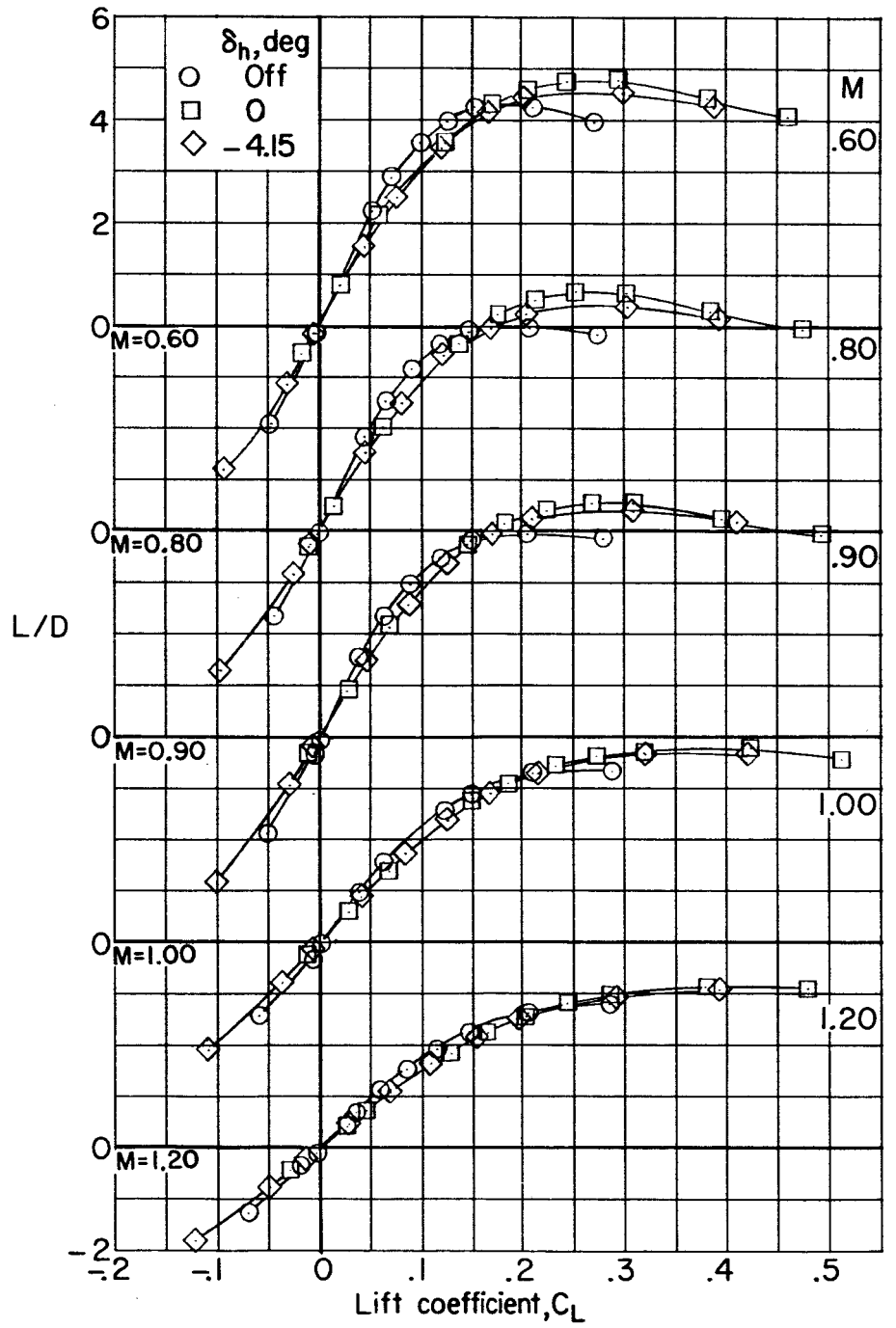

(e) Variation of L/D with C_L.

Figure 17.- Concluded.

[redacted]

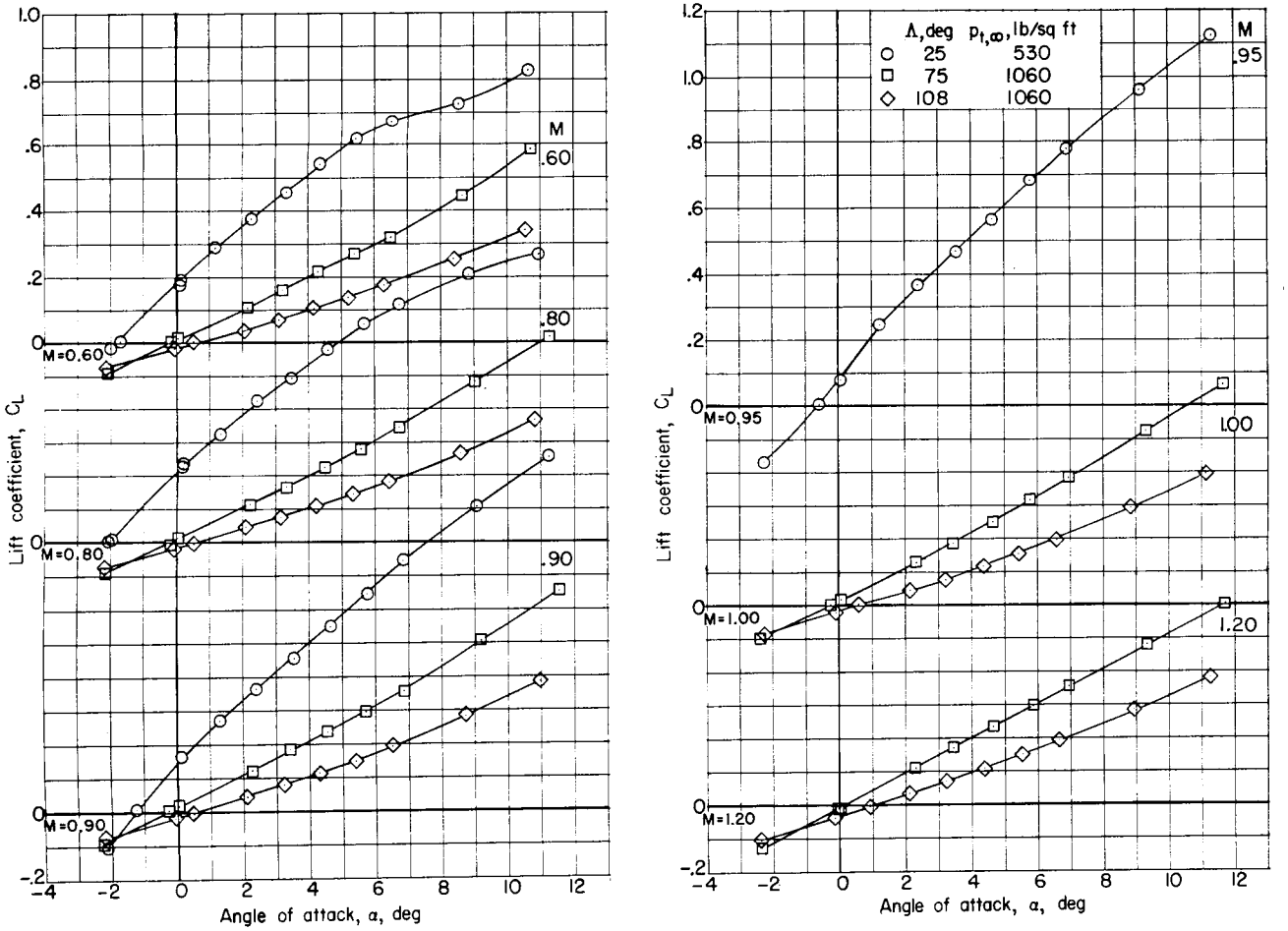

(a) Variation of C_L with α.

Figure 18.- Effect of wing sweep on longitudinal aerodynamic characteristics of model IV-B. Configuration BWVH; $\delta_h = -4.15^\circ$.

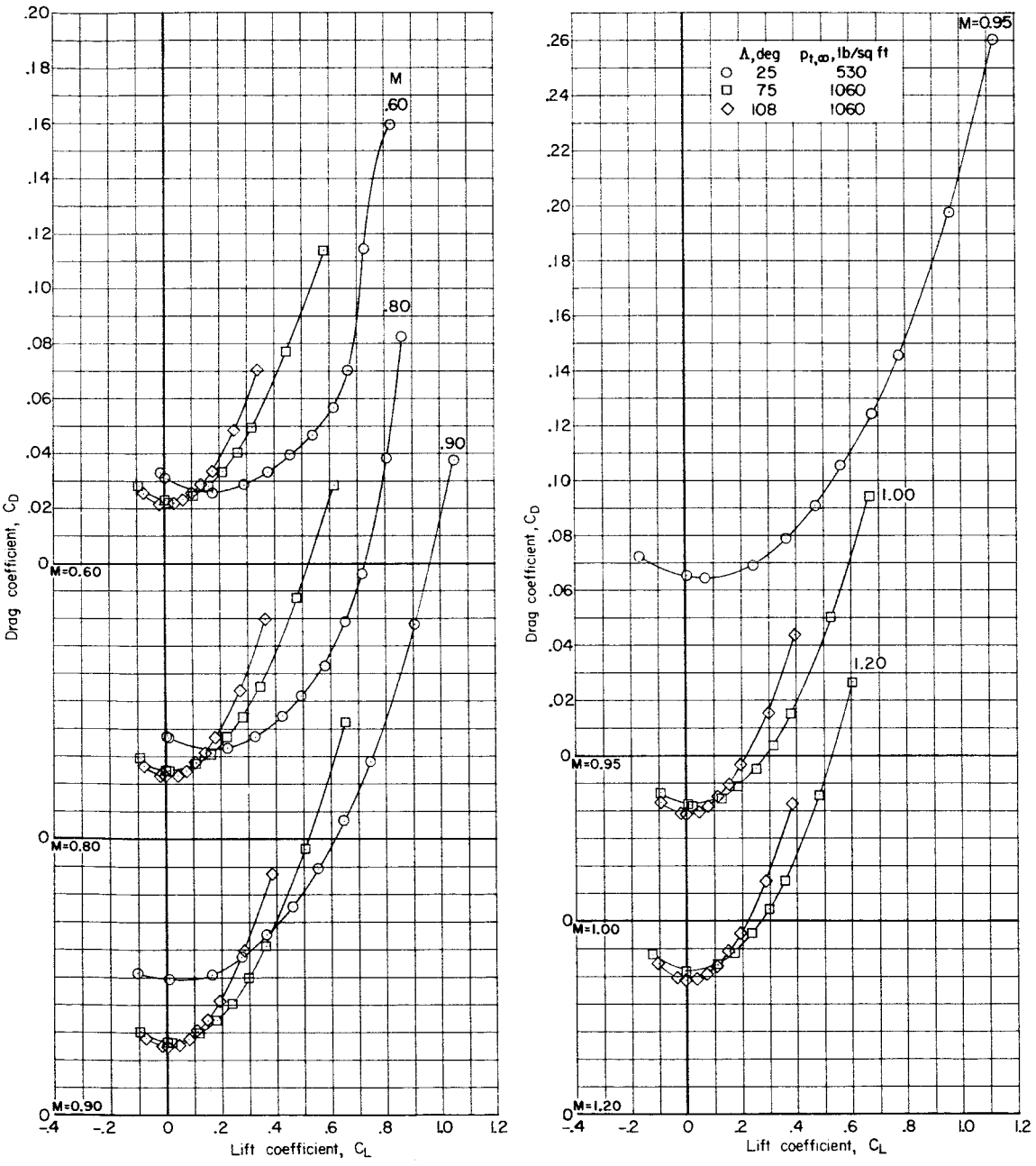

(b) Variation of C_D with C_L.

Figure 18.- Continued.

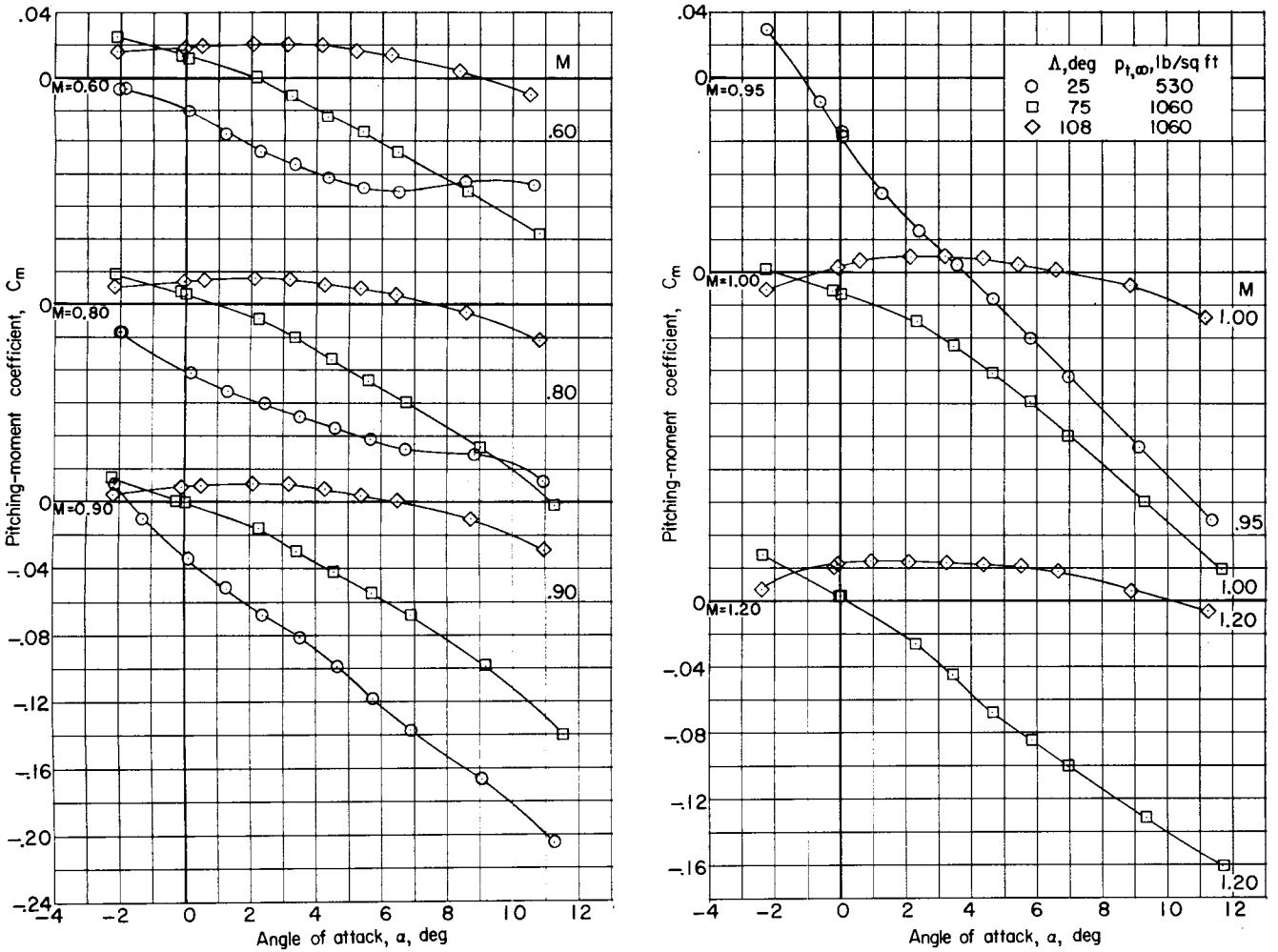

(c) Variation of C_m with α.

Figure 18.- Continued.

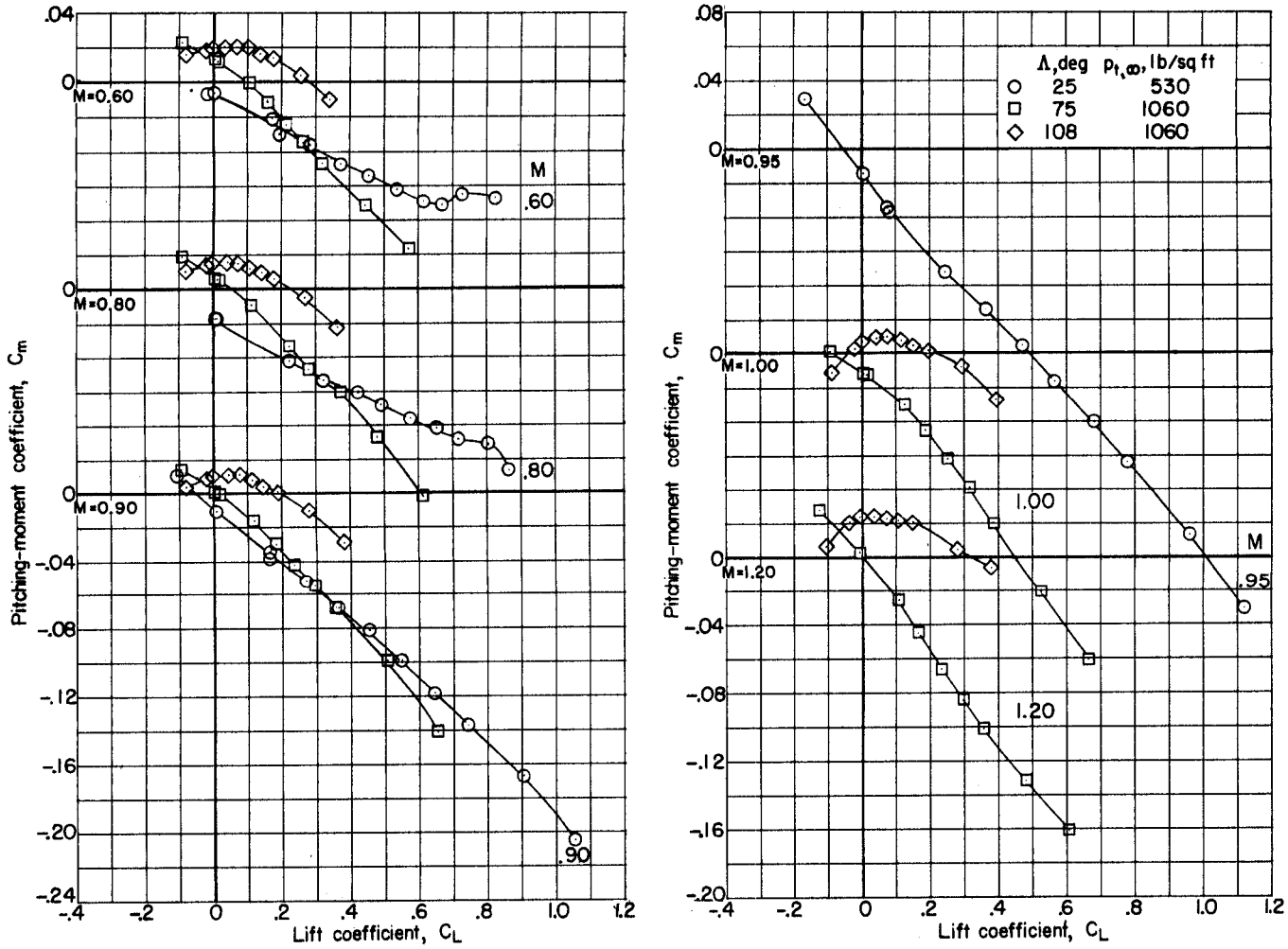

(d) Variation of C_m with C_L.

Figure 18.- Continued.

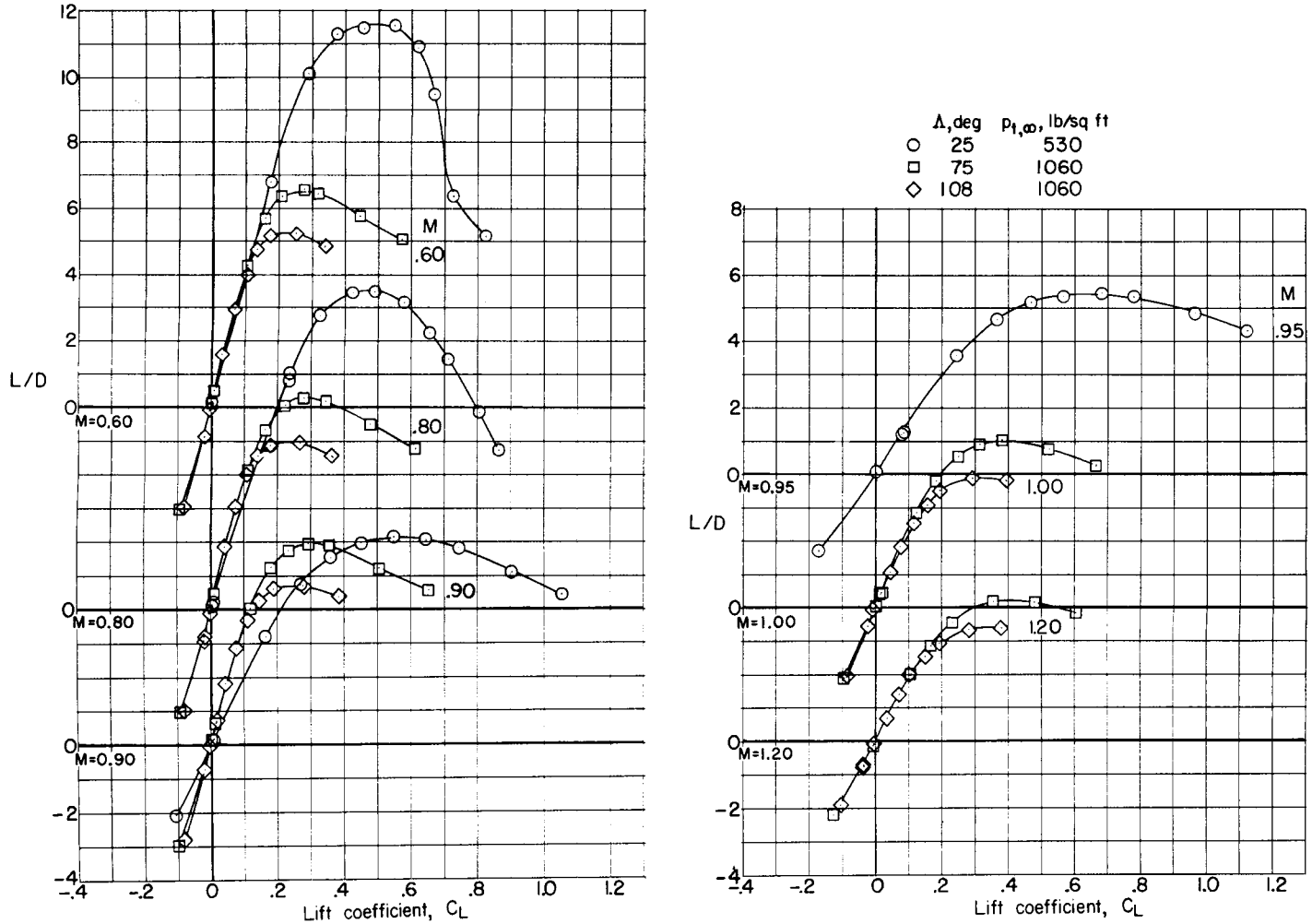

(e) Variation of L/D with C_L.

Figure 18.- Concluded.

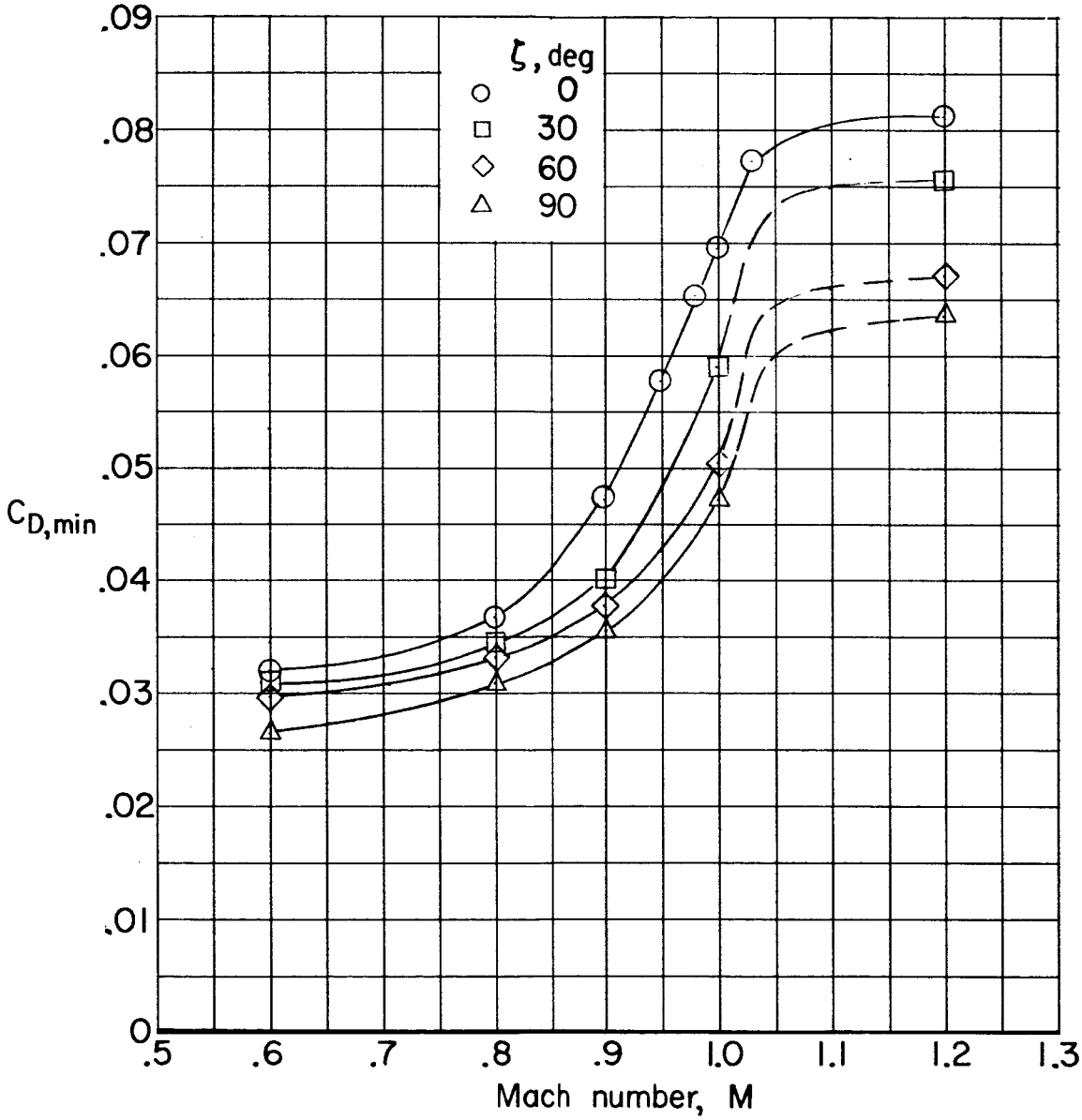

Figure 19.- Effect of wing skew angle on minimum drag of model IV-A. Configuration BWVH; $\delta_h = 0^o$; $p_{t,\infty}$ = 530 lb/sq ft.

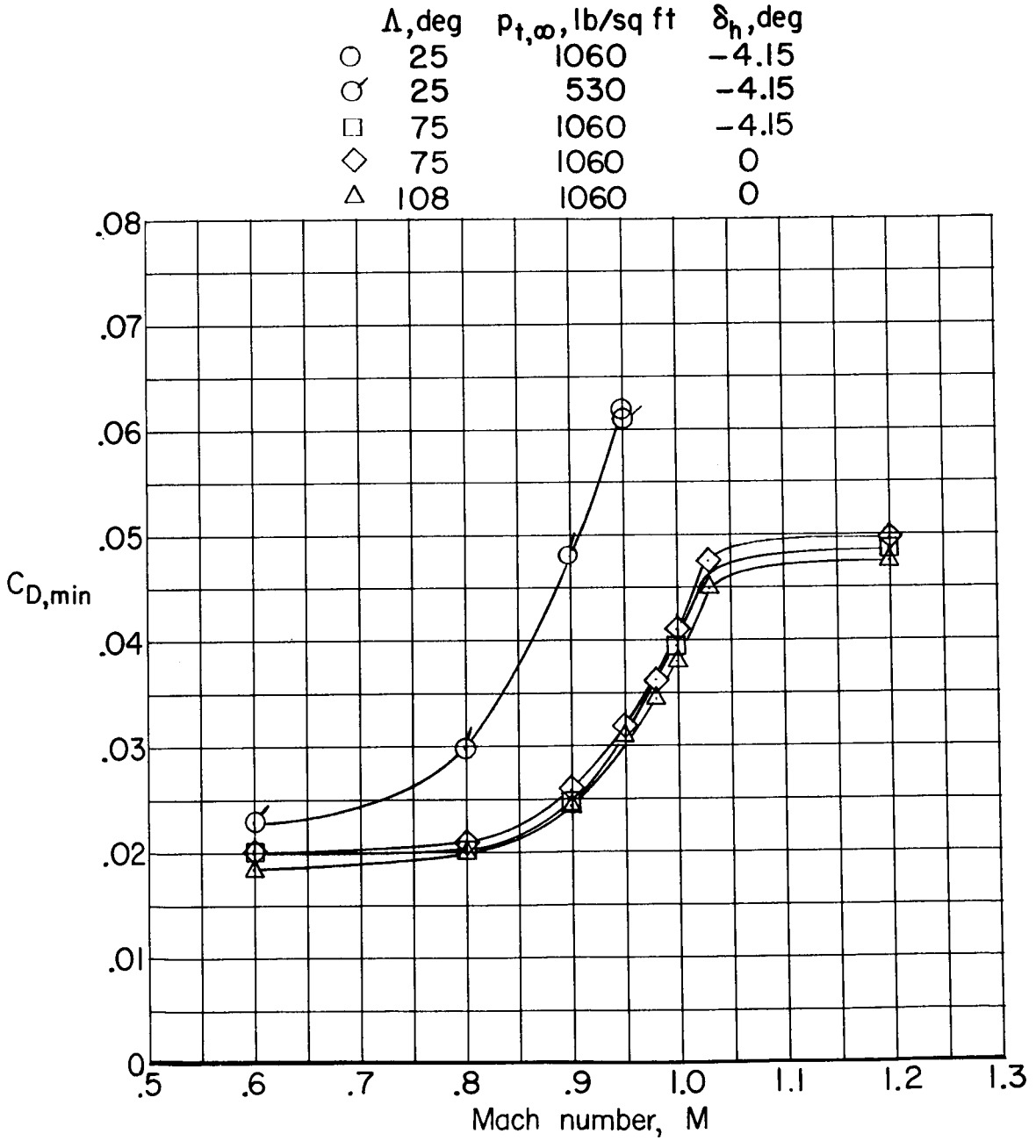

Figure 20.- Effect of wing sweep on minimum drag of model IV-A. Configuration BWVH.

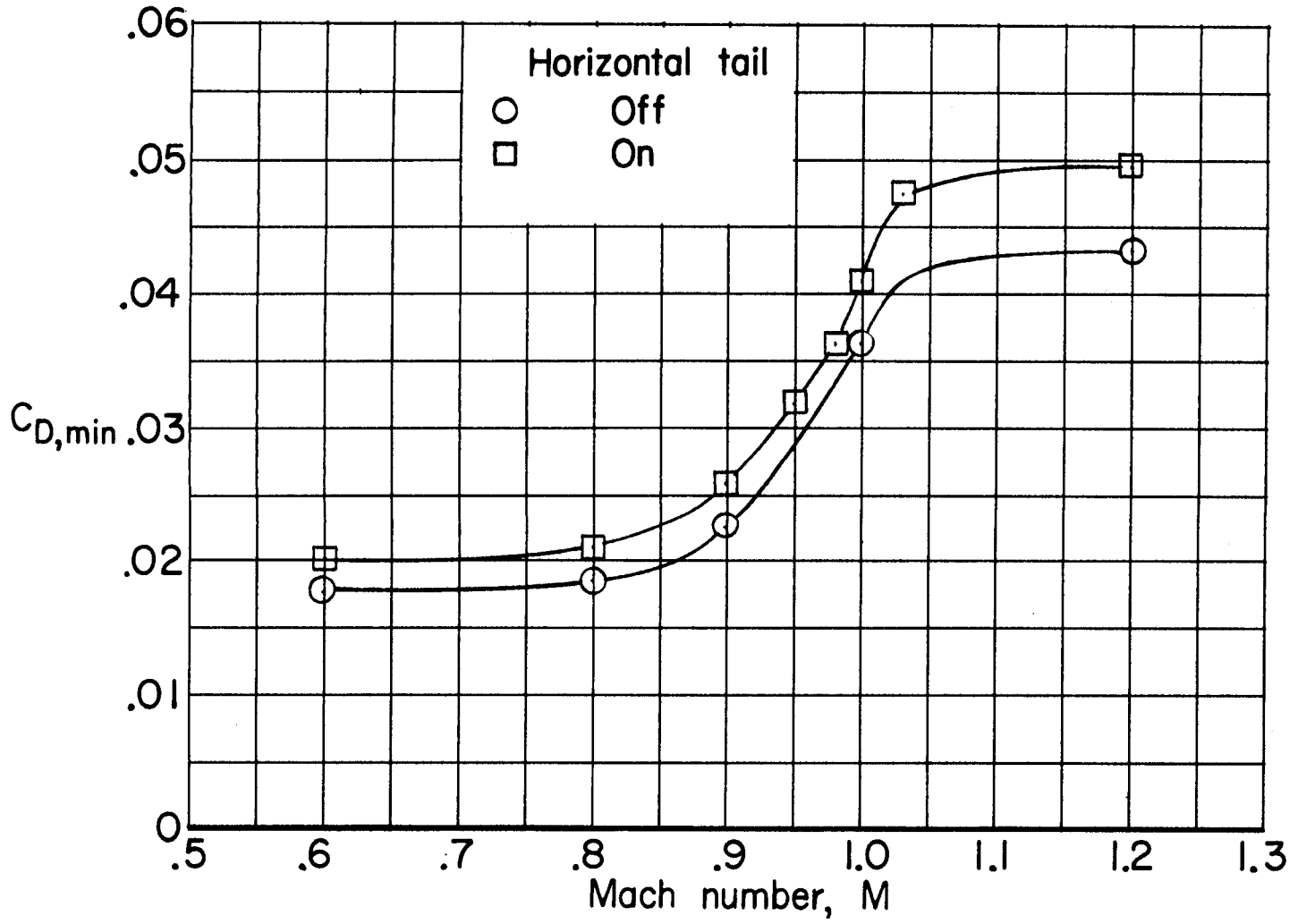

Figure 21.- Incremental effect of horizontal tail on minimum drag of model IV-A with 75° swept wing. Configuration BWVH; $\delta_h = 0°$; $p_{t,\infty} = 1{,}060$ lb/sq ft.

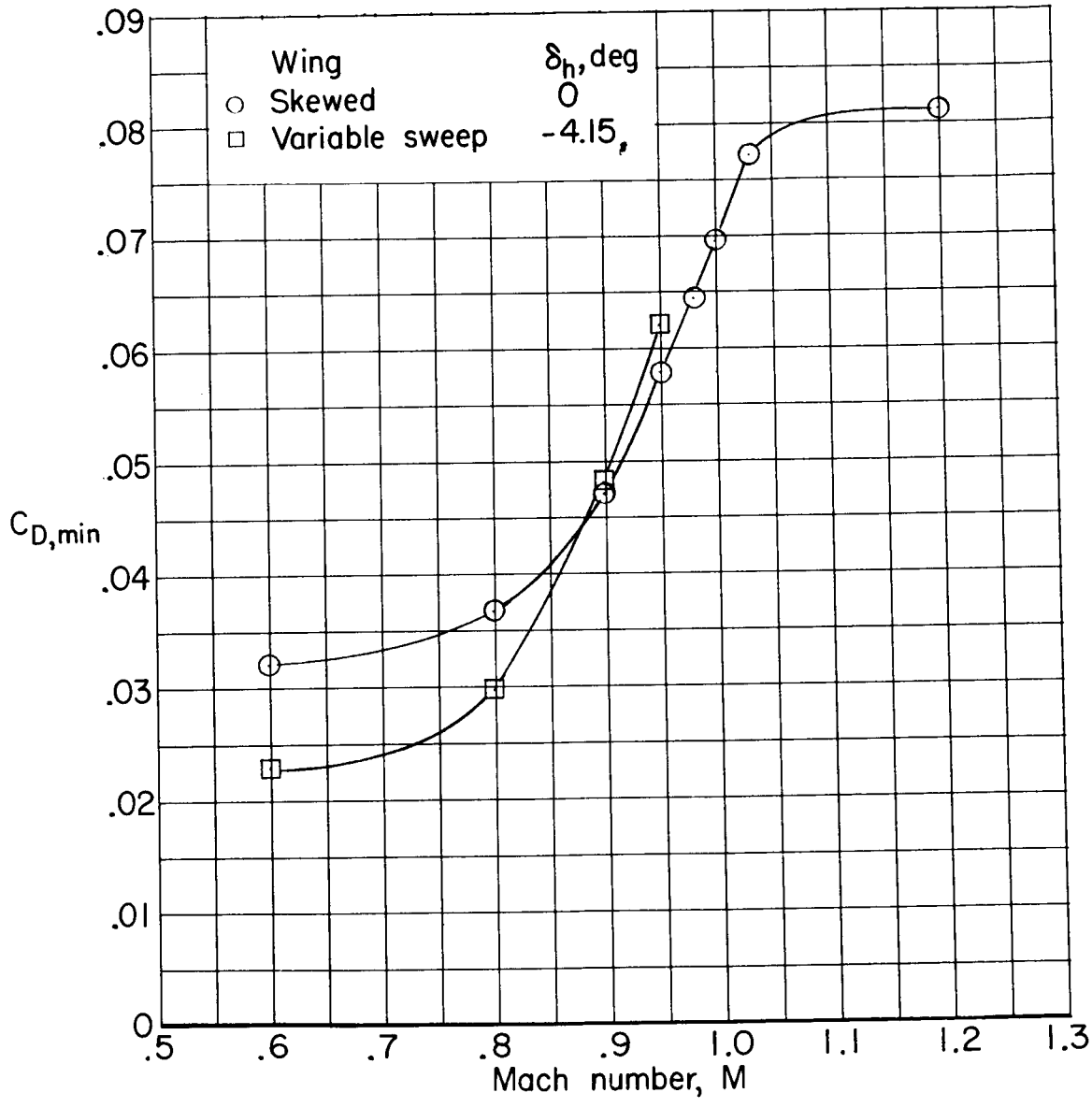

(a) $\zeta = 0^\circ$ and $\Lambda = 25^\circ$; $p_{t,\infty}$ = 530 lb/sq ft.

Figure 22.- Comparison of minimum drag of model IV-A with skewed and variable-sweep wings. Configuration BWVH.

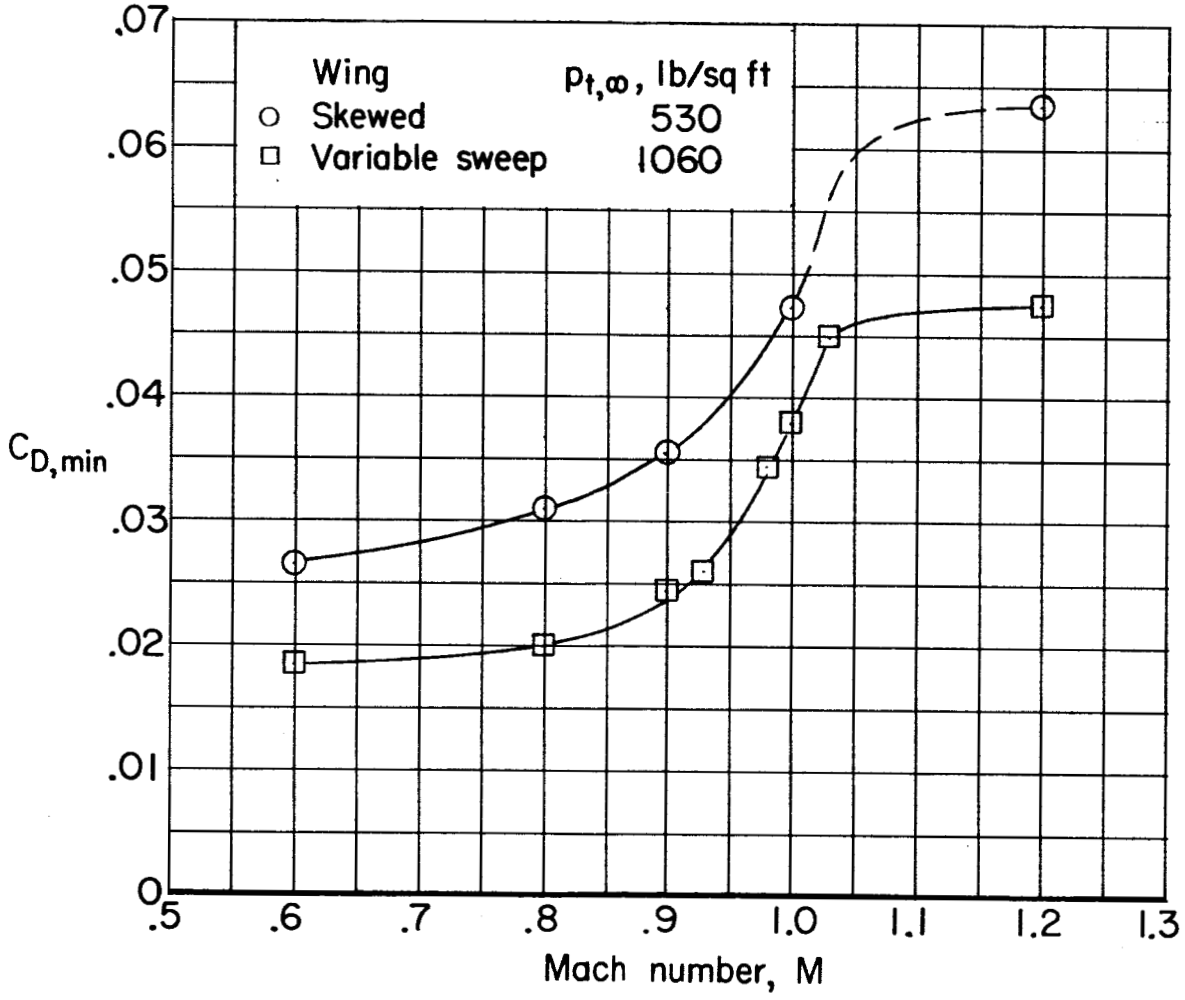

(b) $\zeta = 90^\circ$ and $\Lambda = 108^\circ$; $\delta_h = 0^\circ$.

Figure 22.- Concluded.

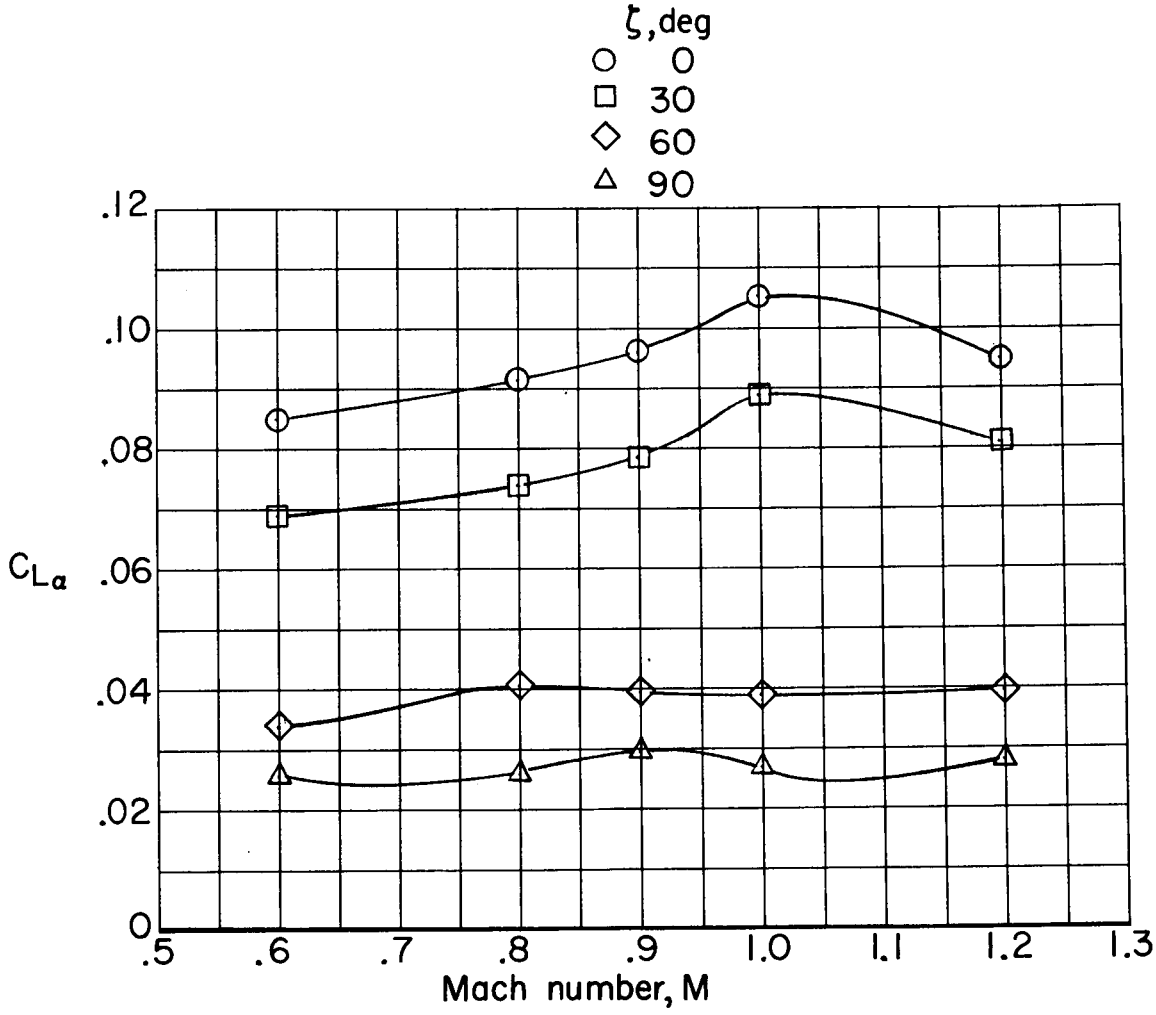

(a) Skewed wing; $\delta_h = 0^o$; $p_{t,\infty}$ = 530 lb/sq ft.

Figure 23.- Lift-curve slope of model IV-A with skewed and variable-sweep wings. Configuration BWVH.

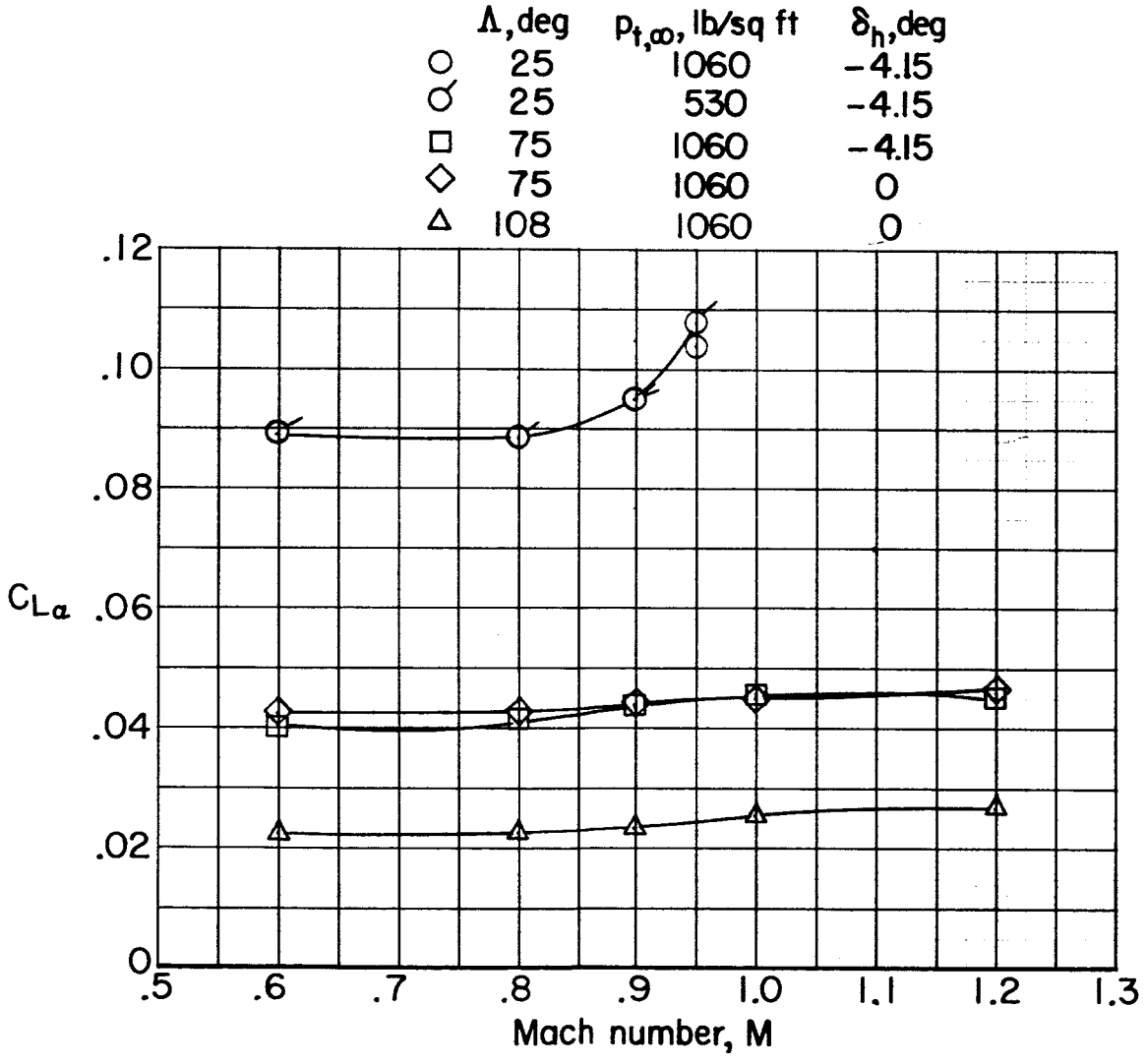

(b) Variable-sweep wing.

Figure 23.- Concluded.

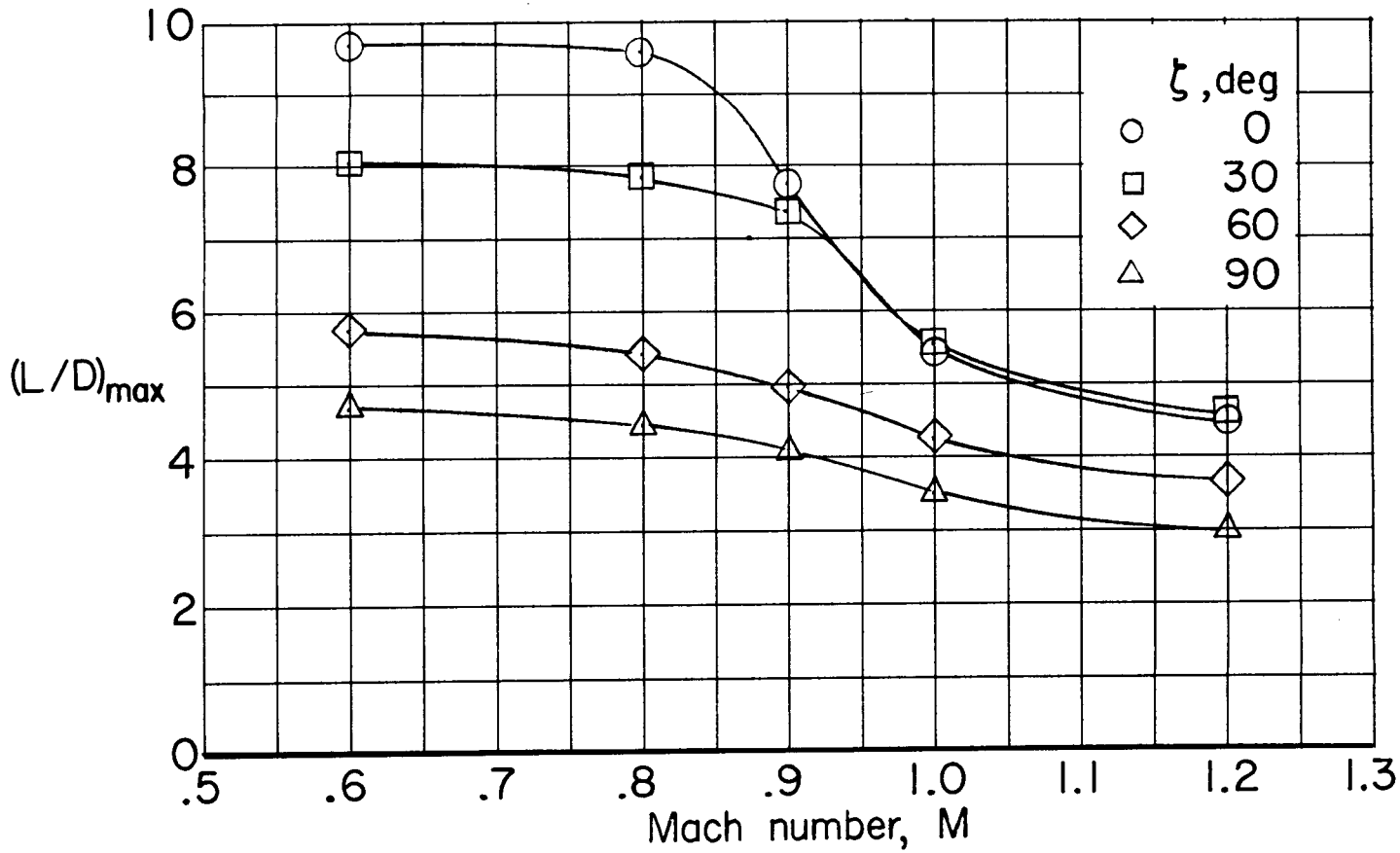

(a) Skewed wing; $\delta_h = 0^o$; $p_{t,\infty}$ = 530 lb/sq ft.

Figure 24.- Maximum lift-drag ratio of model IV-A with skewed and variable-sweep wings. Configuration BWVH.

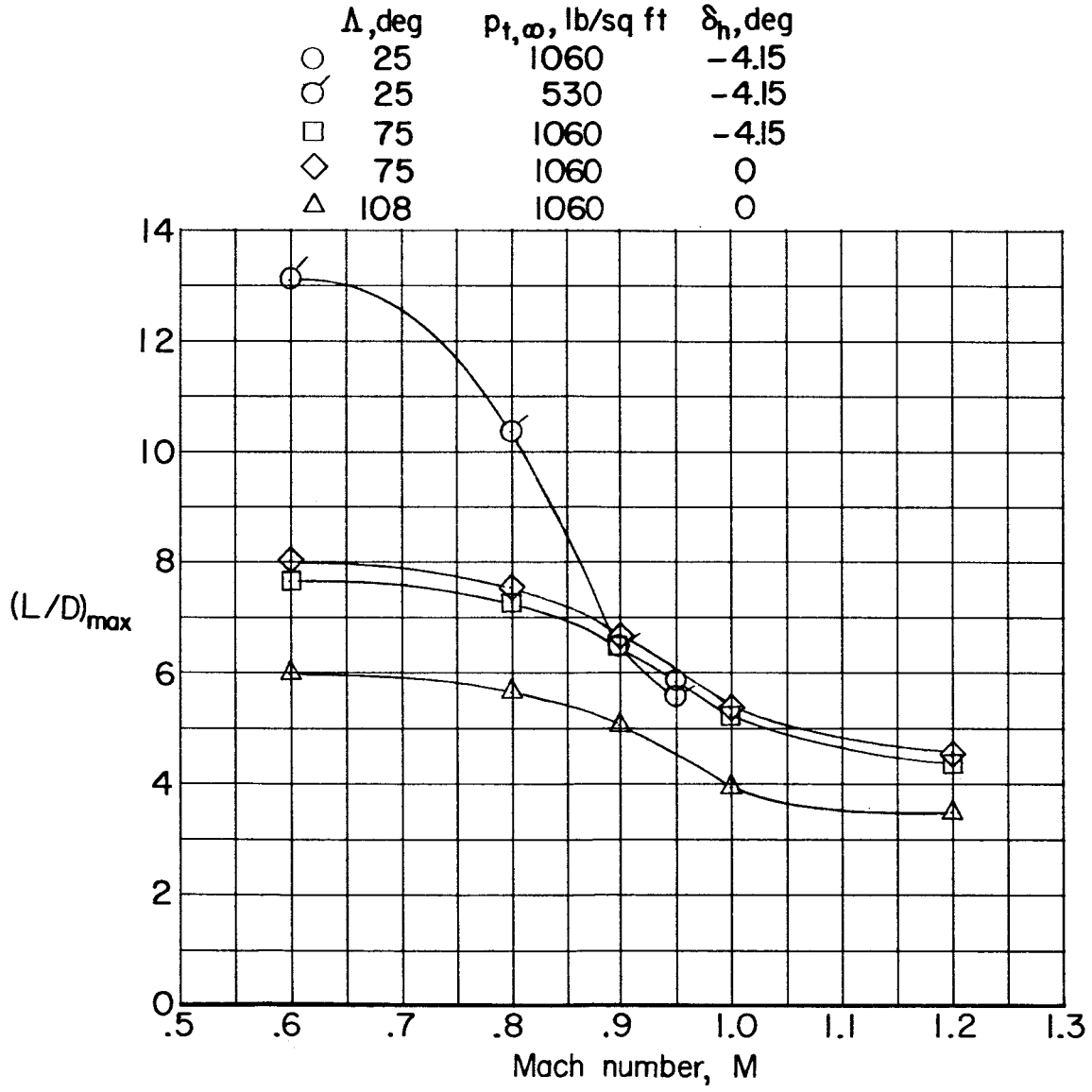

(b) Variable-sweep wing.

Figure 24.- Concluded.

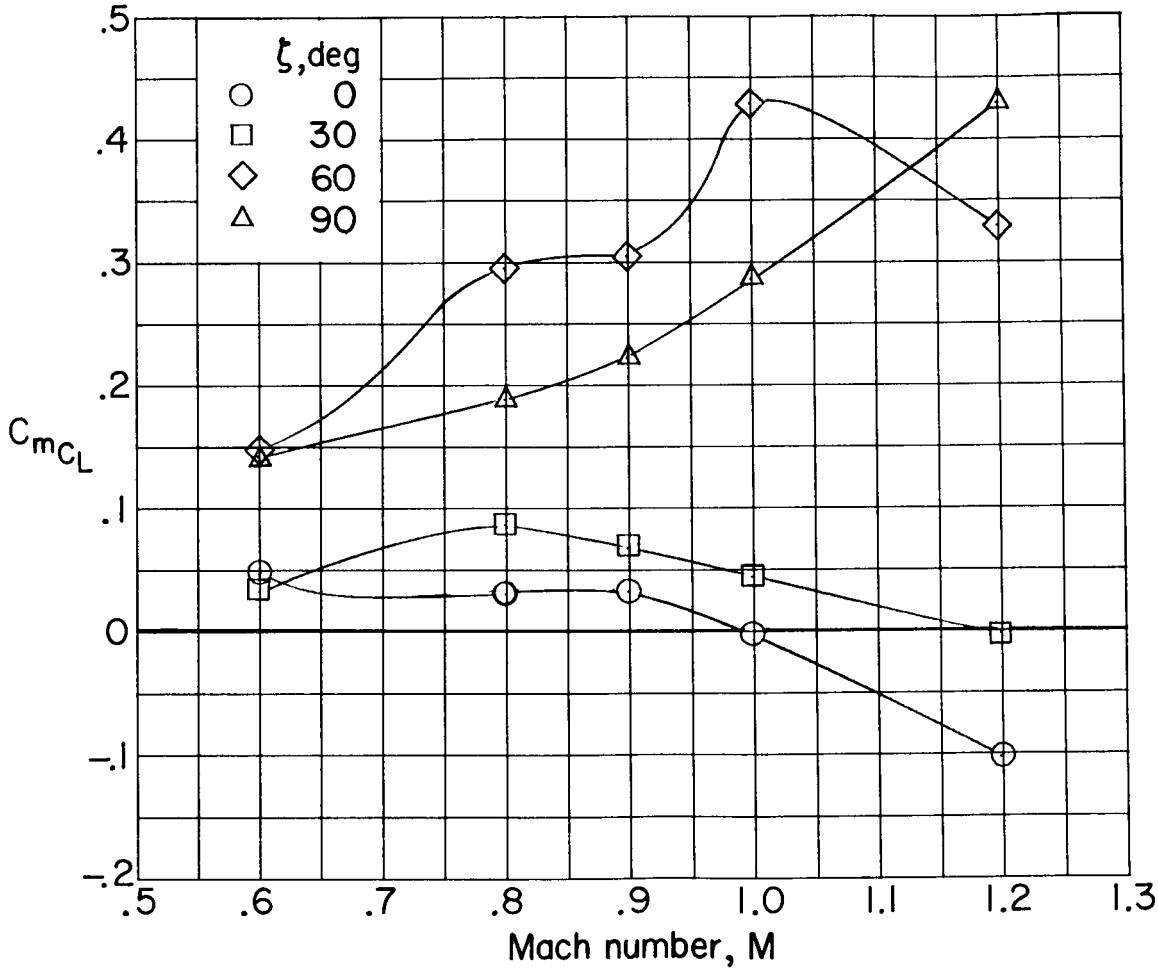

(a) Skewed wing; $\delta_h = 0^\circ$; $p_{t,\infty}$ = 530 lb/sq ft.

Figure 25.- Static longitudinal-stability derivative of model IV-A with skewed and variable-sweep wings. Configuration BWVH.

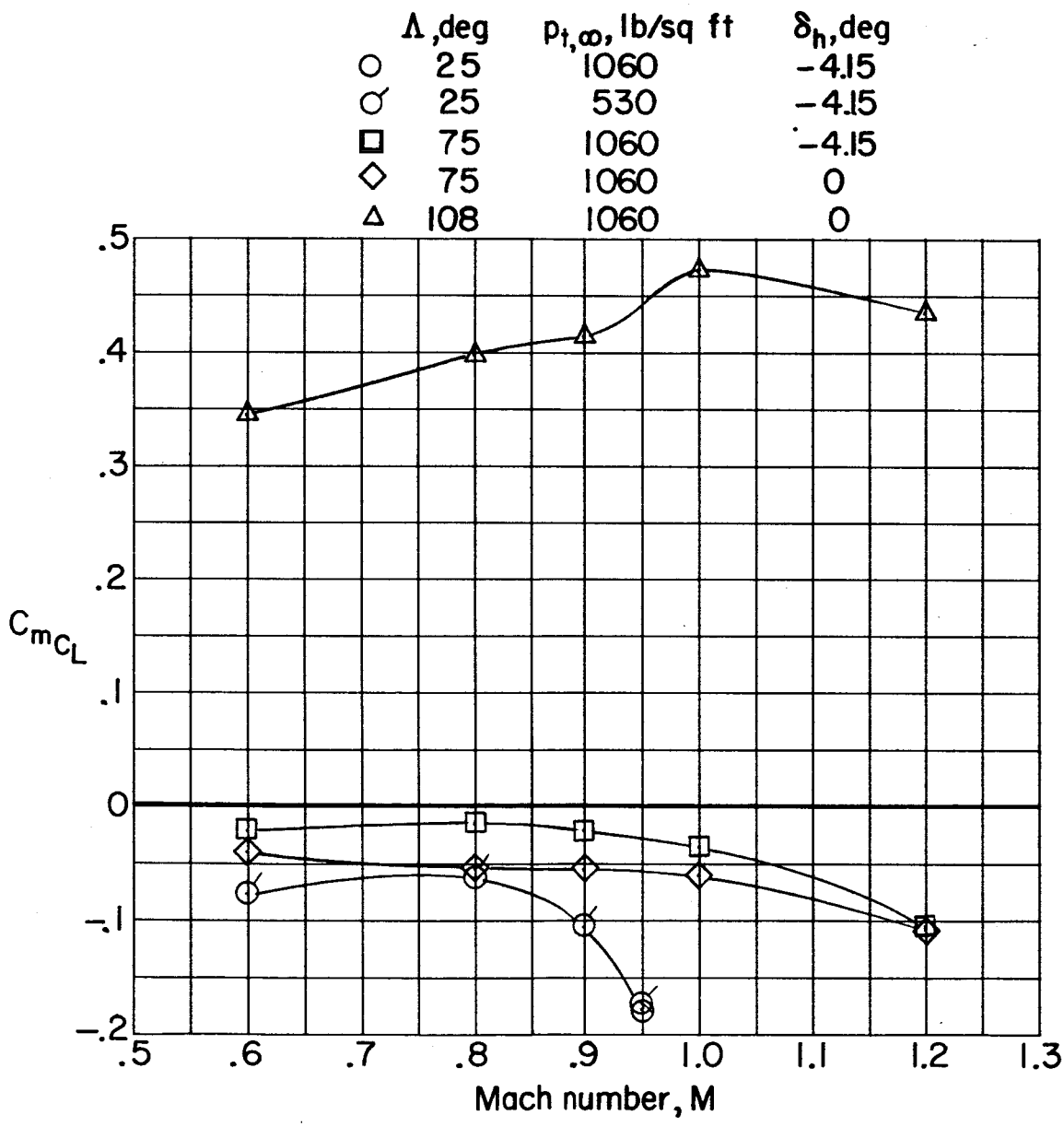

(b) Variable-sweep wing.

Figure 25.- Concluded.

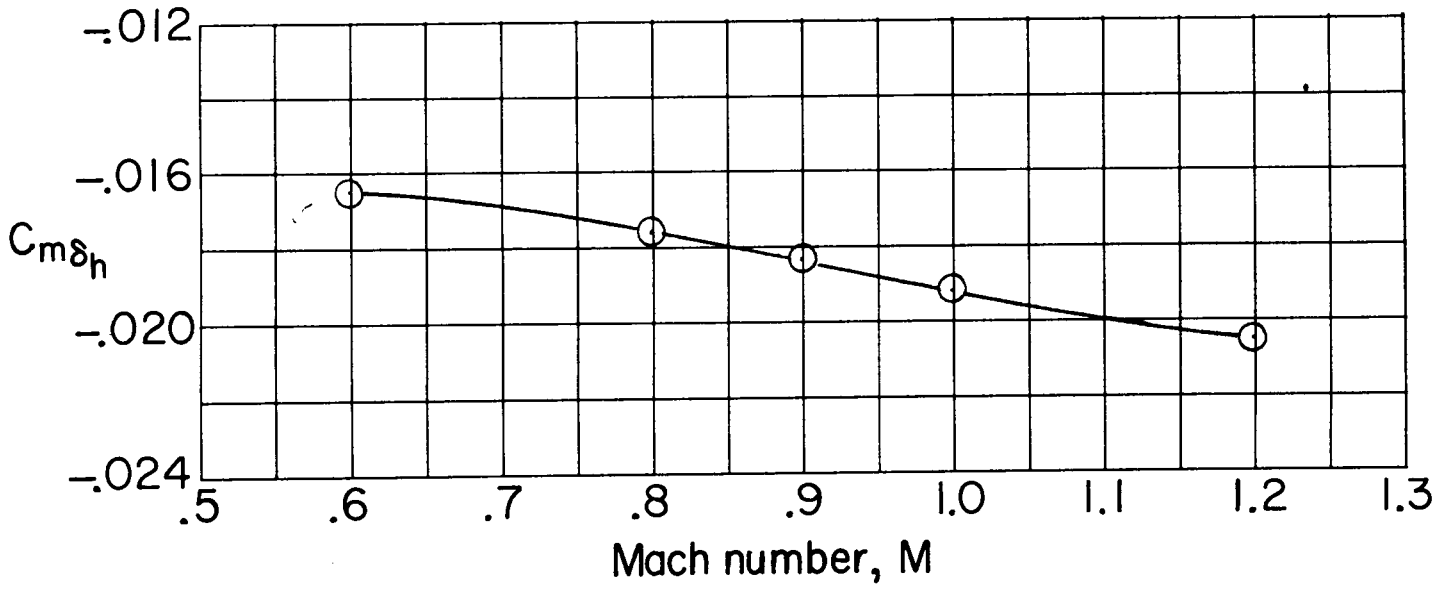

Figure 26.- Horizontal-tail effectiveness of model IV-A with 75° swept wing. Configuration BWVH; $\alpha = 0^{\circ}$; $p_{t,\infty} = 1{,}060$ lb/sq ft.

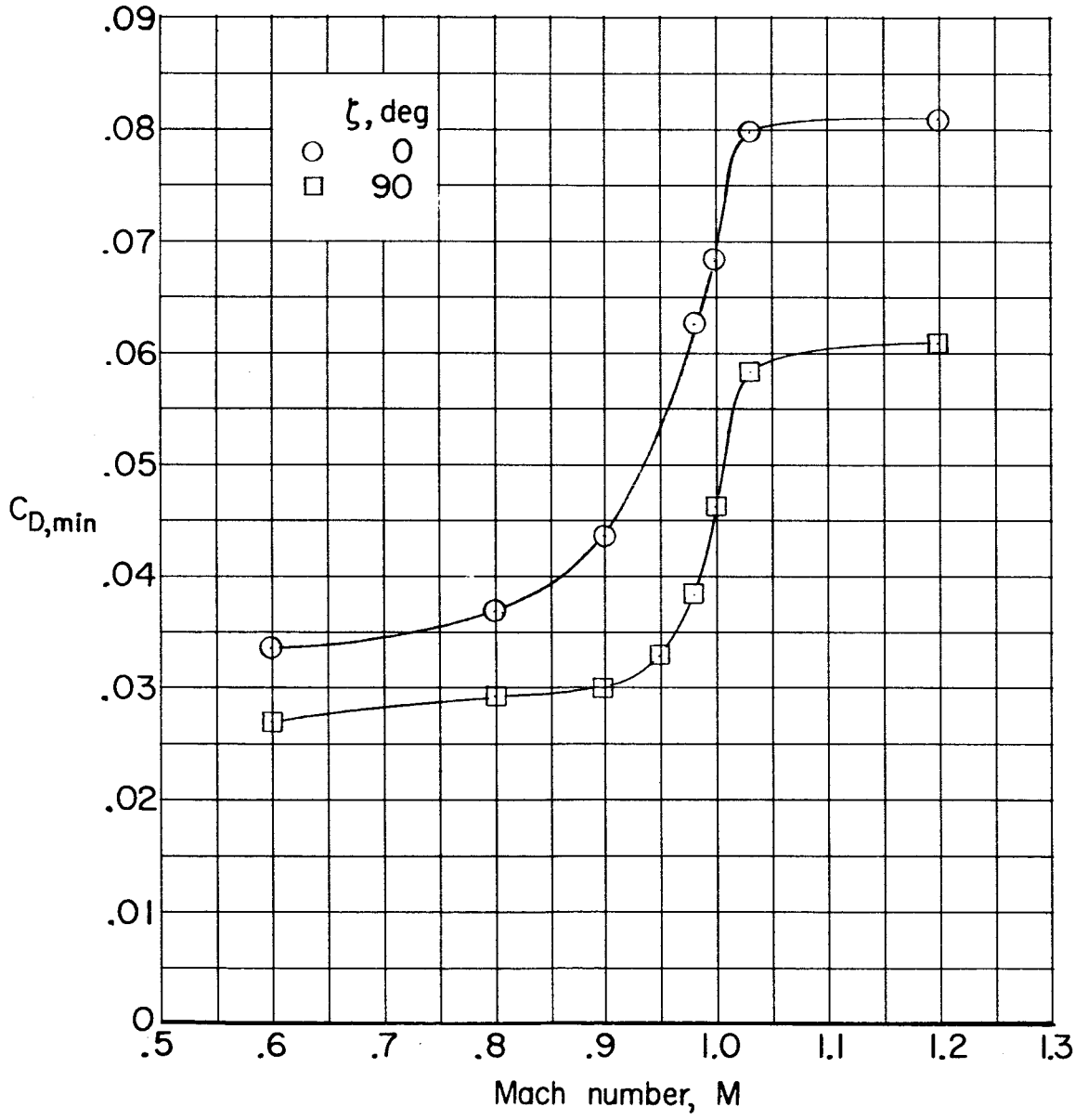

Figure 27.- Effect of wing skew angle on minimum drag of model IV-B. Configuration BWVH; $\delta_h = -4.15^\circ$; $p_{t,\infty} = 1{,}060$ lb/sq ft.

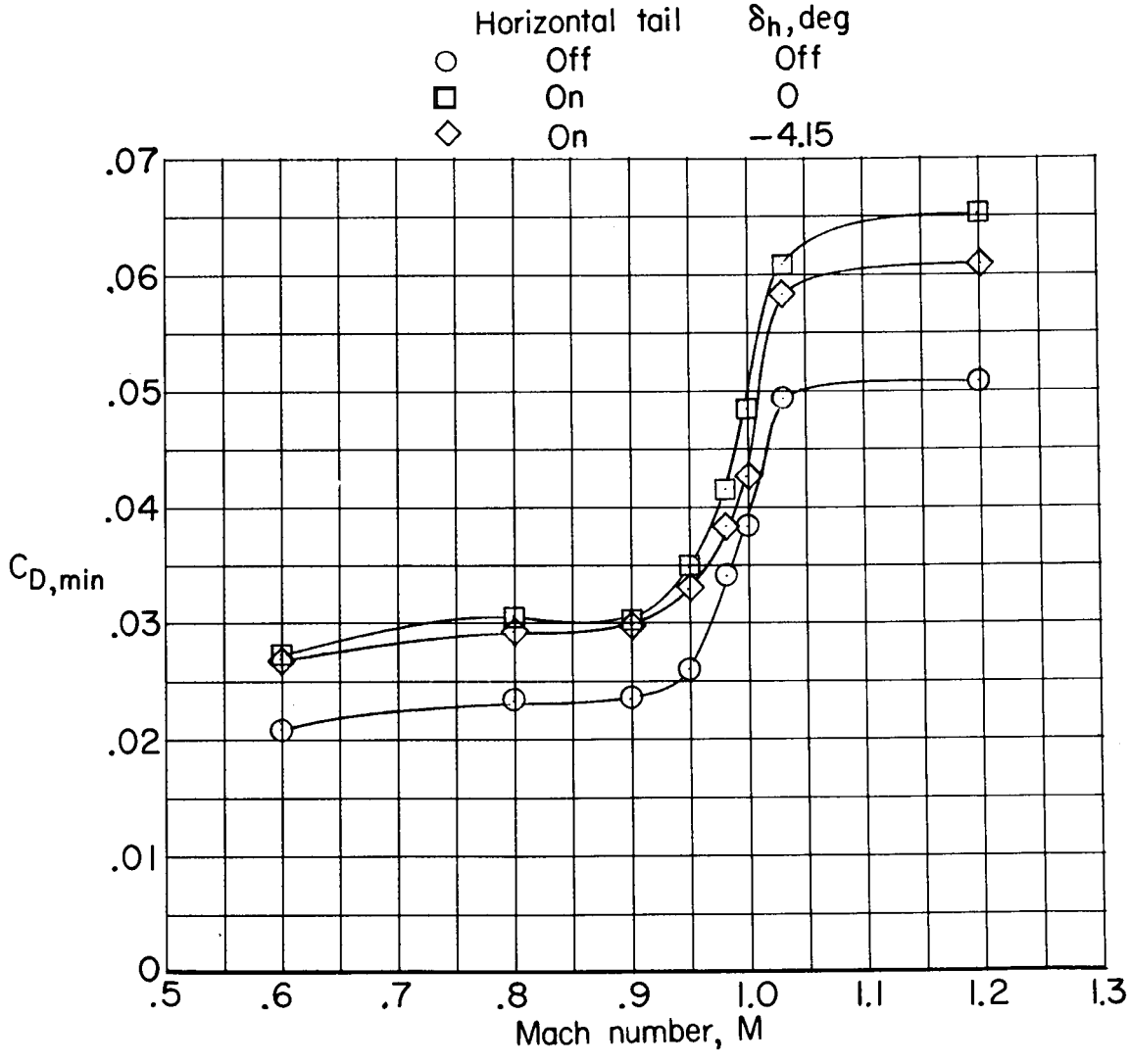

Figure 28.- Incremental effect of horizontal tail on minimum drag of model IV-B with 90° skewed wing. Configuration BWVH; ζ = 90°; $p_{t,\infty}$ = 1,060 lb/sq ft.

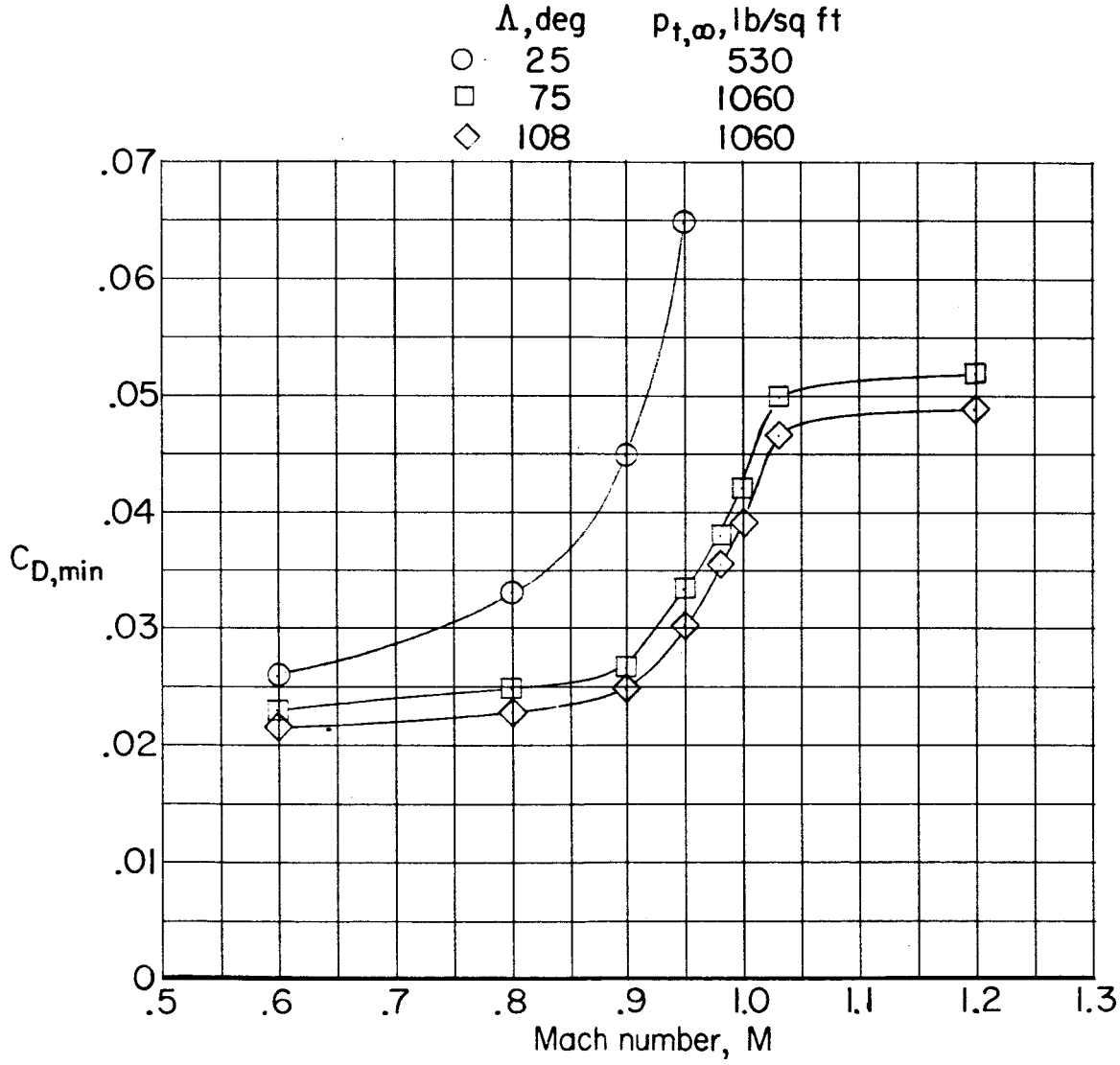

Figure 29.- Effect of wing sweep on minimum drag of model IV-B. Configuration BWVH; $\delta_h = -4.15°$.

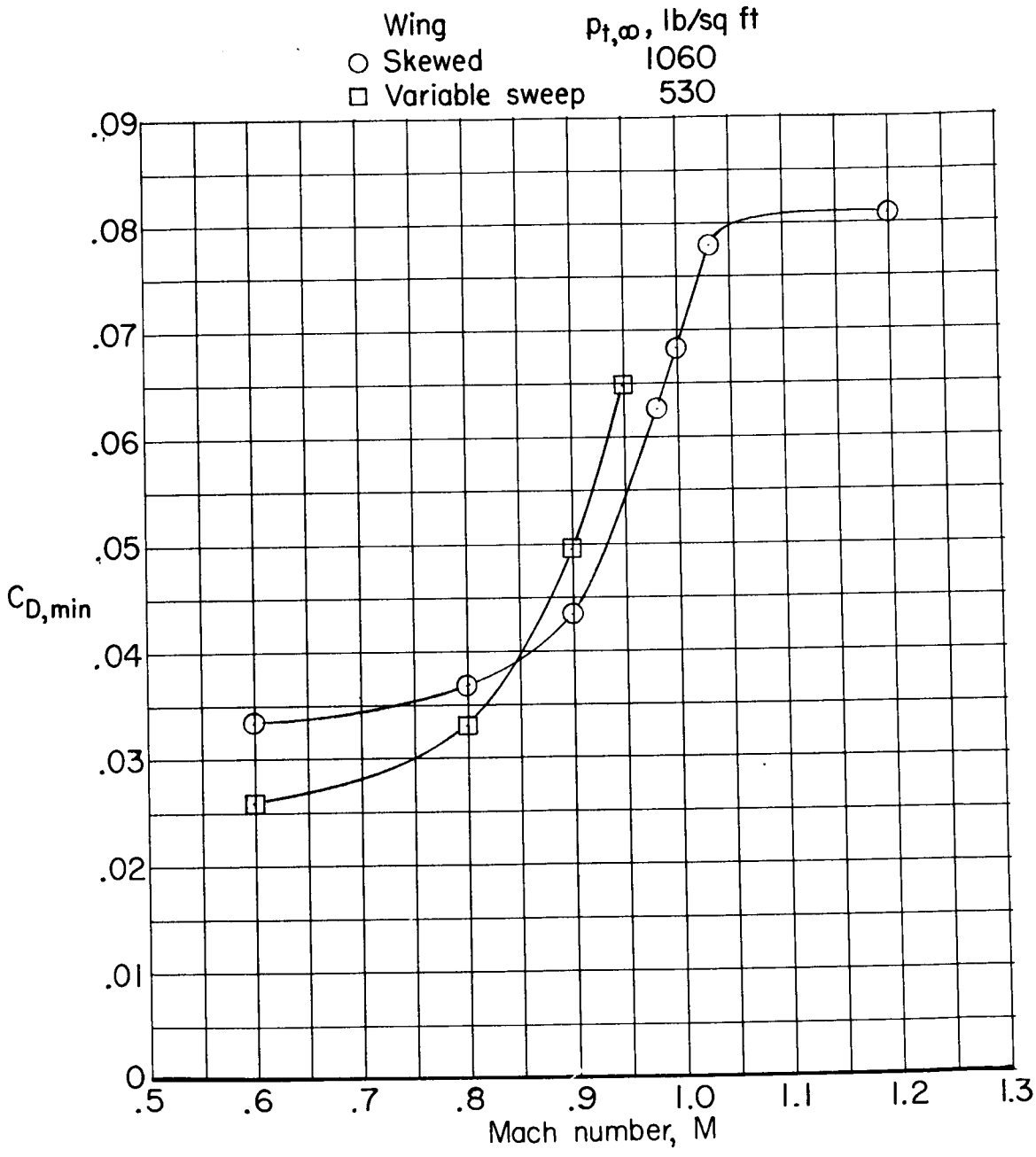

(a) $\zeta = 0^\circ$ and $\Lambda = 25^\circ$.

Figure 30.- Comparison of minimum drag of model IV-B with skewed and variable-sweep wings. Configuration BWVH; $\delta_h = -4.15^\circ$.

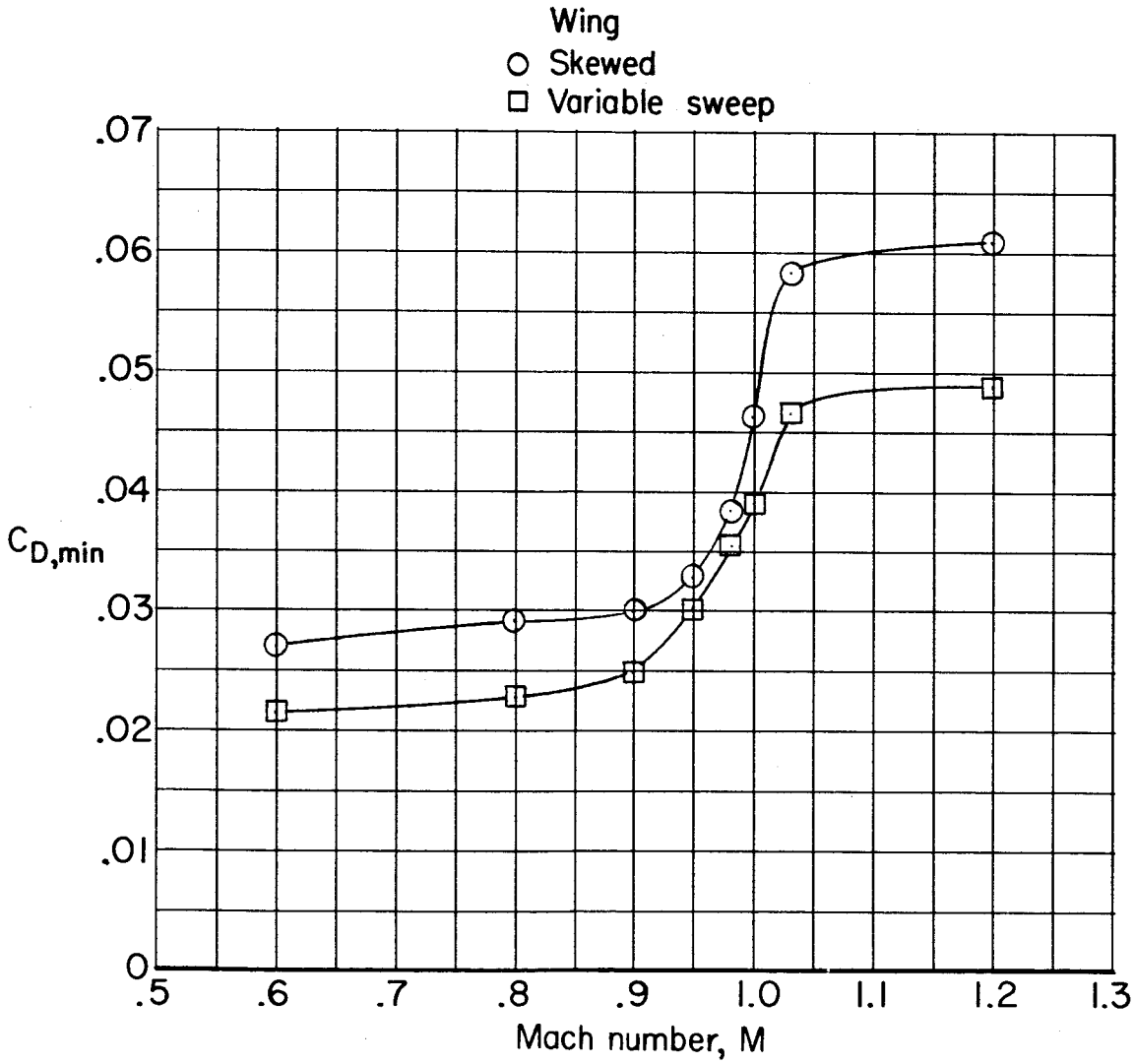

(b) $\zeta = 90^{\circ}$ and $\Lambda = 108^{\circ}$; $p_{t,\infty} = 1{,}060$ lb/sq ft.

Figure 30.- Concluded.

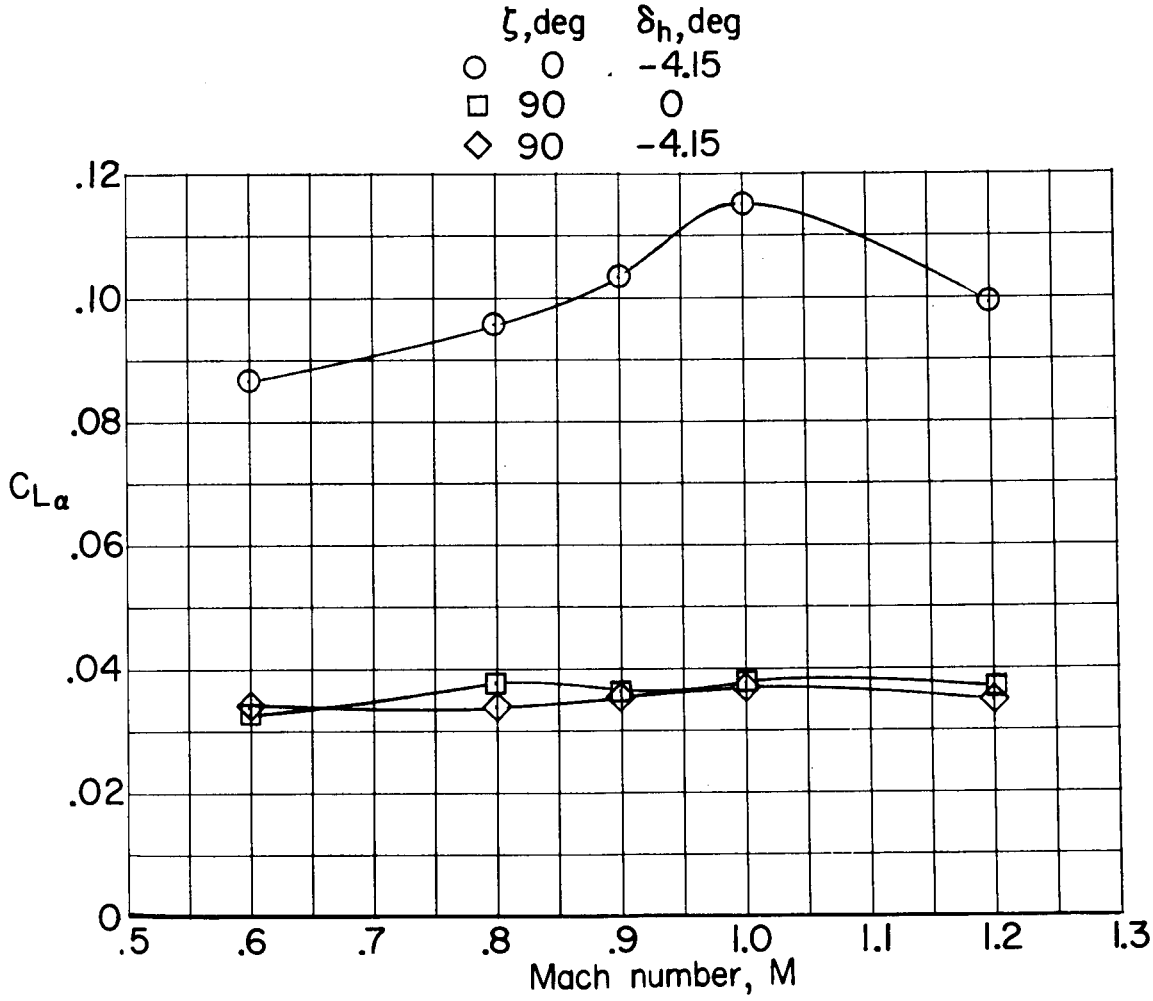

(a) Skewed wing; $p_{t,\infty}$ = 1,060 lb/sq ft.

Figure 31.- Lift-curve slope of model IV-B with skewed and variable-sweep wings. Configuration BWVH.

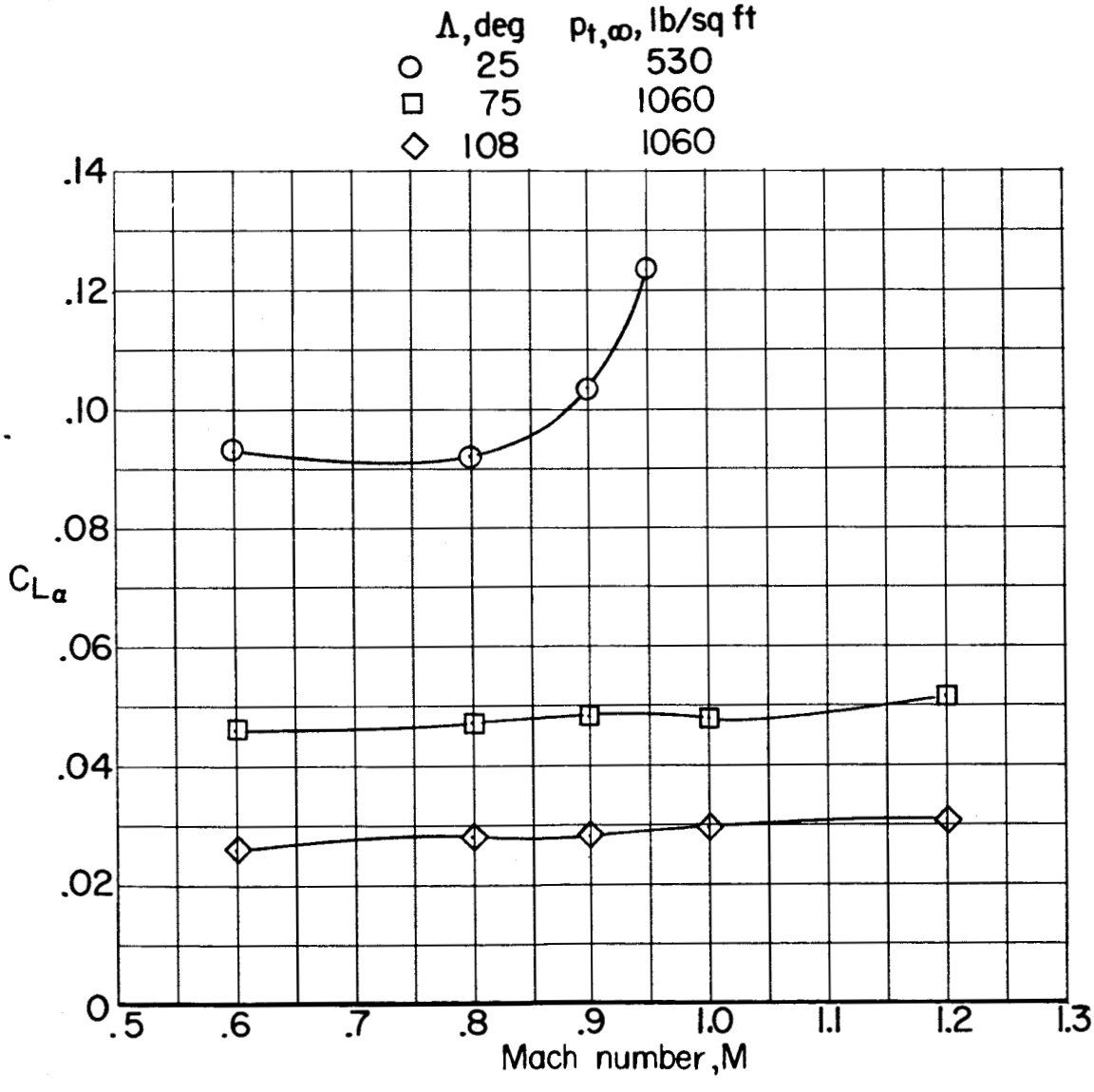

(b) Variable-sweep wing; $\delta_h = -4.15°$.

Figure 31.- Concluded.

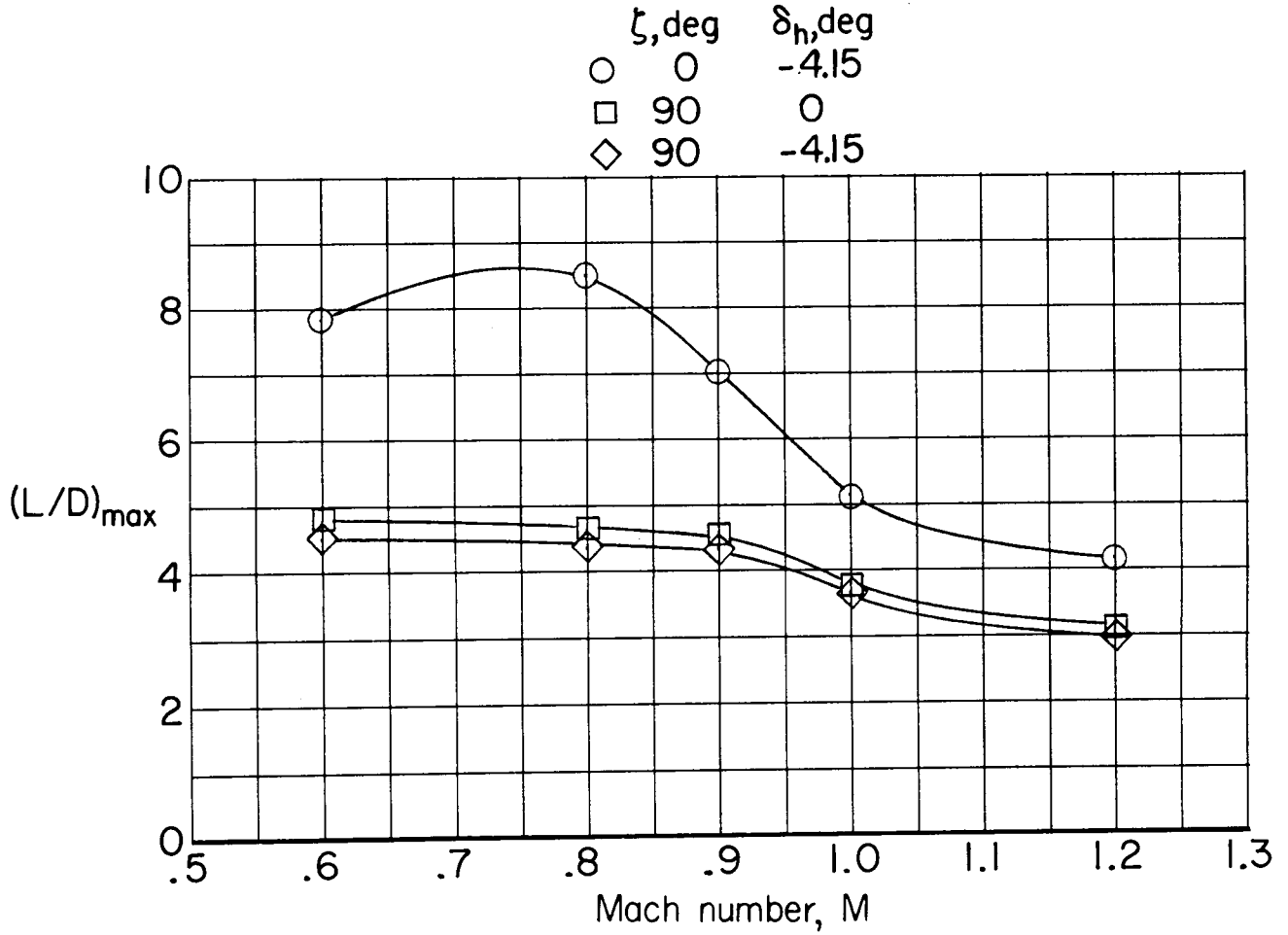

(a) Skewed wing; $p_{t,\infty}$ = 1,060 lb/sq ft.

Figure 32.- Maximum lift-drag ratio of model IV-B with skewed and variable-sweep wings. Configuration BWVH.

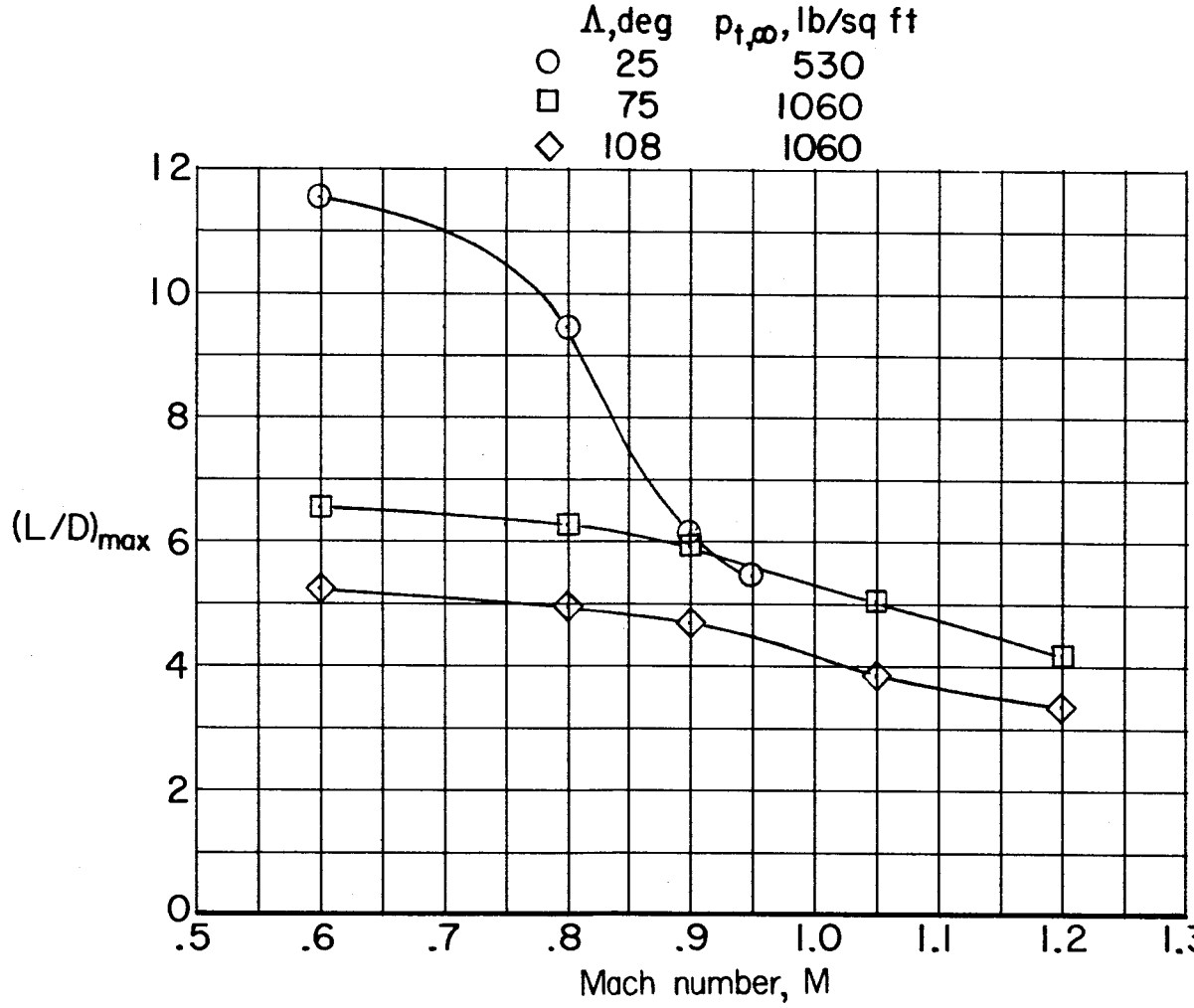

(b) Variable-sweep wing; $\delta_h = 0^o$.

Figure 32.- Concluded.

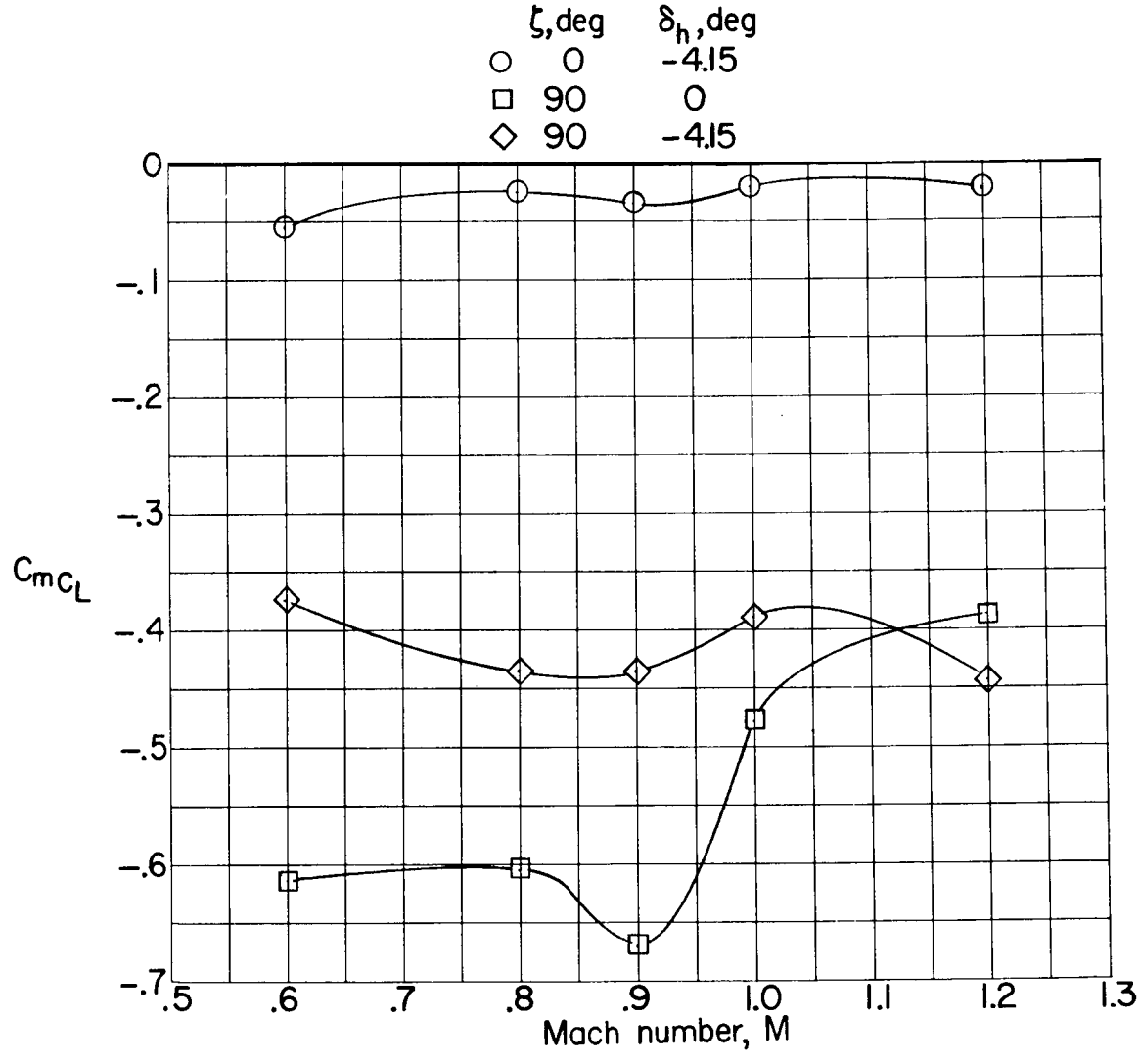

(a) Skewed wing; $p_{t,\infty}$ = 1,060 lb/sq ft.

Figure 33.- Static longitudinal-stability derivatives of model IV-B with skewed and variable-sweep wings. Configuration BWVH.

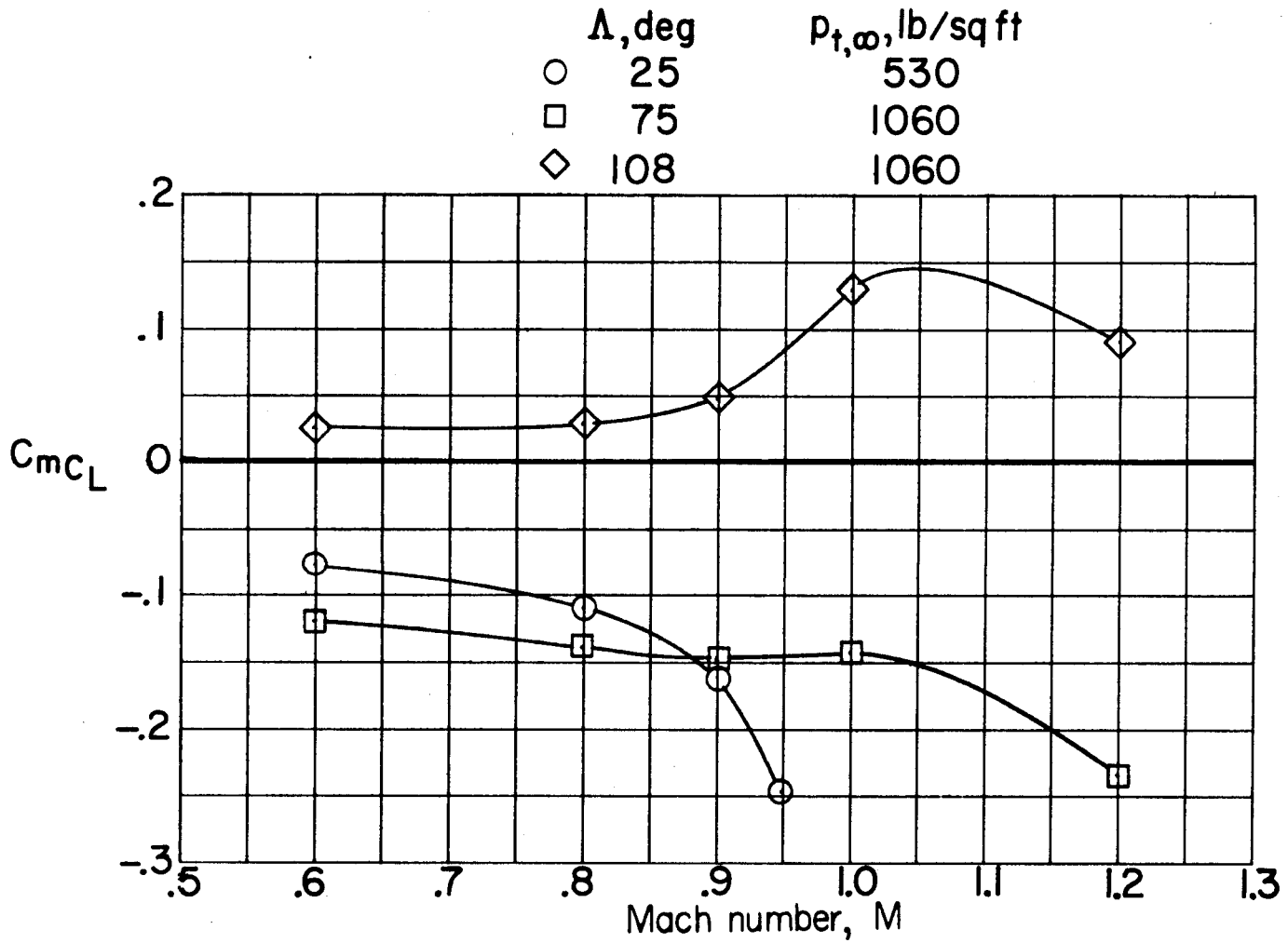

(b) Variable-sweep wing; $\delta_h = -4.15^\circ$.

Figure 33.- Concluded.

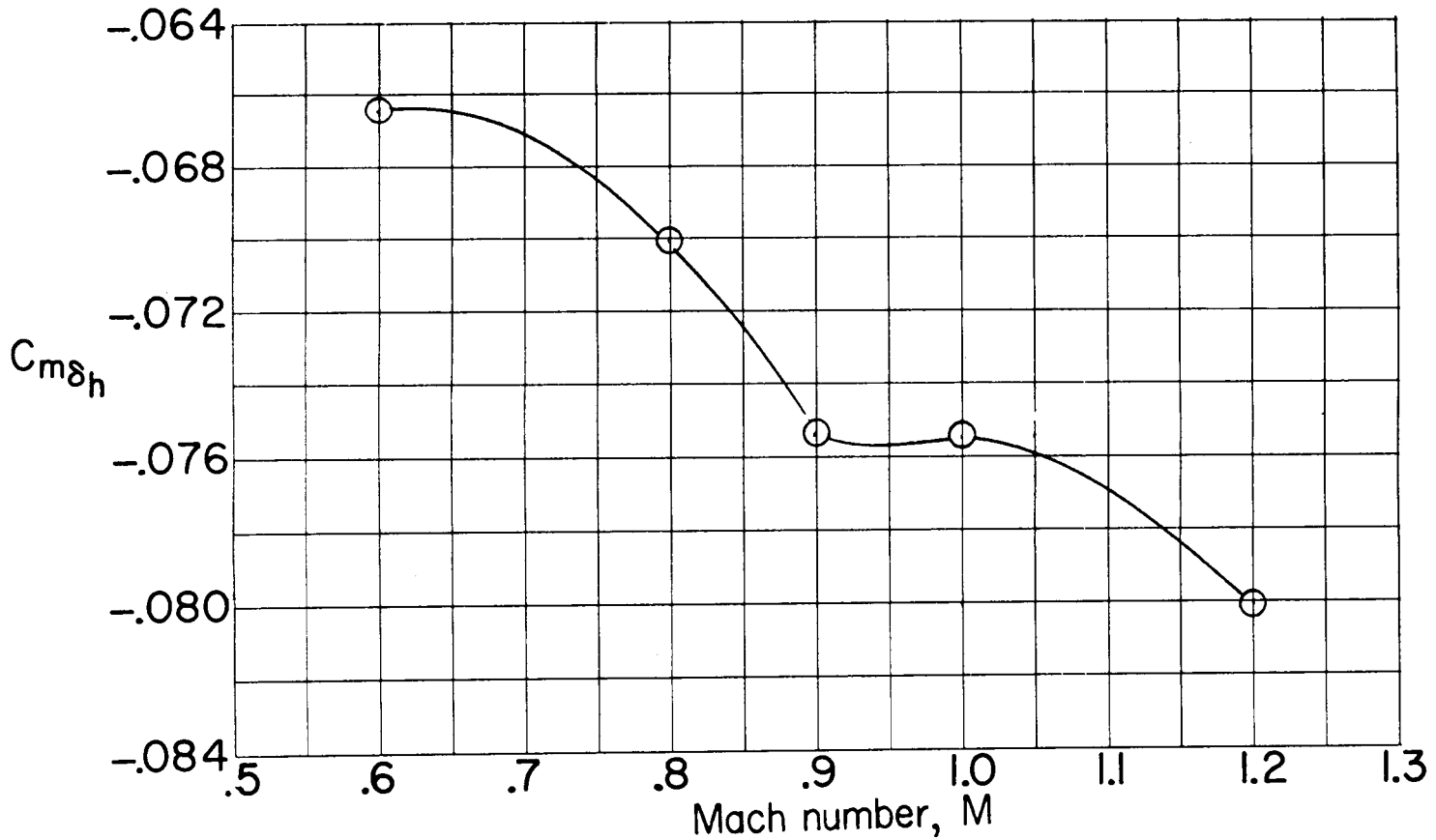

Figure 34.- Horizontal-tail effectiveness of model IV-B with 90° skewed wing. Configuration BWVH; ζ = 90°; α = 0°; $p_{t,\infty}$ = 1,060 lb/sq ft.

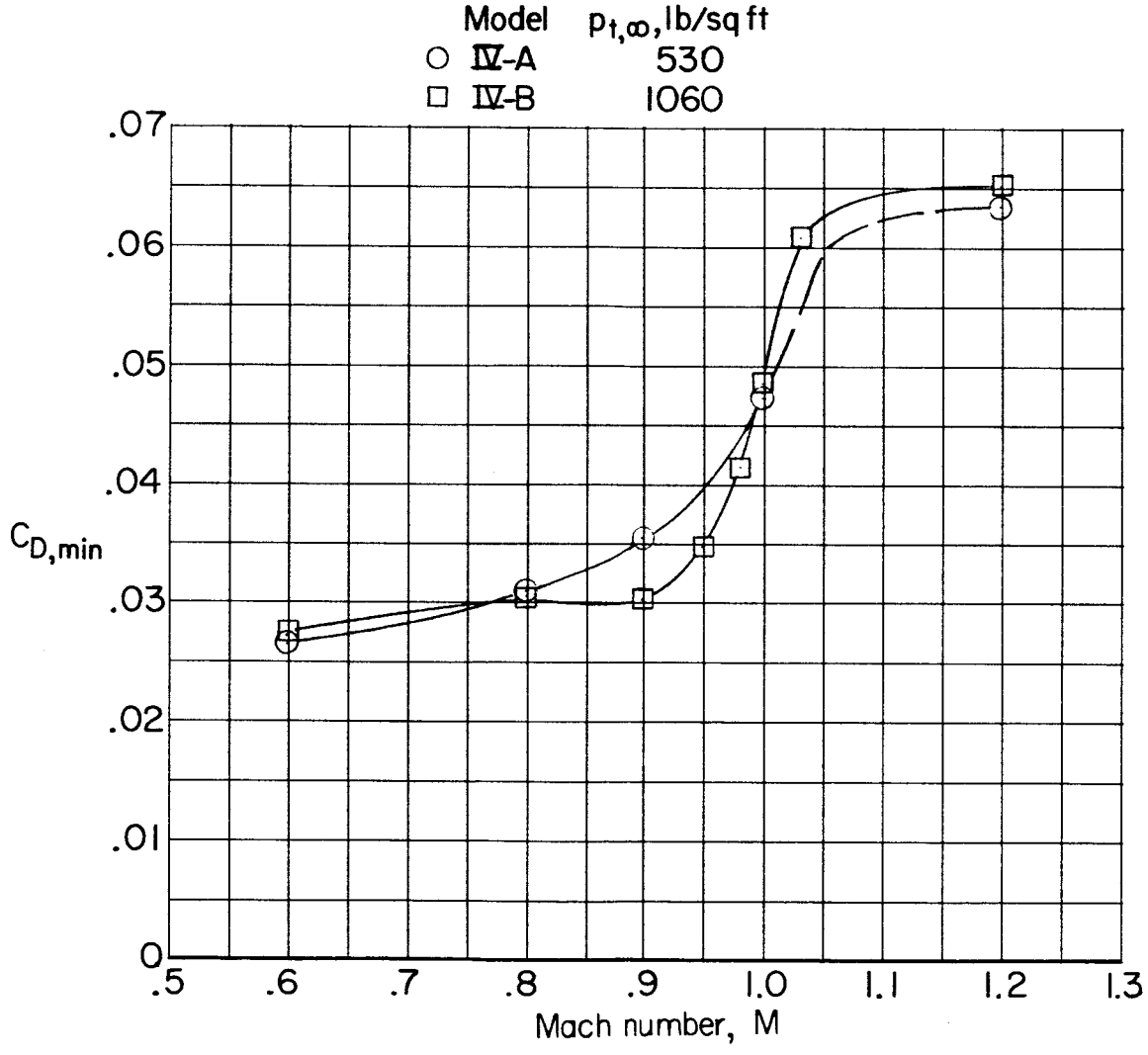

(a) Skewed wing; $\zeta = 90^{\circ}$; $\delta_h = 0^{\circ}$.

Figure 35.- Comparison of minimum drag of models IV-A and IV-B with skewed and variable-sweep wings. Configuration BWVH.

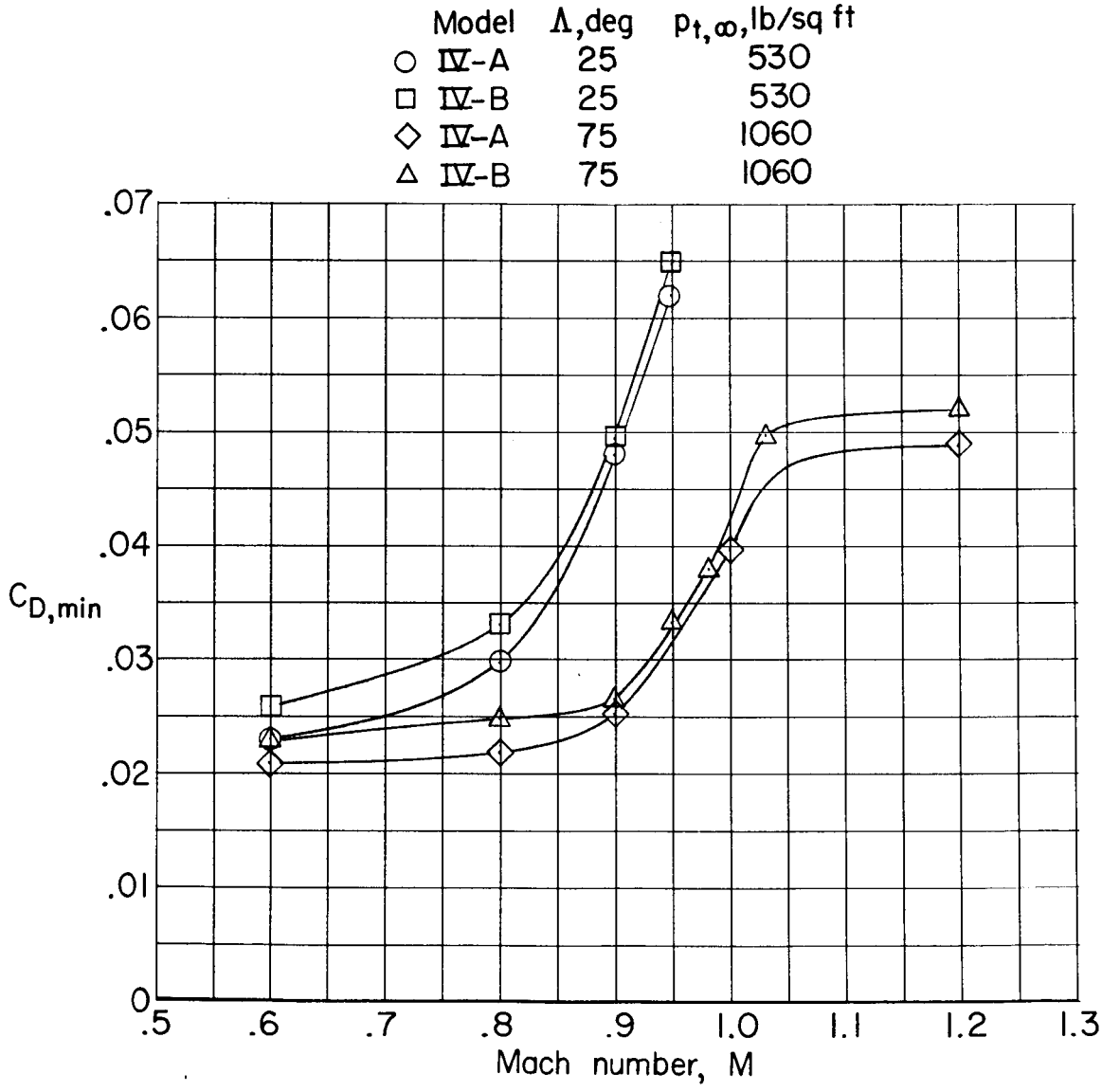

(b) Variable-sweep wing; $\delta_h = -4.15°$.

Figure 35.- Concluded.